Par **Batoul ABDELAZIZ**

Direct algorithms for solving some inverse source problems

Thèse présentée pour l'obtention du grade de Docteur de l'UTC

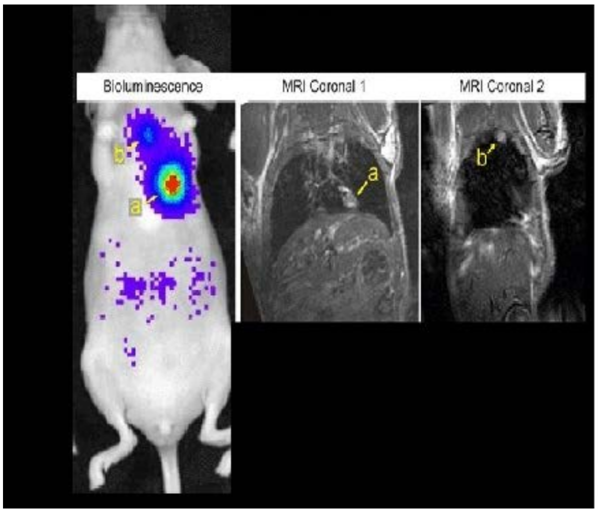

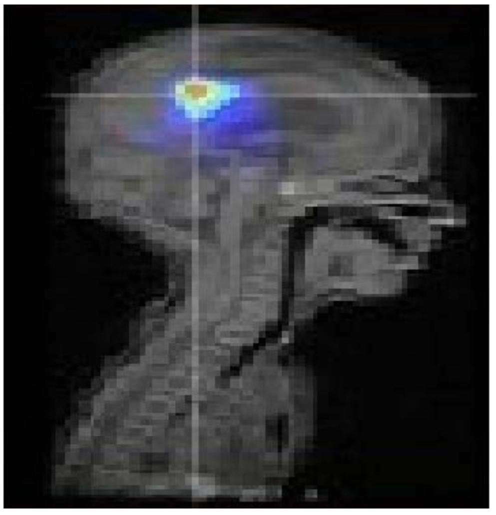

Soutenue le 16 septembre 2014

Spécialité : Mathématiques Appliquées et Problèmes Inverses

D1956

Algorithmes directs pour résoudre quelques problèmes inverses de sources

Batoul ABDELAZIZ

Thèse soutenue le **date** devant le jury composé de :

Président:

Olivier GOUBET
Professeur des Universités
Univ. de Picardie Jules Verne

Directeur de Thèse:

Abdellatif EL BADIA
Professeur des Universités
Univ. de Technologie de Compiègne

Rapporteurs:

Marc BONNET
Directeur de Recherche au CNRS
ENSTA, Unité de Mathématiques Appliquées, POems

William RUNDELL
Professeur des Universités
Texas A&M Univ.

Examinateurs:

Ahmad EL HAJJ
Maître de Conférences
Univ. de Technologie de Compiègne

Mustafa JAZAR
Professeur des Universités
Univ. Libanaise, Tripoli

Université de Technologie de Compiègne

Laboratoire LMAC EA 2222

16 Septembre 2014

- This thesis was typeset with LaTeX using a modified version of `scrbook` class. The majority of the figures where done with TikZ. A great part of the design of the document was inspired by the following communities:

  www.tex.stackexchange.com

  www.texample.net

- The images presented in the front page of this thesis are taken respectively from:

  The Molecular Imaging Center in University of Virginia, USA -
  http://www.medicine.virginia.edu/research/cores/MolecularImagingCore/micservices-page

  Laboratoire GRAMFC, Amiens, France -
  http://www.u-picardie.fr/labo/GRAMFC

To the most affectionate and lovely woman, To MOM

Contents

List of Figures

List of Tables

Preface

Acknowledgements

I would like to express my special appreciation and thanks to my advisor Professor Abdellatif El Badia, whose expertise and knowledge added considerably to my thesis experience. I would like to thank you for your useful comments and remarks and for encouraging me in the research and for allowing me to grow as a research scientist. Your advice on both research as well as on my career have been priceless.

Furthermore, I would like to thank and express my gratitude for Dr. Ahmad El Hajj, whose vast skills in many areas helped me, for working along with us. I thank you for your engagement through the learning process of this thesis as well for the support on the way.

A special thanks for Professor Mustapha Jazar for believing in me, motivating me and for helping me to get a thesis. I wouldn't be here if it wasn't for you so a great thank you.

I would also like to thank the rest of my thesis committee: Professor Olivier Goubet, for presiding the committee and Professors Marc Bonnet and William Rundell for accepting to be the thesis manuscript referees. I thank you all for serving as my committee members and for the fruitful ideas and insightful comments you gave me. Thank you for letting my defense be a very enjoyable moment.

I also want to thank the French Ministry of National Education, Higher Education and Research for the financial support, the scholarship, granted to me through my doctoral fellowship years.

I want to thank all the members of LMAC (Laboratoire de Mathématiques Appliques de Compiègne). Thank you all, you have been extremely helpful and a supportive network of friends especially Djalil, Sergio and Salim.

I thank also, the secretary of the laboratory, Beatrice Barbier for her availability and for helping in all the administrative issues. Moreover, I thank the staff of the Ecole Doctorale especially Julie Jarek as well as the human resources staff for their efficient work and help in the paper work related to my PHD and ATER years.

In addition, a thank you is for Dr. Ammar Assoum who introduced me and helped me with Matlab toolboxes in the beginning of my thesis.

I would also like to thank all of my friends, Mahmoud, Hayat, Souad, Luis, Zoulficar, Diana, Irene, Chrysanthi, Samar, Fatima, Quiocho, Violaine, Alfredo and Mike who incented me to strive towards my goal. Thank you all for the unforgettable moments that we shared together, for the crazy adventures and for our trips together. I will be grateful forever for your love.

Last but not least, very special thanks to my parents and brothers, Mohammad and Ali, for their endless love and support. Words cannot express how grateful I am to my mother for all of the sacrifices that she's made on my behalf. Your prayer for me was what sustained me thus. Thank you very much and I love you a lot.

Finally, I thank Allah for the great opportunities He gave me and for the magnificent years I spent in my PHD thesis. Thank you!!

Publications and Conferences during the P.H.D.

Published articles in international journals

- Batoul Abdelaziz, Abdellatif El Badia, and Ahmad El Hajj. “Reconstruction of extended sources with small supports in the elliptic equation Δu+ μu= F from a single Cauchy data,” in: *Comptes Rendus Mathematique* 351.21 (2013), pp. 797–801
- Batoul Abdelaziz, Abdellatif El Badia, and Ahmad El Hajj. “Identification of monopolar sources in a bioluminescent tomography problem”. In: *ESAIM: PROCEEDINGS AND SURVEYS*. Vol. 45. EDP Sciences, SMAI. 2014, pp. 390–399
- Batoul Abdelaziz, Abdellatif El Badia, and Ahmad El Hajj. “Direct algorithm for multipolar sources reconstruction”. In: *to appear in Journal of Mathematical Analysis and Applications* (2014)

Articles submitted to international journals

- Batoul Abdelaziz, Abdellatif El Badia, and Ahmad El Hajj. “Algebraic method to identify impulse sources in 2D Helmholtz equtaion”. In: *submitted* (2014)

Conferences:

- “Identification in an inverse conductivity problem”, Oral Communication in IPMS, The 6th International Conference "Inverse Problems: Modeling and Simulation", Antalya, Turkey, 21-26/05/2012.
- “Identification dans un problème inverse de conductivité”, Oral Communication in Journée Scientifique du LMAC, UTC, Compiègne, France, 12/06/2012.
- “Identification of a combination of monopolar and dipolar sources for Helmholtz’s equation”, Poster in SMAI 2013, 6e Biennale Française des Mathématiques Appliquées et Industrielles, Seignosse Le Penon, Landes, France, 27-31/05/2013.
- “Reconstruction of extended sources with small supports in the elliptic equation $\Delta u + \mu u = F$”, Poster in 40 èmes journées EDP, Biarritz, 3-7 juin 2013.
- “ Identification of multipolar sources in the elliptic equation $\Delta u + \mu u = F$ ”, Oral Communication in IPDO, The 4th International Symposium on Inverse Problems, Design, and Optimisation, Albi, France, 26-28/06/2013.
- “ Identification de sources monopolaire dans un problème de tomographie par bioluminescence”, Oral Communication in Canum, 42e Congrès National d’Analyse Numérique, Carry-le-Rouet, Bouches-du-Rhône, France, 31/03-04/04/2014.
- “Reconstruction of extended sources with small supports in some elliptic equations from a single Cauchy data”, Oral Communication in IPMS, The 7th International Conference "Inverse Problems: Modeling and Simulation", Olündeniz, Fethiye, Turkey, 26-31/05/2014.

Foreword

Beauty is the first test; there is no permanent place in the world for ugly mathematics

(G.H. Hardy)

0.1. The objective and organization of the thesis

The object of this thesis is to establish effective and robust identification methods, using boundary measurements, able to reconstruct stationary and non-stationary sources describing certain physical and biomedical phenomena. In particular, these sources are taken as pointwise form sources (up to multipolar sources) and sources having compact support within a finite number of subdomains modeling epileptic foci in Electroencephalography (EEG) problems and early reporter gene activity distribution in Bioluminescence Tomography (BLT) problems.

Indeed, these two applications, along with Helmholtz equation and other motivations, can be represented by an inverse source problem over the elliptic equation

$$\nabla \cdot (\sigma \nabla u) + \mu u = F \qquad in\ \Omega \subset \mathbb{R}^n, \quad n = 2, 3 \tag{0.1}$$

where μ is taken as a fixed constant in $\mathbb{R}$ that changes sign based on the underlying physical problem, σ is the diffusion/conductivity coefficient and F is the source term that we are looking for.

Moreover, in this thesis, we also consider the parabolic case which, in addition to the previous stated applications, is motivated by the problem of the identification of pollution sources in a contaminant. The goal is to recover, from a single Cauchy data pair, a non-stationary pointwise source $F := F(x, t)$ in the diffusion equation

$$\frac{1}{c}\frac{\partial u}{\partial t} - \nabla \cdot (\sigma \nabla u) + \mu u = F \qquad in\ \Omega \times [0, T], \quad T > 0. \tag{0.2}$$

This manuscript is organized in the following way.

Chapter 1 presents the different biomedical and physical motivations behind the inverse source problems we are interested in. Moreover, a wide concentration is given for the Bioluminescence Tomography study due to its recent developments and advantages. Later, the mathematical modeling represented by the Boltzamnn equation is introduced and the needed approximations are briefly stated arriving to the desired diffusion equation. Finally, the different system of equations considered in this thesis are presented.

Chapter 2 treats the three-dimensional case of the stationary equation (0.1) considering multipolar sources and sources with small support. In this chapter, after proving the uniqueness in the case of a combination of monopolar and dipolar sources and presenting the corresponding stability estimates, a direct and non-iterative algebraic method is proposed to recover this type of sources. Then, this method is generalized to the case of multipoles. Later, we study the case of sources having compact support within a finite number of subdomains. Finally, we present and interpret numerical simulations related to our proposed reconstruction method to prove its robustness and to show the effect of the different parameters that have an impact on the identification process.

Chapter 3 deals with the two-dimensional stationary equation (0.1). Using a single wave number, although a very simple extension is available to multipolar sources, we develop our study over monopolar sources and sources having small compact support. The method proposed to solve this 2D inverse source problem is based on a proper passage to a 3-dimensional one importing, therefore, specific changes on the source term. Then, to recover this transformed source, we apply an algebraic method similar to that proposed in the previous chapter. Later, we consider the possibility of having multiple frequencies. In such a case, a simpler algebraic method is shown applied on equation (0.1) itself with the same type of sources. Finally, numerical results are presented and interpreted using multiple frequencies to prove the effectiveness of this reconstruction method.

Chapter 4 aims to resolve an inverse source problem over the parabolic equation (0.2) in a three-dimensional space. After simplifying the equation under study, the goal of this chapter is to recover monopolar sources having a fixed location but with time-variable intensities. A direct algebraic method is proposed to reconstruct the number and the positions of these monopoles and quantities related to the intensities are recovered. Then, a Kohn-Vogelius optimization method is presented in order to identify these intensities. An adjoint state method along with a BFGS- gradient conjugate algorithm with Morozov's stop criterion are proposed to accomplish this latter identification. Finally, some numerical results are shown to prove the robustness of this quasi-algebraic method.

CHAPTER 1

General Introduction

It is the perennial youthfulness of mathematics itself which marks it off with a disconcerting immortality from the other sciences.

(Eric Temple Bell)

The object of this chapter is to present the biological, biomedical and the mathematical context of the resolution of an inverse source problem whose one of other applications appears in Bioluminescence Tomography (BLT).

Section 1.1 is intended to introduce the applications of the considered inverse problem. This section is divided into two subsections. In the first subsection Section 1.1.1, we state the physiological and medical context of the problem. We start by explaining the BLT problem and the motivation behind it especially gene therapy. Later, we explain the experiment done and the Optical Tomography technique crucial for BLT. Then, the second subsection, Section 1.1.2, presents the mathematical modeling of the problem represented by Boltzmann transfer equation which is approximated, due to the domination of the scattering phenomena over the absorption ones, by a diffusion equation.

Section 1.2 presents the different problem models to be considered in our work.

Inverse problems are in the core of many engineering and biomedical applications. Among these, inverse source problems (ISP) have attracted great attention of many researchers over recent years because of their applications to many practical domains. The inverse source problem, mentioned in our work, is based, in addition to the Helmholtz equation, on a particular framework that has several practical motivations particularly in certain non-invasive biomedical imaging techniques. More precisely, one of the important applications is the inverse electroencephalography/-magnetoencephalography (EEG/MEG) problem [Das09; Jer+02; Jer+04; MLL92]. The aim of this problem, used in the epilepsy disease treatment, is to obtain a fairly accurate localization of the epileptogenic sources using electrical and magnetic measures over the scalp. On the other hand, another recent related developing problem is the inverse source problem of the Bioluminescence Tomography (BLT). In fact, BLT, [WLJ04], consists in determining an internal bioluminescent source distribution generated by luciferase inducted by reporter genes from external optical measurements. It is an increasingly important tool for biomedical researchers that can help diagnose diseases and evaluate and monitor therapies by allowing real time tomographic localization of the disease foci. In both latter mentioned applications, these foci and their distribution are described mathematically as sources that one aims to reconstruct. In addition to that, other related applications are utilized also throughout the literature such as pollution in the environment [EBHD02; Isa98], photo- and thermo-acoustic tomography [Ana+07; SU09], optical tomography [Arr99] and discrete dislocations in materials [EBEH13].

In this chapter and for the convenience of the reader, we concentrate our study over the inverse source problem related to Bioluminescence Tomography (BLT) and we give the medical, physiological and mathematical context of this study arriving to the associated inverse problem.

1.1. Medical Context and Modelization of the BLT Study

1.1.1. Mechanism of Bioluminescent Tomography and Its Application

In molecular/cellular imaging, small animal organs and tissues are often labeled with reporter probes that generate detectable signals. Bioluminescence Tomography (BLT) is a newly and recently developed technique, first conducted by researchers at the University of Southern California, Los Angeles, USA in 2005, for molecular imaging allowing *in vivo* studies on small animals, especially living mice. It is based on the use of luciferase, an enzyme responsible for light emission. Indeed, bioluminescent probes usually use luciferase extracted from three main organisms: the North American firefly "Photinus Pyralis" (FLuc) of wavelength $\simeq 490 - 620nm$, the sea pansy "Renilla Reniformis" (RLuc) of wavelength $\simeq 480nm$, and bacterias like Photorhabdus Luminescens and Vibrio Fisheri (Figure 1.1). Then, this extracted luciferase is confined to a cell (or a gene) and afterwards introduced in the body of the animal model for later detection.

Figure 1.1.: *firefly Photinus pyralis, Sea pansy, Photorhabdus-luminescens bacteria (from left to right)*

The aim of BLT is to reconstruct, localize and quantify the 3D bioluminescent source distribution (the reporter cell activity) inside the living mouse based on external bioluminescent optical measures. In fact, the bioluminescent photons cover a red region of the spectrum (or can be red-shifted) with a good penetration depth. Hence, with an adequate exposure time, a significant number of photons can escape to reach the mouse body surface and be detected using a highly sensitive charged-coupled device (CCD) camera. Then this 2D image is superposed with the photograph of a mouse to get localization of the reporter cell activity. However, the bioluminescent imaging view is only a planar image [WLJ04] since it detects only surface light signals and cannot generate a depth location because it is incapable of tomographic reconstruction of the internal optical features inside a mouse which represent the 3D distribution of a BLT source. Thus, in BLT we need a complete knowledge on the internal optical properties of anatomical structures of the mouse established from an independent pre-scanned tomographic study, an Optical Tomography study.

BLT can be applied to study almost all diseases in every small animal model and promises to have major impacts on small animal studies towards the development of molecular medicine. Hence, it becomes an increasingly important tool for biomedical researchers due to its aid in the localization and the monitoring of the diseases. In addition to its application in gene therapy, BLT is already widely used is the investigation of cancer tumors and cancer progression [MV+12; Con+05], cardiac diseases, studying protein-protein interactions, cystic fibrosis [Tay+98], studies of infection, reconstitution kinetics [Cao+06; Wu+03] and so on.

BLT for gene therapy

The key for the development of the gene therapy is to monitor the gene transfer and evaluate its distribution in a living model. Monitoring gene expression is crucial for studying the responses of gene therapy and clarifying gene function in various environments. BLT is used to fulfill this goal. It is used to express a reporter gene with luciefrase driven by a promoter of the gene of interest into target tissue(s) to test the expression of that particular gene. The expression level of the target gene is assessed by monitoring luciferase expression which can be interpreted from the photon output.

In fact, once a gene therapy vector has been administrated, the researcher needs to know:

1. the location of the gene within the body
2. the degree of activity and the magnitude of the gene expression over time
3. the time of the activity of the transferred gene.

These information are found and analyzed using a BLT study. Thus, BLT felicitates the visualization of critical gene expression patterns in different stages of any disease and advances the understanding of a disease progression *invivo*. This method has been used to the study of DNA vaccines [Jeo+06], to monitor insulin gene expression for diabetes [Che+10], for studying human prostate cancer [Ada+02], for breast cancer [LM10], for measuring ATP released from CF and non CF-human epithelial monolayers [Tay+98], for cell trafficking [HYC11] and so many other genetic diseases.

Let us, now, explain the mechanism of this method. In fact, following its imaging experiment, one needs both the anatomy of the used model and an indispensable Optical Tomography study to complete the 3D BLT technique.

The Bioluminescence Imaging (BLI) Experiment: bioluminescent data acquisition

BLI systems, Figure 1.2, have been built and used by many research groups in USA and China.

1. • Several days before the experiment, luciferase probes, which are biological

entities (cells,genes,...) tagged with luciferase enzyme, are implanted into the mouse.

2.
   - At the beginning of the BLT experiment, luciferase substrate, luciferin, is injected into the mouse.
   - A biochemical reaction of luciferase with oxygen and adenosine triphosphate (ATP) generates bioluminescent photons in the biological tissues. These photons of light contain significant red components and are with a wavelength of about 600nm.
   - A significant number of bioluminescent photons escape from their attenuating environment to reach the mouse body surface.
3.
   - A highly sensitive (high quantum efficiency)charge-coupled device CCD camera is used to collect the emitted light knowing that it detects even very low levels of visible light. Note that the camera is usually super cooled to less than $-80°C$ to reduce thermal noise.
   - The mouse is placed at the suitable distance (well adjusted and measured) from the lens and marks are placed on the mouse's skin for registration.
   - A holder maintains the mouse in a vertical position while a stage rotates vertically using computer control.
   - Note that, this experiment is performed in a total dark environment. To do so, all the objects specified in the steps above are placed in a light-tight enclosure chamber that just has a small entry to accommodate the wires. The chamber has a removable part to help manipulate the mouse.
   - Two images are obtained in each orientation one of the mouse body surface and another of the corresponding bioluminescent view.
   - The $2D$ bioluminescent image is superposed over the photograph of the mouse.
4.
   - Finally, the bioluminescent photon rate can be detected on the body surface of the mouse. The external (observable) optical data are calculated from pixel values in the bioluminescent images taken by the CCD camera.

Remark 1. *This system can be enhanced to a multiview system with multispectral data [Wan+06b]. Such a system employs several mirrors and a special mouse holder to provide much more information. Its advantage is that it gives the same results but costs less in time and gives the capability of using more than one bioluminescent probe.*

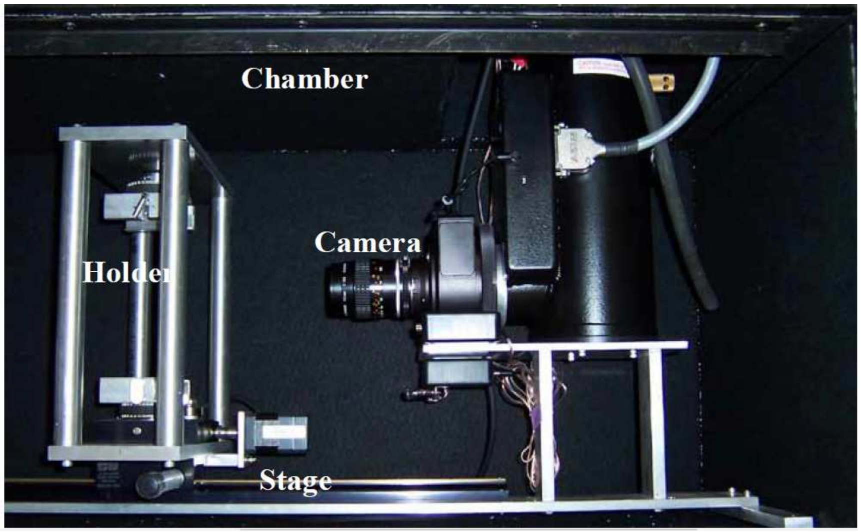

Figure 1.2.: BLT experiment [Wan+06a]

Anatomical structure of the mouse

The anatomic structure information of the small animal can be imaged by X-ray Computed Tomography and Magnetic Resonance Imaging techniques. The geometric shapes of the major organ regions are established by 3D computer graphic techniques. The anatomical structure of the small animal is then segmented into its major components (heart, liver, lungs, stomach, bones, ...) and then a convenient mesh is used to mesh the whole mouse domain or a certain organ of interest. As seen in Figure 1.3, in [Wan+06a], the authors established mouse geometric model with 80670 tetrahedral and 14757 nodes using Amira 4.0 program.

Optical Tomography

The larger the variation of the optical properties, the poorer the BLT reconstruction quality one obtains. This reflects the critical importance to estimate *in vivo* optical properties as accurately as possible. Indeed, every organ region is associated with its tissue optical parameters, its scattering and absorption coefficients, as seen, for instance, in Table 1.1 for the mouse organs. These parameters can be determined using optical tomographic approaches. Optical Tomography uses incoming visible or near infrared light to probe a scattering object and reconstructs the distribution of internal optical properties such as one or both of scattering and absorption coefficients. Note that the BLT problem is fundamentally different from the so-called diffuse opti-

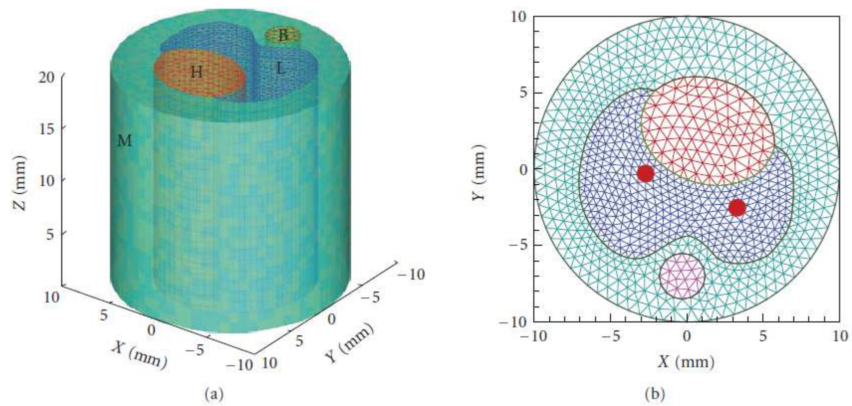

Figure 1.3.: *mouse meshing [Wan+06b]*

Organ	Muscle	Lung	Heart	Liver	Kidney	Stomach
μ_a $[mm^{-1}]$	0.23	0.35	0.11	0.45	0.12	0.21
$\mu_s^{'}$ $[mm^{-1}]$	1.00	2.30	1.10	2.00	1.20	1.70

Table 1.1.: *Optical parameters for the mouse organ regions*

cal tomography. Using the diffusion approximation, the optical tomography problem is to find optical properties of an object from diffuse signals generated by a controllable optical simulation and measured on the external surface of the object. In other words, in the BLT problem, the source is unknown while in the optical tomography problem, the optical properties are to be determined.

Several units and data

Several data:

- Bioluminescence data acquisition takes from 5 to 10 minutes for one exposure if the source is deep inside the mouse.
- Bioluminescence signal decays over about 1 hour.
- In most cases, we prefer 4 image-views of the mouse (front, back, two sides).

Several units:

- the photon fluency rate/density : $Watts/mm^2$
- the bioluminescence source distribution density : $Watts/mm^3$
- absorption and scattering coefficients: mm^{-1}

1.1.2. Mathematical modeling of the problem

a. Boltzmann Equation

The basic equation governing the light migration in a random medium Ω is the radiative transfer equation (RTE), also known as Boltzmann equation, and is given by,

$$\boxed{\begin{array}{c}\left(\frac{1}{c}\frac{\partial}{\partial t} - \hat{s}\cdot\nabla_{\mathbf{x}} + \mu(\mathbf{x})\right) u(\mathbf{x},\hat{s},t) = \mu_s(\mathbf{x}) \int\limits_{\mathcal{S}^2} \Theta(\hat{s}\cdot\hat{s}')\, u(\mathbf{x},\hat{s}',t)\;\, d\hat{s}' + q(\mathbf{x},\hat{s},t) \\ \text{for} \quad t>0, \mathbf{x}\in\Omega\end{array}} \tag{1.1}$$

where $u(\mathbf{x},\hat{s},t)$ is the light flux in the direction $\hat{s}\in\mathcal{S}^2$, $\mathcal{S}^2$ being the unit sphere. Moreover, c denotes the particle speed, $\mu=\mu_a+\mu_s$ with μ_a and μ_s being the absorption and scattering coefficients respectively, the scattering kernel $\Theta(\hat{s},\hat{s}')$ is the normalized phase function $(\int\limits_{\mathcal{S}^2}\Theta(\hat{s}\cdot\hat{s}')d\hat{s}'=1)$ and $q(\mathbf{x},\hat{s},t)$ is the internal source.

The boundary and the initial conditions are defined by:

$$\left\{\begin{array}{lcllll} u(\mathbf{x},\hat{s},t) & = & g^{-}(\mathbf{x},\hat{s},t) & \text{for} \quad t>0, & \mathbf{x}\in\Gamma, \quad \hat{s}\in\mathcal{S}^2, & (\nu(\mathbf{x})\cdot\hat{s}\leq 0) \\ u(\mathbf{x},\hat{s},0) & = & 0 & \text{for} \quad \mathbf{x}\in\Omega, & \hat{s}\in\mathcal{S}^2 & \end{array}\right. \tag{1.2}$$

where g^- represents the incoming flux and ν denotes the exterior normal at $\mathbf{x}$ on Γ, the medium's boundary. In a typical BLT, g^- is identically null since the BLT experiment is performed in a totally dark environment and no external photon travels into Ω through its boundary Γ.

Given the internal source q and the incoming flux g^-, the forward problem consists in solving (1.1-1.2) in order to calculate the outgoing radiation denoted by $\overline{g}$ and defined as, [Arr99; NW01],

$$\overline{g}(\mathbf{x},\hat{s},t) = \int_{\mathcal{S}^2} \nu(\mathbf{x})\cdot\hat{s}u(\mathbf{x},\hat{s},t)\,d\hat{s} \qquad \text{for} \quad t>0, \quad \mathbf{x}\in\Gamma. \tag{1.3}$$

Based upon the model's geometry and its optical properties, the BLT study comes back to an inverse source problem whose goal is to reconstruct the internal light source q from the given data g^- and the measurement of the outgoing radiation $\overline{g}$.

b. Diffusion Approximation

Solving BLT problem using RTE equation (1.1,1.2,1.3) is quite complex. Therefore, it is commonly accepted to replace it by a diffusion approximation in a medium where the light propagation is highly scattering and low absorptive. Indeed, since the mean-free path of the particle of our subject study is between 0.005 and 0.01 mm in biological tissues, scattering phenomena dominates absorption ones. This enables us to utilize a diffusion approximation. For more details concerning the diffusion approximation, we refer the reader to the work of [Arr99] and the references within.

In fact, let u and F be the average photon flux and the source in all directions defined respectively as

$$u(\mathbf{x},t) = \frac{1}{4\pi}\int_{\mathcal{S}^2} u(\mathbf{x},\hat{s},t)\,d\hat{s}$$

and

$$F(\mathbf{x},t) = \frac{1}{4\pi}\int_{\mathcal{S}^2} q(\mathbf{x},\hat{s},t)\,d\hat{s}.$$

Then, the diffusion equation is given by

$$\boxed{\begin{cases} \left(\frac{1}{c}\frac{\partial}{\partial t} - \nabla\cdot\sigma(\mathbf{x})\nabla + \mu_a(\mathbf{x})\right)u(\mathbf{x},t) &= F(\mathbf{x},t) \quad \text{for} \quad t>0, \mathbf{x}\in\Omega \\ u(\mathbf{x},t) + 2\sigma(\mathbf{x})\frac{\partial u}{\partial \nu}(\mathbf{x},t) &= g^{-}(\mathbf{x},t) \quad \text{for} \quad t>0, \mathbf{x}\in\Gamma \\ u(\mathbf{x},0) &= 0 \quad \text{for} \quad \mathbf{x}\in\Omega \end{cases}} \tag{1.4}$$

where

$$\sigma = \frac{1}{3(\mu_a + \mu_s^{'})}$$

with $\mu_s^{'}$ being the effective scattering coefficient.

Hence, the forward problem becomes the problem: having as given σ, μ_a, F and the boundary condition g^{-}, our aim is to determine the external optical measures (1.3), which using this approximation becomes

$$\boxed{\overline{g}(\mathbf{x},t) = -\sigma(\mathbf{x})\frac{\partial u}{\partial \nu}(\mathbf{x},t) \qquad t>0, \quad \mathbf{x}\in\Gamma.} \tag{1.5}$$

Inversely, the goal of the BLT problem is to reconstruct the internal bioluminescent source F given σ, μ_a, the observation of the Robin boundary condition g^{-} and the measurement of the flux $\overline{g}$ on the boundary Γ.

c. Stationary case

Since the internal bioluminescence distribution induced by the reporter genes is relatively stable, one can start by considering the stationary version of (1.4) as a model for the BLT problem. Therefore, the BLT elliptic equation is represented as

$$\begin{cases} -\nabla \cdot (\sigma(\mathbf{x})\nabla u(\mathbf{x})) + \mu_a u(\mathbf{x}) = F(\mathbf{x}) & \text{for} \quad \mathbf{x} \in \Omega \\ \\ u(\mathbf{x}) + 2\sigma(\mathbf{x})\frac{\partial u}{\partial \nu}(\mathbf{x}) = g^-(\mathbf{x}) & \text{for} \quad \mathbf{x} \in \Gamma, \end{cases} \tag{1.6}$$

where the current of the photons, measured on the body surface, is defined as:

$$g(\mathbf{x}) = \sigma(\mathbf{x})\frac{\partial u}{\partial \nu}(\mathbf{x}) \qquad \mathbf{x} \in \Gamma. \tag{1.7}$$

Due to the existence of the measurement g and assuming the existence of the source F, the boundary condition and the measurement can be added to get

$$u(\mathbf{x}) = g^-(\mathbf{x}) - 2g(\mathbf{x}) := f \qquad \mathbf{x} \in \Gamma.$$

Remark 2. *Normally, as mentioned before, in a typical BLT problem, one considers the boundary condition g^- to be identically null. However, here, in the stationary system (1.6), we will consider the general case having $g^- \neq 0$ which can be used, for example, in the case of studying 2 mice simultaneously. Moreover, in here, for simplicity, we don't take into account the mismatch between the refractive indices n for Ω and n' for the surrounding (for air $n' = 1$). However, if one wants to do so, the boundary condition considered would be*

$$g^-(\boldsymbol{x}) = u(\boldsymbol{x}) + 2\mathcal{A}(\boldsymbol{x}; n, n')\sigma(\boldsymbol{x})\frac{\partial u}{\partial \nu}(\boldsymbol{x})$$

with

$$\mathcal{A}(\boldsymbol{x}; n, n') = \frac{1 + R(\boldsymbol{x})}{1 - R(\boldsymbol{x})}$$

where the approximated value of R, [Sch+95], is $R = -1.4399\,n^{-2} + 0.7099\,n^{-1} + 0.6681 + 0.0636\,n$.

Remark 3. *To reconstruct the optical properties σ and μ_a, a traditional optical tomography is used, for a pre-BLT study, which utilizes a visible or near infrared light to establish the reconstruction of the internal optical properties. This pre-scanned study supposes* *that no source is present in the medium under study. The solution of this tomographic study is represented by determination of σ and μ_a in the over-determined problem*

$$\begin{cases} -\nabla.(\sigma\nabla u) + \mu_a u = 0 & \textit{in} \quad \Omega \\ u = f & \textit{on} \quad \Gamma \\ \sigma\frac{\partial u}{\partial \nu} = g & \textit{on} \quad \Gamma. \end{cases} \tag{1.8}$$

1.2. Problems considered in this thesis

The inverse source problems considered in this thesis are:

1. The stationary inverse source problem whose aim is to determine a source F in the elliptic equation

$$\Delta u + \mu u = F \qquad \text{in} \qquad \Omega \tag{1.9}$$

   from a single Cauchy data

$$(f, g) := (u_{|\Gamma}, \frac{\partial u}{\partial \nu}_{|\Gamma})$$

   prescribed on the boundary Γ of an open bounded domain Ω in $\mathbb{R}^3$.

2. The inverse source problem in the Helmholtz equation whose aim is to determine a source F in

$$\Delta u + \kappa^2 u = F \qquad \text{in} \qquad \Omega \tag{1.10}$$

   where Ω is an open bounded domain in $\mathbb{R}^2$, first, from a single Cauchy data at a fixed wave number κ and then in a multi-frequencial case.

3. The non-stationary inverse source problem whose aim is to determine a time-dependant source F in the parabolic equation

$$\frac{1}{c}\frac{\partial u}{\partial t} - \sigma\Delta u + \mu u = F \qquad \text{in} \qquad \Omega \times (0, T) \tag{1.11}$$

   where T is a positive real constant, from a single Cauchy data

$$(f, g) := (u_{|\Sigma_T}, \frac{\partial u}{\partial \nu}_{|\Sigma_T})$$

   prescribed on the boundary Σ_T.

The main type of sources considered here, whose motivation is clarified later, are pointwise multipolar sources and sources of compact support within a finite number of subdomains.

CHAPTER 2

3D Stationary Inverse Source Problem

If I were again beginning my studies, I would follow the advice of Plato and start with mathematics.

(Galileo Galilei)

The object of this chapter is to study the inverse source problem related to (1.9) in a three-dimensional space mainly in the case of stationary multipolar sources and sources with small supports where we discuss the uniqueness and the stability issues and propose a suitable identification method.

Section 2.1 is intended to introduce the main three-dimensional problem then states the inverse problem we are interested in. Later, we present the different principal source identification techniques existing in the literature. Finally, we specify the main type of sources considered in our study.

Section 2.2 is divided into two subsections where the first presents, for the particular case of monopoles and dipoles, the uniqueness issue for sources and illustrates the stability estimates already established in [EBEH12] then discusses an algebraic identification algorithm employed to reconstruct a combination of monopolar and dipolar sources. The second subsection generalizes the algebraic identification algorithm for multipolar sources.

Section 2.3 introduces the uniqueness issue and the use of the algebraic algorithm on sources with small supports and states a remark on using this algorithm on general poles of meromorphic functions.

Section 2.4 is consecrated to introduce the numerical framework used.

Section 2.5 shows the numerical results for the reconstruction of dipoles, a combination of monopoles and dipoles and sources having small compact support. Other effects as the number of sensors, the number of sources, the separability between the sources, the coefficient μ and the noise effect are also studied and analyzed numerically.

Section 2.6 presents the same numerical experiments performed in the previous subsection in the case of BLT and compares between this case and the Helmholtz numerical results.

2.1. Introduction and statement of the problem

In this chapter, we consider an inverse source problem whose aim is to reconstruct a source F in the elliptic equation

$$\Delta u + \mu u \quad = \quad F \quad \text{in} \quad \Omega, \tag{2.1}$$

from a single Cauchy data $(f, g) := (u_{|\Gamma}, \frac{\partial u}{\partial \nu}_{|\Gamma})$ prescribed on a sufficiently regular boundary Γ of an open bounded volume $\Omega \subset \mathbb{R}^3$. Here, μ is a fixed real number assumed to be known and ν denotes the outward unit normal to Γ.

To be more precise, if one defines, for all F, the following application in $H^{\frac{1}{2}}(\Gamma) \times H^{-\frac{1}{2}}(\Gamma)$

$$\Lambda : F \to (u_{|\Gamma}, \frac{\partial u}{\partial \nu}_{|\Gamma}),$$

then our inverse problem is formulated as follows:

$$\text{Given} \quad (f, g) \in H^{\frac{1}{2}}(\Gamma) \times H^{-\frac{1}{2}}(\Gamma), \quad \text{determine } F \text{ such that} \quad \Lambda(F) = (f, g). \tag{2.2}$$

Physically, a boundary condition in direct problem is imposed and sensors on Γ permit to measure the other quantity related to u so that the Cauchy data $f = u_{|\Gamma}$ and $g = \frac{\partial u}{\partial \nu}_{|\Gamma}$ are obtained.

Note that the choice of the space $H^{\frac{1}{2}}(\Gamma) \times H^{-\frac{1}{2}}(\Gamma)$ will be justified later by the nature of the sources considered.

Three questions are important in the resolution of an inverse problem for recovering the source F:

1. *Identifiability*: Does the Cauchy pair (f, g) uniquely determine F? (i.e. the injectivity of Λ)
2. *Stability*: What is the behavior of source term F with respect to the perturbation on the Cauchy data denoted by $(\epsilon f, \epsilon g)$?
3. *Reconstruction method*: What are the reconstruction algorithms that could be employed for determining F?

It is rather interesting to note that several applications are related to this particular inverse source problem. While the Bioluminescence Tomography [WLJ04] corresponds to the case with μ negative, that of Helmholtz equation in an interior domain corresponds to taking μ positive, [EBN11a], and EEG/MEG problems [Jer+02; Jer+04;

MLL92] are also possible applications for the inverse source problem that we consider here for μ identically null (Poisson equation) but they are not the only applications.

These inverse source problems have interested many to work on due to their wide applications. Since there is a vast literature treating this type of problems, we will just mention the work of few in this domain. In the three-dimensional space, the general case where sources $F \in L^2(\Omega)$ was used in [HCW06; Con+05]. Pointwise source were considered by many authors as in [Bar+99; AK04; EBHD00a; EB05; EBF10; EBN11a; CC09; CKC12; Nar08; Nar12], with different values of μ, using different approaches to recover the sources. One can also mention the work of Ikehata in [Ike99] where the author has considered Helmholtz problem in a two-dimensional space with F is either of the form $\chi_B \rho(x)$ where B is an open subset of Ω , χ_B is the characteristic function of B, or of the form $div[\rho(x)\chi_B(x)a]$, where a is a nonzero constant vector. Under additional conditions the convex hull of B was reconstructed iteratively using the Cauchy data. Related to our problem, let us mention the interesting and relevant paper [KR13] on the reconstruction of extended sources for the 2D Helmholtz equation. See also references therein, notably [HR11]. Moreover, in the case of the exterior Helmholtz problem, the paper [AKS09] treats, proposing an iterative scheme, the reconstruction of monopolar sources having a known source number.

2.1.1. Different Identification Techniques

To solve inverse source problems from boundary measurements, many theoretical and numerical identification techniques were and can be employed for the process of the identification of sources. For special defined source structures, there are sometimes identification methods that are specially used in their cases. As the assumed structure becomes less and less defined, the identification method needs to be more and more general.

Method of meromorphic approximations

This method is used in order to reconstruct pointwise and small sized distributed sources. The concept was first developed by Baratchart *et al*, in [Bar+99], to express conductivity inhomogeneities in Electrical Impedance Tomography (EIT) problems and then used for the purpose of source reconstruction in [AK04; Han08]. It was, then, applied for the reconstruction of monopole and dipole sources in [Bar+05] over

2D Poisson equation (case with $\mu = 0$) then extended over 3D domains in [BLM+06]. It is based on the existence of a meromorphic function f in a ball surrounding the point sources and on the analyticity of the solution u of the considered differential equation over the domain except on the point sources. The inverse source problem is by then transformed into the problem of finding the singularities of the meromorphic function f and thus finding the desired sources. A remark on this approach applied on our case of study is shown throughout this chapter.

Optimization methods

In the general case where the source $F \in L^2(\Omega)$, optimization methods could be employed to recover the desired source term. These methods seek basically to minimize the error between the observable data and the solution of the forward problem for obtaining the source parameters. The most known optimization approach is the Least Square Method whose objective is to minimize the quadratic error between the optimal measures and those calculated using the direct problem. This iterative approach was used in [HCW06; Con+05] employing techniques based on the finite element resolution of the forward problem and on a permissible source region. Moreover, the recent concept used initially by R. Kohn and M. Vogelius [KV85] can be employed to reconstruct the needed source term. This approach seeks basically on minimizing the energetic gap between the forward problem with Neumannn boundary condition and that with Dirichlet boundary condition. This iterative method was used, for example, in [EBF10], in order to recover the parameters of dipoles in the Poisson equation ($\mu = 0$).

Algebraic methods

These methods, which have been developed over recent years, consist in transforming the inverse source problem into an infinity of algebraic relationships between the source parameters and the observable data, obtained from Green's formula. Compared to iterative algorithms for inverse problems, the algebraic method has an advantage that it requires neither the initial solution nor the iterative computation of the forward problem. From the practical viewpoint, the solution obtained by an algebraic method can be used as an initial solution to the iterative algorithm, which is quite important to prevent it from converging to local minima.

The algebraic method was originally developed by El Badia and H.Doung, [EBHD00a], on monopolar or dipolar sources in the case of 2D and 3D Poisson equation because of their interest in the inverse EEG/MEG problem. Their method consists in decomposing a Hankel-type matrix H into ADA^t, where A is a Vandermonde matrix and D is a diagonal matrix. Then, the number of projected point sources onto a complex-plane are given by the rank of the Hankel matrix H built up from the Dirichlet and the Neumann data and the projected point sources are the eigenvalues of a companion matrix. The latter work was revisited in [Nar08] considering a combination of dipoles and quadrupoles and [CC09] with a combination of monopoles and dipoles and recently in [CKC12; Nar12] considering sources of general order poles always on the Poisson equation. The proposed algorithms in the previous papers are based on the invertibility of a Hankel-type matrix H, using the calculation of its determinant. It is rather important to say that the calculation is very long and tedious. Finally, the approach adopted in [EB05; EBHD00a] was then extended by El Badia end Nara, [EBN11a], for Helmholtz equation ($\mu > 0$) but only in the case of monopoles.

2.1.2. Form of the sources

One of difficulties of the inverse source problem from boundary measurements concerns the non-uniqueness of the source, for example, because of the possible existence of non-radiating sources, see e.g. [BC77; DW73]. Thus, in the general case, a source F cannot be identified from boundary measurements.

Although identification in the L^2 sense can be obtained if the boundary data with multiple coefficients μ (all of the coefficients on some open set) are given, as it was shown in [AMR09], with a single μ, one can expect a well-posed inverse source problem only if *a priori* information is available. Usually this information takes the form of certain conditions on admissible sources depending on the underlying physical problem. When no *a priori* information is available, which is generally the case for distributed sources that belongs, for example, to $L^2(\Omega)$, one seeks a special solution F_H of the minimal L^2 norm among all the solutions F.

And then every solution would be, as shown in [EBD98] for the Laplace equation and in [WLJ04] for our studied equation, of the form

$$F = F_H + L[m] \qquad \forall m \in H_0^2(\Omega)$$

where L is, in here, the operator: $\Delta + \mu$.

In the present chapter, two types of sources F will be considered . The first type is a source of multipolar pointwise form

$$F = \sum_{\ell=1}^{L} \sum_{j=1}^{N^\ell} \sum_{\alpha=0}^{K^\ell} \lambda_{j,\ell}^{\{\alpha_1,\alpha_2,\alpha_3\}} \frac{\partial^\alpha}{\partial_x^{\alpha_1} \partial_y^{\alpha_2} \partial_z^{\alpha_3}} \delta_{\mathbf{S}_j^\ell} \tag{2.3}$$

where $\delta_{\mathbf{S}}$ stands for the Dirac distribution at the point $\mathbf{S}$, the quantities L, N^ℓ, K^ℓ are integers, the coefficients $\lambda_{j,\ell}^{\{\alpha_1,\alpha_2,\alpha_3\}}$ are scalar non-null quantities and $\alpha = \alpha_1+\alpha_2+\alpha_3$ with $(\alpha_1, \alpha_2, \alpha_3) \in \mathbb{N}^3$. The points $\mathbf{S}_j^\ell = (x_j^\ell, y_j^\ell, z_j^\ell) \in \Omega$ and the orders of derivation K^ℓ are, respectively, assumed to be mutually distinct . The second type is a source having compact support within a finite number of subdomains, namely

$$F = \sum_{j=1}^{N} h_j \chi_{D_j} \quad \text{with} \quad D_j = \mathbf{S}_j + \varepsilon B_j \tag{2.4}$$

where, as seen in Figure 2.1, $B_j \subset \mathbb{R}^3$ is a bounded domain containing the origin, the densities h_j are non-null functions belonging to the space $L^1(\Omega)$, the points $\mathbf{S}_j = (x_j, y_j, z_j) \in \Omega$ and ε is a positive real number less than or equal to 1.

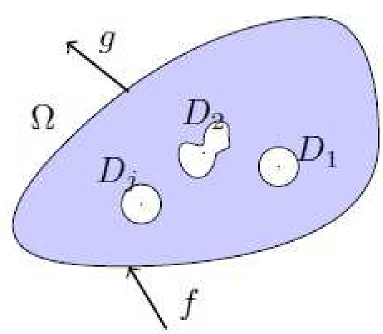

Figure 2.1.: *Inverse source problem concept*

As we have mentioned, compared to optimization iterative methods, the algebraic method has an advantage that it doesn't require the initial solution and the iterative computation of the froward problem. Moreover, the approach developed in [CC09; CKC12; Nar08; Nar12] can not be extended to the inverse problem that we consider in this paper when $\mu \neq 0$. Therefore, we propose, following the approach adopted in [EB05; EBHD00a; EBN11a], a simple and elegant proof of the invertibility of a Hankel matrix H built up from the Cauchy data (f, g) by establishing its decomposition into ATA^t, where T is a symmetrical tridiagonal matrix (see (2.21) and (2.34)). In this sense, our work generalizes and extends previous works on this subject. The main objective of this chapter is to establish such relationships and provide an algebraic algorithm allowing us to solve them and consequently identify the source F when given by (2.3) or (2.4).

2.2. Multipolar Sources

This section focuses on the inverse problem (2.2) when the source F is of the form (2.3). Before studying the reconstruction of these sources, two main issues are essential : their uniqueness and their stability. The uniqueness, in the case of monopolar and dipolar sources, which corresponds to the framework studied in Subsection 2.2.1, is valid. However, in the general case, where the order of derivation $K^\ell \geq 2$, the uniqueness is not valid as shown in Subsection 2.2.2.

Therefore, for an easy reading of our identification algorithm and also for the identifiability reason, it is reasonable to study these two cases separately and so, we divide this section into two subsections. First, in Subsection 2.2.1, we consider the particular case where the source F is a finite linear combination of monopolar and dipolar sources ($K^\ell = 0, 1$), namely

$$F = \sum_{j=1}^{N^1} p_j \delta_{\mathbf{S}_j^1} + \sum_{j=1}^{N^2} q_j \delta_{\mathbf{S}_j^2} + \sum_{j=1}^{N^2} \mathbf{r}_j . \nabla \delta_{\mathbf{S}_j^2}, \quad \mathbf{S}_j^1,\ \mathbf{S}_j^2 \in \Omega, \tag{2.5}$$

where p_j, q_j and $\mathbf{r}_j$ are, respectively, non-null scalar and vector quantities and $\mathbf{S}_j^1$ and $\mathbf{S}_j^2$ are mutually distinct. Then, in Subsection 2.2.2, we consider the general case of multipolar sources (2.3).

2.2.1. Monopolar and dipolar sources

In this subsection, we assume that the source F is a finite linear combination of monopolar and dipolar point sources given by (2.5). This represents a particular case of sources F satisfying (2.3) corresponding to $L = 2$, $K^1 = 0$ and $K^2 = 1$. Thus, our goal is to identify the numbers N^1, N^2, the locations $\mathbf{S}_j^1$, $\mathbf{S}_j^2$, the intensities p_j, q_j and the moments $\mathbf{r}_j$ algebraically from the Cauchy data (f, g). Here, N^1 and N^2 are, respectively, the number of monopolar and dipolar sources.

1. Uniqueness

A source F satisfying (2.5), which is a combination of monopoles and dipoles, can be uniquely determined using a single Cauchy data as shown in the following theorem.

Theorem 1. *Let F^ℓ, $\ell = 1, 2$ be two sources of the form (2.5) and let u_ℓ be the corresponding solutions of (2.1) such that $(f^1, g^1) = (f^2, g^2)$. Then,*

$$N^{1,1} = N^{1,2} = N^1, \qquad N^{2,1} = N^{2,2} = N^2$$

and there exists a permutation π^1 of the integers $1, ..., N^1$ and a permutation π^2 of the integers $1, ..., N^2$ such that

$$\boldsymbol{S}_j^{1,1} = \boldsymbol{S}_{\pi^1(j)}^{1,2}, \qquad \boldsymbol{S}_k^{2,1} = \boldsymbol{S}_{\pi^2(k)}^{2,2}, \qquad j = 1, ..., N^1, k = 1, ..., N^2$$

$$p_j^1 = p_{\pi^1}^2(j), \qquad q_k^1 = q_{\pi^2(k)}^2, \qquad \boldsymbol{r}_k^1 = \boldsymbol{r}_{\pi^2(k)}^2, \quad j = 1, ..., N^1, k = 1, ..., N^2.$$

* * *

Proof: Consider $w = u_2 - u_1$. Then, w is the solution of the problem

$$\begin{cases} \Delta w + \mu w = F^2 - F^1 & \text{in} \quad \Omega \\ w = 0 & \text{on} \quad \Gamma \\ \frac{\partial w}{\partial \nu} = 0 & \text{on} \quad \Gamma. \end{cases}$$

Thus, using Holmgrem's theorem, one gets

$$w = 0 \qquad \text{in} \quad \Omega \setminus \bigcup_{j,\ell} \{S_j^{1,\ell}, S_j^{2,\ell}\}.$$

Therefore, from the structure theorem [Sch43], w is a finite linear combination of the dirac mass and its derivative at points $S_j^{1,\ell}$ and $S_j^{2,\ell}$. Furthermore, since $F^i \in H^{-s}, s > \frac{5}{2}$, we have $w \in H^{-\epsilon}, \epsilon > \frac{1}{2}$. Then, w is identically null over Ω. Therefore, we have $F^1 = F^2$.

Let us begin by proving the uniqueness of the monopole parameters and that with dipoles is done analogously. Indeed, suppose that $N^{1,1} \neq N^{2,1}$, for example, $N^{1,1} >$

$N^{2,1}$. Then, there exists $r \in \{1, \cdots, N^{1,1}\}$ such that

$$\mathbf{S}_r^{1,1} \neq \mathbf{S}_j^{1,2} \qquad \text{for all } j = 1, \cdots, N^{1,2}.$$

Moreover, one has

$$\mathbf{S}_r^{1,1} \neq \mathbf{S}_j^{1,1}, \qquad j = 1, \cdots, N^{1,1}, j \neq r.$$

Therefore, there exists a neighborhood of $\mathbf{S}_r^{1,1}$, $V(\mathbf{S}_r^{1,1})$, that doesn't contain any point of the set $\bigcup\limits_{j,\ell,j\neq r} \{S_j^{1,\ell}, S_j^{2,\ell}\}$. Now, consider a positive continuous test function φ having a compact support in $V(\mathbf{S}_r^{1,1})$. Then, as $F_1 = F_2$, one has

$$< F_1, \varphi > = < F_2, \varphi > .$$

This leads to

$$p_r^1 = 0$$

which contradicts the fact that the intensities are not null and therefore $N^{1,1} = N^{1,2} = N^1$. Then, the same idea is used to obtain the uniqueness of the locations and the intensities of the sources. $\square$

2. Stability

Formerly, the stability issue has been considered with the general form. We mention that in [BLT11], the authors have studied the stability using a general form source but with a variable frequency μ in the Helmholtz case (not fixed as supposed in here) . For our case, the stability has been thoroughly studied in [EBEH12]. They distinguished in their study between the case of the monopoles and that of dipoles. In here, we will just present the theorems on the sources locations stability, that will then be verified numerically in Section 2.4, without their proves consulting the interested readers to refer to the corresponding article [EBEH12] for more details.

Theorem 2. *[EBEH12] (for monopoles ($L = 1$, $K^1 = 0$) locations)*
If u^ℓ, $\ell = 1, 2$ is the solution of (2.1) corresponding to two sources characterized by the configuration $(N^1, \lambda_j, \mathbf{S}_j^{1,\ell})$, then there exist three constants c, c_1, c_2 and a permutation

π of the integers $1, ..., N^1$ such that

$$\max_{1\le j\le N^1} ||\boldsymbol{S}_j^{1,2} - \boldsymbol{S}_{\pi(j)}^{1,1}|| \le 2c\frac{\beta^2}{\varrho}\left[\frac{\sqrt{|\Gamma|}}{c_1}\frac{\varrho}{\beta}\left[||g^2-g^1||_{L^2(\Gamma)} + c_2||f^2-f^1||_{L^2(\Gamma)}\right]\right]^{\frac{1}{N^1}} \tag{2.6}$$

where $(f^\ell, g^\ell) = (u^\ell_{|\Gamma}, \frac{\partial u^\ell}{\partial \nu}_{|\Gamma})$, $\sqrt{|\Gamma|} = \int_\Gamma ds$, β is the distance of the sources from the boundary and ϱ is the separability coefficient between the sources defined consecutively by:

$$\beta = diam(\Omega) - \alpha, \quad \textit{where} \quad \alpha = \min_{1\le j\le N^1} d(\Gamma, \boldsymbol{S}_j)$$

and

$$\varrho = \min(\varrho_1, \varrho_2), \quad \textit{where} \quad \varrho_1 = \min_{1\le j,n\le N^1, j\ne n} ||P_j - P_n|| \quad \textit{and} \quad \varrho_2 = \min_{1\le j,n\le N^1, j\ne n} ||Q_j - Q_n||$$

with P_j and Q_j are respectively the xy and yz projections of $\boldsymbol{S}_j^1$. The constant c depends on μ and c_1 and c_2 can be written explicitly as

$$c_1 = \min_{1\le j\le N^1} |\lambda_j|$$

and

$$c_2 = \sqrt{2\frac{(2N^1-1)^2}{\beta^2} + \kappa^2}.$$

* * *

Theorem 3. *[EBEH12] (for dipoles ($L = 1$, $K^1 = 1$) locations)*
If u^ℓ, $\ell = 1, 2$, is the solution of (2.1) corresponding to two sources characterized by the configuration $(N^2, \boldsymbol{q}_j, \boldsymbol{S}_j^{2,\ell})$, then there exists three constants $\tilde{c}$, c_3, c_4 and a permutation π of the integers $1, ..., N^2$ such that

$$\max_{1\le j\le N^2} ||\boldsymbol{S}_j^{2,2} - \boldsymbol{S}_{\pi(j)}^{2,1}|| \le 2\tilde{c}\frac{\beta^2}{\varrho}\left[\frac{\sqrt{|\Gamma|}}{c_3}\frac{\varrho}{\beta}\left[||g^2-g^1||_{L^2(\Gamma)} + c_4||f^2-f^1||_{L^2(\Gamma)}\right]\right]^{\frac{1}{2N^2}} \tag{2.7}$$

having the same notations as (2.6) replacing $\boldsymbol{S}_j^1$ by $\boldsymbol{S}_j^2$. The constant $\tilde{c}$ depends on μ and c_3 and c_4 can be written explicitly as

$$c_3 = \min_{1\le j\le N^2} \left(||\boldsymbol{q}_{j,x} + i\boldsymbol{q}_{j,y}||, ||\boldsymbol{q}_{j,y} + i\boldsymbol{q}_{j,z}||\right)$$

and

$$c_4 = \sqrt{2\frac{(4N^2-1)^2}{\beta^2} + \kappa^2}.$$

* * *

This proves that the error in the localization reconstruction depends not only on the number of monopoles and dipoles but also on many other factors as the separability between the sources, the distance from the boundary and also the coefficient μ. These effects are studied and verified numerically in Section 2.4.

Remark 4. *We note that in [EBEH12] the authors considered only the case with $\mu \geq 0$, where (2.6,2.7) were obtained with $c = \widetilde{c} = 1$. However, in the case where $\mu < 0$, one obtains in the same manner the theoretical stability estimates mentioned above but with positive constants c and $\widetilde{c}$ proportional to e^{μ}.*

3. Identification Method

In what follows, we will issue a full algebraic algorithm allowing us to identify the source term (2.5).

Indeed, first, we introduce the following space

$$\mathcal{H}_\mu = \{v \in H^1(\Omega) : \Delta v + \mu v = 0\} \tag{2.8}$$

and define the operator $\mathcal{R}$ as follows

$$\mathcal{R}(v, f, g) = \int_\Gamma \left(gv - f\frac{\partial v}{\partial \nu} \right) ds \quad \text{for all} \quad v \in \mathcal{H}_\mu. \tag{2.9}$$

Multiplying equation (2.1)-(2.5) by v, an element of $\mathcal{H}_\mu$, integrating by parts and using Green's formula lead to

$$\mathcal{R}(v, f, g) = \sum_{j=1}^{N^1} p_j v(\mathbf{S}_j^1) + \sum_{j=1}^{N^2} q_j v(\mathbf{S}_j^2) - \sum_{j=1}^{N^2} \mathbf{r}_j.\nabla v(\mathbf{S}_j^2) \quad \text{for all} \quad v \in \mathcal{H}_\mu. \tag{2.10}$$

Now, the question is how to choose the special functions $v \in \mathcal{H}_\mu$ that would allow us to determine

$$N^1,\ N^2,\ p_j,\ q_j,\ \mathbf{r}_j = (r_{j,1}, r_{j,2}, r_{j,3}),\ \mathbf{S}_j^1 = (x_j^1, y_j^1, z_j^1),\ \mathbf{S}_j^2 = (x_j^2, y_j^2, z_j^2).$$

In fact, observe that, for all $n \in \mathbb{N}$, the functions

$$v_n^a(x,y,z) = (x+iy)^n e^{kz} \quad \text{with} \quad k = \begin{cases} i\sqrt{\mu} & \text{if } \mu \geq 0 \\ \sqrt{-\mu} & \text{if } \mu < 0 \end{cases} \tag{2.11}$$

belong to the space $\mathcal{H}_\mu$.

Therefore, replacing v by v_n^a in formula (2.10), we obtain, for all $n \in \mathbb{N}$, the following relationships, which are behind our identification algorithm:

$$\mathcal{R}(v_n^a, f, g) = \sum_{j=1}^{N^1} p_j e^{kz_j^1} (P_j^{1,a})^n + \sum_{j=1}^{N^2} (q_j - kr_{j,3}) e^{kz_j^2} (P_j^{2,a})^n - n \sum_{j=1}^{N^2} (r_{j,1} + ir_{j,2}) e^{kz_j^2} (P_j^{2,a})^{n-1} \tag{2.12}$$

where $P_j^{1,a} = x_j^1 + iy_j^1$ and $P_j^{2,a} = x_j^2 + iy_j^2$ are the projected points, respectively, of $\mathbf{S}_j^1$ and $\mathbf{S}_j^2$ onto the $xy-$complex plane. For simplicity, we rewrite the relationships (2.12) as

$$\alpha_n^a = \sum_{j=1}^{N^1} \lambda_j^a (P_j^{1,a})^n + \sum_{j=1}^{N^2} \nu_j^a (P_j^{2,a})^n + n \sum_{j=1}^{N^2} \mu_j^a (P_j^{2,a})^{n-1} \quad \forall n \in \mathbb{N} \tag{2.13}$$

with

$$\alpha_n^a = \mathcal{R}(v_n^a, f, g), \quad \lambda_j^a = p_j e^{kz_j^1}, \quad \nu_j^a = (q_j - kr_{j,3}) e^{kz_j^2} \quad \text{and} \quad \mu_j^a = -(r_{j,1} + ir_{j,2}) e^{kz_j^2}.$$

Remark 5. *We note that if $\mu \neq 0$ even in the absence of monopolar sources, the dipolar sources produce algebraic equations similar to those in the case of a linear combination of monopolar and dipolar sources.*

Before solving the equations (2.13), we need to know if the projections $P_j^{1,a}$, $P_j^{2,a}$ are mutually distinct and if $\mu_j^a \neq 0$, which is necessary in order to use the algebraic method proposed below. Indeed, one can remark that there is only a finite number of planes containing the origin such that at least two points among $\mathbf{S}_j^1$, $\mathbf{S}_j^2$ are projected onto the same point on this plane and at least one moment $\mathbf{r}_j$ is projected onto 0

on the same plane. So, if a basis is chosen randomly, one is almost sure that the points $\mathbf{S}_j^1$, $\mathbf{S}_j^2$ are projected onto distinct points and $\mathbf{r}_j$ is not projected onto 0 on every coordinate plane. Therefore, without loss of generality (see also Remark 8), we assume that:

(H) The projections onto the xy, yz and xz-planes of the points $\mathbf{S}_j^1$, $\mathbf{S}_j^2$ and the moments $\mathbf{r}_j$ are respectively mutually distinct and not null.

Before presenting our identification algorithm we introduce, for simplicity, some notations and definitions that are used throughout this subsection.

First, denote by $P_j^{1,b}$, $P_j^{2,b}$ and $P_j^{1,c}$, $P_j^{2,c}$, the projections of $\mathbf{S}_j^1$, $\mathbf{S}_j^2$ onto the yz and xz-complex planes respectively. Then, using, in (2.10), the following test functions

$$v_n^b = (y+iz)^n e^{kx} \quad \text{and} \quad v_n^c = (x+iz)^n e^{ky}, \tag{2.14}$$

elements of $\mathcal{H}_\mu$, one has, as in (2.13), the following algebraic equations

$$\alpha_n^b = \sum_{j=1}^{N^1} \lambda_j^b (P_j^{1,b})^n + \sum_{j=1}^{N^2} \nu_j^b (P_j^{2,b})^n + n \sum_{j=1}^{N^2} \mu_j^b (P_j^{2,b})^{n-1} \quad \forall n \in \mathbb{N} \tag{2.15}$$

and

$$\alpha_n^c = \sum_{j=1}^{N^1} \lambda_j^c (P_j^{1,c})^n + \sum_{j=1}^{N^2} \nu_j^c (P_j^{2,c})^n + n \sum_{j=1}^{N^2} \mu_j^c (P_j^{2,c})^{n-1} \quad \forall n \in \mathbb{N} \tag{2.16}$$

where we note

$$\alpha_n^b = \mathcal{R}(v_n^b, f, g), \quad \lambda_j^b = p_j e^{kx_j^1}, \quad \nu_j^b = (q_j - k r_{j,1}) e^{kx_j^2}, \quad \mu_j^b = -(r_{j,2} + i r_{j,3}) e^{kx_j^2},$$

and

$$\alpha_n^c = \mathcal{R}(v_n^c, f, g), \quad \lambda_j^c = p_j e^{ky_j^1}, \quad \nu_j^c = (q_j - k r_{j,2}) e^{ky_j^2}, \quad \mu_j^c = -(r_{j,1} + i r_{j,3}) e^{ky_j^2}.$$

Finally, bringing together the three equations (2.13), (2.15) and (2.16), we can write

$$\alpha_n^r = \sum_{j=1}^{N^1} \lambda_j^r (P_j^{1,r})^n + \sum_{j=1}^{N^2} \nu_j^r (P_j^{2,r})^n + n \sum_{j=1}^{N^2} \mu_j^r (P_j^{2,r})^{n-1} \text{ for } r = a, b, c \text{ and } n \in \mathbb{N}. \quad (2.17)$$

Remark 6. *Let us note that in equations (2.17), the terms with a power* $(n-1)$ *are assumed to be zero in the case* $n = 0$.

Therefore, the non-linear algebraic system (2.17) can be solved in order to determine

- the number of monopoles N^1
- the number of dipoles N^2
- the projections $P_j^{\ell,r}$, $\ell = 1, 2$
- the coefficients λ_j^r, ν_j^r and μ_j^r.

To do so, first, assume that we know an upper bound $\bar{J}$ for the number

$$J = N^1 + 2N^2.$$

Then, define, for all $n \in \mathbb{N}$, the complex vectors

$$\xi_n^r = (\alpha_n^r, \cdots, \alpha_{\bar{J}+n-1}^r)^t, \quad \Lambda^r = (\lambda_1^r, \cdots, \lambda_{N^1}^r, \nu_1^r, \cdots, \nu_{N^2}^r, \mu_1^r, \cdots, \mu_{N^2}^r)^t.$$

Now, consider, for all $n \in \mathbb{N}$, the complex matrices A_n^r of size $\bar{J} \times J$

$$A_n^r = (V_{n,1}^r \ \ V_{n,2}^r) \quad (2.18)$$

where $V_{n,1}^r$ are the following $\bar{J} \times N^1$ Vandermonde matrices

$$V_{n,1}^r = \begin{pmatrix} (P_1^{1,r})^n & \cdots & (P_{N^1}^{1,r})^n \\ (P_1^{1,r})^{n+1} & \cdots & (P_{N^1}^{1,r})^{n+1} \\ \vdots & \ddots & \vdots \\ (P_1^{1,r})^{\bar{J}+n-1} & \cdots & (P_{N^1}^{1,r})^{\bar{J}+n-1} \end{pmatrix}$$

and $V_{n,2}^r$ are the confluent $\bar{J} \times 2N^2$ Vandermonde matrices

$$V^r_{n,2} = \begin{pmatrix} (P^{2,r}_1)^n & \cdots & (P^{2,r}_{N^2})^n & n(P^{2,r}_1)^{n-1} & \cdots & n(P^{2,r}_{N^2})^{n-1} \\ (P^{2,r}_1)^{n+1} & \cdots & (P^{2,r}_{N^2})^{n+1} & (n+1)(P^{2,r}_1)^n & \cdots & (n+1)(P^{2,r}_{N^2})^n \\ \vdots & \ddots & \vdots & \vdots & \ddots & \vdots \\ (P^{2,r}_1)^{\bar{J}+n-1} & \cdots & (P^{2,r}_{N^2})^{\bar{J}+n-1} & (\bar{J}+n-1)(P^{2,r}_1)^{\bar{J}+n-2} & \cdots & (\bar{J}+n-1)(P^{2,r}_{N^2})^{\bar{J}+n-2} \end{pmatrix},$$

introduce the Hankel matrix

$$H^r_{\bar{J}} = \begin{pmatrix} \alpha^r_0 & \alpha^r_1 & \cdots & \alpha^r_{\bar{J}-1} \\ \alpha^r_1 & \alpha^r_2 & \cdots & \alpha^r_{\bar{J}} \\ \vdots & \vdots & \vdots & \vdots \\ \alpha^r_{\bar{J}-1} & \alpha^r_{\bar{J}} & \cdots & \alpha^r_{2\bar{J}-2} \end{pmatrix}, \tag{2.19}$$

and the block tridiagonal matrix

$$\bar{I}^r = \begin{pmatrix} \lambda^r_1 & \cdots & 0 & 0 & \cdots & 0 & 0 & \cdots & 0 \\ \vdots & \ddots & \vdots & \vdots & \ddots & \vdots & \vdots & \ddots & \vdots \\ 0 & \cdots & \lambda^r_{N^1} & 0 & \cdots & 0 & 0 & \cdots & 0 \\ 0 & \cdots & 0 & \nu^r_1 & \cdots & 0 & \mu^r_1 & \cdots & 0 \\ \vdots & \ddots & \vdots & \vdots & \ddots & \vdots & \vdots & \ddots & \vdots \\ 0 & \cdots & 0 & 0 & \cdots & \nu^r_{N^2} & 0 & \cdots & \mu^r_{N^2} \\ 0 & \cdots & 0 & \mu^r_1 & \cdots & 0 & 0 & \cdots & 0 \\ \vdots & \ddots & \vdots & \vdots & \ddots & \vdots & \vdots & \ddots & \vdots \\ 0 & \cdots & 0 & 0 & \cdots & \mu^r_{N^2} & 0 & \cdots & 0 \end{pmatrix}. \tag{2.20}$$

Therefore, the identification process is attained in two steps.

1. Determination of the number of sources:

The first step consists in determining the number of sources. This is object of the following theorem.

Theorem 4. *Let $H^r_{\bar{J}}$ be the Hankel matrix defined in (2.19) where $\bar{J}$ is a known upper* *bound of J. Under hypothesis **(H)**, we have*

$$rank\left(H^r_{\bar{J}}\right) = N^1 + 2N^2.$$

* * *

Before proving Theorem 4, we start by establishing the following interesting decomposition lemma.

Lemma 1. *Let $H^r_{\bar{J}}$ be the Hankel matrix defined in (2.19), $\bar{I}^r$ the block tridiagonal matrix defined in (2.20), A^r_0 the Vandermonde matrix defined in (2.18) and $(A^r_0)^t$ its matrix transpose. Then,*

$$H^r_{\bar{J}} = A^r_0 \bar{I}^r (A^r_0)^t. \tag{2.21}$$

Proof: First, using the Vandermonde matrices (2.18), one can rewrite the algebraic formulae (2.17) in the matrix form as

$$\xi^r_n = A^r_n \Lambda^r, \qquad \forall n \in \mathbb{N}.$$

On the other hand, if we denote by T^r the block upper triangular complex matrix

$$T^r = \begin{pmatrix} P^{1,r}_1 & \cdots & 0 & 0 & \cdots & 0 & 0 & \cdots & 0 \\ \vdots & \ddots & \vdots & \vdots & \ddots & \vdots & \vdots & \ddots & \vdots \\ 0 & \cdots & P^{1,r}_{N^1} & 0 & \cdots & 0 & 0 & \cdots & 0 \\ & & & & & & & & \\ 0 & \cdots & 0 & P^{2,r}_1 & \cdots & 0 & 1 & \cdots & 0 \\ \vdots & \ddots & \vdots & \vdots & \ddots & \vdots & \vdots & \ddots & \vdots \\ 0 & \cdots & 0 & 0 & \cdots & P^{2,r}_{N^2} & 0 & \cdots & 1 \\ & & & & & & & & \\ 0 & \cdots & 0 & 0 & \cdots & 0 & P^{2,r}_1 & \cdots & 0 \\ \vdots & \ddots & \vdots & \vdots & \ddots & \vdots & \vdots & \ddots & \vdots \\ 0 & \cdots & 0 & 0 & \cdots & 0 & 0 & \cdots & P^{2,r}_{N^2} \end{pmatrix} \tag{2.22}$$

one gets, for all $n \in \mathbb{N}$,

$$A^r_{n+1} = A^r_n T^r = A^r_0 (T^r)^{n+1}$$

and therefore

$$\xi_n^r = A_0^r (T^r)^n \Lambda^r \qquad \forall n \in \mathbb{N}. \tag{2.23}$$

Then, by using (2.23), one can rewrite the Hankel matrix $H_{\bar{J}}^r$ as,

$$H_{\bar{J}}^r = A_0^r [\Lambda^r, T^r \Lambda^r, ..., (T^r)^{\bar{J}-1} \Lambda^r]. \tag{2.24}$$

Now, it remains to prove that

$$[\Lambda^r, T^r \Lambda^r, ..., (T^r)^{\bar{J}-1} \Lambda^r] = \bar{I}^r (A_0^r)^t.$$

Indeed, first, $\bar{I}^r (A_0^r)^t =$

$$\begin{pmatrix} \lambda_1^r & \cdots & 0 & 0 & \cdots & 0 & 0 & \cdots & 0 \\ \vdots & \ddots & \vdots & \vdots & \ddots & \vdots & \vdots & \ddots & \vdots \\ 0 & \cdots & \lambda_{N^1}^r & 0 & \cdots & 0 & 0 & \cdots & 0 \\ \\ 0 & \cdots & 0 & \nu_1^r & \cdots & 0 & \mu_1^r & \cdots & 0 \\ \vdots & \ddots & \vdots & \vdots & \ddots & \vdots & \vdots & \ddots & \vdots \\ 0 & \cdots & 0 & 0 & \cdots & \nu_{N^2}^r & 0 & \cdots & \mu_{N^2}^r \\ \\ 0 & \cdots & 0 & \mu_1^r & \cdots & 0 & 0 & \cdots & 0 \\ \vdots & \ddots & \vdots & \vdots & \ddots & \vdots & \vdots & \ddots & \vdots \\ 0 & \cdots & 0 & 0 & \cdots & \mu_{N^2}^r & 0 & \cdots & 0 \end{pmatrix} \begin{pmatrix} 1 & P_1^{1,r} & \cdots & (P_1^{1,r})^{\bar{J}-1} \\ \vdots & \vdots & \cdots & \vdots \\ 1 & P_{N^1}^{1,r} & \cdots & (P_{N^1}^{1,r})^{\bar{J}-1} \\ \\ 1 & P_1^{2,r} & \cdots & (P_1^{2,r})^{\bar{J}-1} \\ \vdots & \vdots & \cdots & \vdots \\ 1 & P_{N^2}^{2,r} & \cdots & (P_{N^2}^{2,r})^{\bar{J}-1} \\ \\ 0 & 1 & \cdots & (\bar{J}-1)(P_1^{2,r})^{\bar{J}-2} \\ \vdots & \vdots & \cdots & \vdots \\ 0 & 1 & \cdots & (\bar{J}-1)(P_{N^2}^{2,r})^{\bar{J}-2} \end{pmatrix}$$

$$= \begin{pmatrix} \lambda_1^r & \lambda_1^r P_1^{1,r} & \cdots & \lambda_1^r (P_1^{1,r})^{\bar{J}-1} \\ \vdots & \vdots & \cdots & \vdots \\ \lambda_{N^1}^r & \lambda_{N^1}^r P_{N^1}^{1,r} & \cdots & \lambda_{N^1}^r (P_{N^1}^{1,r})^{\bar{J}-1} \\ \nu_1^r & \nu_1^r P_1^{2,r} + \mu_1^r & \cdots & \nu_1^r (P_1^{2,r})^{\bar{J}-1} + (\bar{J}-1)\mu_1^r (P_1^{2,r})^{\bar{J}-2} \\ \vdots & \vdots & \cdots & \vdots \\ \nu_{N^2}^r & \nu_{N^2}^r P_{N^2}^{2,r} + \mu_{N^2}^r & \cdots & \nu_{N^2}^r (P_{N^2}^{2,r})^{\bar{J}-1} + (\bar{J}-1)\mu_{N^2}^r (P_{N^2}^{2,r})^{\bar{J}-2} \\ \mu_1^r & \mu_1^r P_1^{2,r} & \cdots & \mu_1^r (P_1^{2,r})^{\bar{J}-1} \\ \vdots & \vdots & \cdots & \vdots \\ \mu_{N^2}^r & \mu_{N^2}^r P_{N^2}^{2,r} & \cdots & \mu_{N^2}^r (P_{N^2}^{2,r})^{\bar{J}-1} \end{pmatrix}.$$

On the other hand, we can see that

$$(T^r)^n = \begin{pmatrix} (P_1^{1,r})^n & \cdots & 0 & 0 & \cdots & 0 & 0 & \cdots & 0 \\ \vdots & \ddots & \vdots & \vdots & \ddots & \vdots & \vdots & \ddots & \vdots \\ 0 & \cdots & (P_{N^1}^{1,r})^n & 0 & \cdots & 0 & 0 & \cdots & 0 \\ 0 & \cdots & 0 & (P_1^{2,r})^n & \cdots & 0 & n(P_1^{2,r})^{n-1} & \cdots & 0 \\ \vdots & \ddots & \vdots & \vdots & \ddots & \vdots & \vdots & \ddots & \vdots \\ 0 & \cdots & 0 & 0 & \cdots & (P_{N^2}^{2,r})^n & 0 & \cdots & n(P_{N^2}^{2,r})^{n-1} \\ 0 & \cdots & 0 & 0 & \cdots & 0 & (P_1^{2,r})^n & \cdots & 0 \\ \vdots & \ddots & \vdots & \vdots & \ddots & \vdots & \vdots & \ddots & \vdots \\ 0 & \cdots & 0 & 0 & \cdots & 0 & 0 & \cdots & (P_{N^2}^{2,r})^n \end{pmatrix},$$

and then for all $n = 1, 2, \cdots, \bar{J}-1$, one has

$$(T^r)^n\Lambda^r = \begin{pmatrix} \lambda_1^r(P_1^{1,r})^n \\ \vdots \\ \lambda_{N^1}^r(P_{N^1}^{1,r})^n \\ \nu_1^r(P_1^{2,r})^n + n\mu_1^r(P_1^{2,r})^{n-1} \\ \vdots \\ \nu_{N^2}^r(P_{N^2}^{2,r})^n + n\mu_{N^2}^r(P_{N^2}^{2,r})^{n-1} \\ \mu_1^r(P_{N^1}^{1,r})^n \\ \vdots \\ \mu_{N^2}^r(P_{N^2}^{2,r})^n \end{pmatrix}.$$

So, assembling the vectors $(T^r)^n\Lambda^r$, $n = 1, \cdots, \bar{J}-1$, we get

$$[\Lambda^r, T^r\Lambda^r, \cdots, (T^r)^{\bar{J}-1}\Lambda^r] = \bar{I}^r(A_0^r)^t.$$

This ends the proof of Lemma 1. □

Remark 7. *It is easy to see that*

- $\bar{I}^r$ *is invertible if and only if* $\lambda_j^r \neq 0, j = 1, \cdots, N^1$ *and* $\mu_j^r \neq 0, j = 1, \cdots, N^2$.
- $rank(A_0^r)^t = J$ *if and only if the projections* $P_j^{2,r}, j = 1, \cdots, N^1$ *and* $P_j^{2,r}, j = 1, \cdots, N^2$ *are mutually distinct.*

Proof of Theorem 4. From **(H)** and Remark 7, we can check that $\bar{I}^r$ is a nonsingular matrix and $rank(A_0^r)^t = J$. This implies that $A_0^r\bar{I}^r$ is surjective and therefore we have $rank(A_0^r\bar{I}^r(A_0^r)^t) = rank(A_0^r)^t$, which leads to the desired result.

2. Reconstruction of the projections $P_j^{1,r}$ and $P_j^{2,r}$

The second step consists in determining the projections onto the xy-, yz- and xz-complex planes of the monopolar and dipolar sources. Since, as we have shown, the rank of $H_{\bar{J}}^r$ is J, we replace in the quantities defined above $\bar{J}$ by J. Then, from (2.23), we can easily derive the following relations:

$$\xi_{n+1}^r = A_0^r (T^r)^{n+1} \Lambda^r \tag{2.25}$$
$$= A_0^r (T^r)(A_0^r)^{-1} A_0^r (T^r)^n \Lambda^r. \tag{2.26}$$

Then, we get

$$\xi_{n+1}^r = B^r \xi_n^r, \qquad \forall n \in \mathbb{N}$$

where we have set

$$B^r = A_0^r T^r (A_0^r)^{-1}. \tag{2.27}$$

Here, the matrix A_0^r is invertible ($(A_0^r)^{-1}$ exists) since the projected points $\{P_j^{1,r}, P_j^{2,r}\}$ are assumed distinct (respecting **H**). Moreover, since $\mathrm{rank}(H_J^r) = J$, the family $(\xi_n^r)_{n=0,\ldots,J-1}$ forms a basis of $\mathcal{C}^J$ and consequently the $J \times J$ complex matrix B^r is given explicitly by

$$B^r = \begin{pmatrix} 0 & 1 & \cdots & 0 & 0 \\ 0 & 0 & 1 & \cdots & 0 \\ \vdots & \vdots & \ddots & \ddots & 0 \\ \vdots & \vdots & \ddots & \ddots & 1 \\ c_0^r & c_1^r & \cdots & \cdots & c_{J-1}^r \end{pmatrix} \tag{2.28}$$

where the vector $C^r = (c_0^r, ..., c_{J-1}^r)^t$ is obtained by solving the linear system

$$H_J^r C^r = \xi_J^r.$$

Thus, the projections $\{P_j^{1,r}, P_j^{2,r}\}$ are given by the following theorem.

Theorem 5. *Let B^r be the companion matrix defined in (2.28). Assume that the hypothesis **(H)** is satisfied, then*

1. *B^r admits N^1 simple eigenvalues and N^2 double eigenvalues.*
2. *The N^1 simple eigenvalues are the projections $P_j^{1,r}$ of the monopolar sources and the N^2 double eigenvalues are the projections $P_j^{2,r}$ of the dipolar sources.*

* * *

Proof: The proof of this theorem is a direct consequence from (2.22) and (2.27). □

3. Determination of the vectors Λ^r

To determine λ_j^r, ν_j^r and μ_j^r, it is sufficient to solve the linear systems

$$A_0^r \Lambda^r = \xi_0^r,$$

which allow us to obtain the coefficients $p_j, q_j, \mathbf{r}_j$, as suggested in the algorithm below.

Theorems 4 and 5 suggest that if one knows an upper bound $\bar{J}$ for the number $J = N^1 + 2N^2$, one can establish an algorithm to identify, in a unique way, the coefficients N^1, N^2, p_j, q_j, $\mathbf{r}_j$, $\mathbf{S}_j^1$ and $\mathbf{S}_j^2$.

4.Algebraic algorithm

Step 1. Using the given Cauchy data (f, g) on the boundary Γ, compute $\alpha_0, \alpha_1, \cdots, \alpha_{2\bar{J}-1}$. Then, the number $J = N^1 + 2N^2$ can be determined by the rank of one of the three Hankel matrices $H_{\bar{J}}^r$, estimated using the Singular Value Decomposition method with an appropriate threshold, following [Han98], see Section 2.4 for more details concerning the choice of the threshold.

Step 2. Solve the linear system $H_J^r C^r = \xi_J^r$. The projection points $P_j^{1,r}$ of monopolar sources are obtained as the N^1 simple eigenvalues of the matrix B^r and the projection points $P_j^{2,r}$ of dipolar sources are obtained as the N^2 double eigenvalues of the same matrix.

Step 3. The three vectors Λ^r are obtained by solving the systems $A_0^r \Lambda^r = \xi_0^r$, which gives λ_j^r, ν_j^r and μ_j^r.

Step 4. To determine the locations $\mathbf{S}_j^1$, $\mathbf{S}_j^2$, it remains to find z_j^ℓ, for $\ell = 1, 2$. To do this, three cases may occur:

a. Case $\mu = 0$. In this case, z_j^ℓ can be determined directly using some adapted test functions of the form $v(x, y, z) = z\phi(x + iy)$, in the same way as it was done in [EB05, Section 5.1.1].

b. Case $\mu < 0$. We replace in (2.12) the test function v_n^a by $\bar{v}_n^a(x, y, z) = (x + iy)^n e^{-kz}$. Then, solving these algebraic equations we can identify, using Step 3, the following quantities

$$\bar{\lambda}_j^a = p_j e^{-kz_j^1} \quad \text{and} \quad \bar{\mu}_j^a = -(r_{j,1} + ir_{j,2})e^{-kz_j^2}.$$

This allows us to determine z_j^1 and z_j^2 using λ_j^a, $\bar{\lambda}_j^a$, μ_j^a, $\bar{\mu}_j^a$, namely,

$$z_j^1 = \frac{1}{2k} \ln\left(\frac{\lambda_j^a}{\bar{\lambda}_j^a}\right), \quad z_j^2 = \frac{1}{2k} \ln\left(\frac{\mu_j^a}{\bar{\mu}_j^a}\right).$$

c. Case $\mu > 0$. First, we set

$$\begin{aligned} P_j^{1,a} &= x_j^{1,a} + iy_j^{1,a}, \quad P_j^{1,b} &= y_j^{1,b} + iz_j^{1,b}, \quad P_j^{1,c} &= x_j^{1,c} + iz_j^{1,c}, \\ P_j^{2,a} &= x_j^{2,a} + iy_j^{2,a}, \quad P_j^{2,b} &= y_j^{2,b} + iz_j^{2,b}, \quad P_j^{2,c} &= x_j^{2,c} + iz_j^{2,c}. \end{aligned}$$

Then, we proceed as in the previous case, by replacing in (2.12) and (2.16) the test functions v_n^a and v_n^c by $\bar{v}_n^a(x,y,z) = (x+iy)^n e^{-kz}$ and $\bar{v}_n^c(x,y,z) = (x+iz)^n e^{-ky}$ respectively. We identify $z_j^{\ell,a}$ and $y_j^{\ell,c}$ (modulo 2π), namely,

$$z_j^{1,a} = \frac{1}{2k} \log\left(\frac{\lambda_j^a}{\bar{\lambda}_j^a}\right) + \frac{im\pi}{k}, \quad z_j^{2,a} = \frac{1}{2k} \log\left(\frac{\mu_j^a}{\bar{\mu}_j^a}\right) + \frac{im\pi}{k} \qquad \forall m \in \mathbb{N}$$

$$y_j^{1,c} = \frac{1}{2k} \log\left(\frac{\lambda_j^c}{\bar{\lambda}_j^c}\right) + \frac{im\pi}{k}, \quad y_j^{2,c} = \frac{1}{2k} \log\left(\frac{\mu_j^c}{\bar{\mu}_j^c}\right) + \frac{im\pi}{k} \qquad \forall m \in \mathbb{N}.$$

Now, for $\ell = 1, \cdots, N^2$, we denote

$$J_\ell = \left\{ j = 1, \cdots, N^2 \quad \text{such that} \quad y_j^{2,b} = y_\ell^{2,a} \text{ and } z_j^{2,b} = \frac{1}{2k} \log\left(\frac{\mu_\ell^a}{\bar{\mu}_\ell^a}\right) + \frac{im\pi}{k} \right\}.$$

Assuming that the hypothesis **(H)** is satisfied, we are almost sure that there will exist only one index, noted σ_ℓ, satisfying the following condition

$$z_{\sigma_\ell}^{2,c} = z_j^{2,b}, \quad x_{\sigma_\ell}^{2,c} = x_\ell^{2,a} \quad \text{and} \quad \frac{1}{2k} \log\left(\frac{\mu_{\sigma_\ell}^c}{\bar{\mu}_{\sigma_\ell}^c}\right) + \frac{im\pi}{k} = y_\ell^{2,a} \qquad \forall j \in J_\ell,$$

and therefore we take

$$\mathbf{S}_\ell^2 = (x_\ell^{2,a}, y_\ell^{2,a}, z_{\sigma_\ell}^{2,c}), \qquad \ell = 1, \cdots, N^2.$$

We repeat the same argument to determine $\mathbf{S}_\ell^1$, for $\ell = 1, \cdots, N^1$.

Step 5. Once the locations of the point sources are identified, the intensities p_j can be determined directly from λ_j^a, the moments $\mathbf{r}_j$ can be determined from μ_j^a, μ_j^b and consequently q_j are determined from ν_j^a.

Remark 8.

1. *In the case where k is non-zero and $q_\ell = 0$, the moments $\boldsymbol{r}_\ell$ can be determined directly from μ_ℓ^a and ν_ℓ^a.*
2. *In the latter algebraic algorithm, we have assumed that, the projected points onto xy-, xz- and yz-complex planes of the point sources $\boldsymbol{S}_j^1$, $\boldsymbol{S}_j^2$ are distinct and also that the projected points of the moments $\boldsymbol{r}_j$ are nonzero. Thus, this enables us to identify the points $\boldsymbol{S}_j^1$ and $\boldsymbol{S}_j^2$ through their projection points. However, if by bad luck one of the projected points onto xy-, xz- or yz-complex planes coincides with another one, we can do the same thing by choosing two other planes, where the projected points are distinct. This is possible, since, for all orthonormal basis $(\vec{u}, \vec{v}, \vec{u} \wedge \vec{v})$, the following function*

$$v_n(\boldsymbol{S}) = (\vec{u}.\boldsymbol{S} + i\vec{v}.\boldsymbol{S})^n e^{k(\vec{u}\wedge\vec{v}).\boldsymbol{S}} \quad \text{with} \quad \boldsymbol{S} = (x, y, z)$$

remains in the space $\mathcal{H}_\mu$, for all $n \in \mathbb{N}$. Let us mention that, to reach a better identification of point sources, it is desirable to project the point sources on a plane $(\vec{u}, \vec{v})$ where the absolute gap between the singular values of the corresponding Hankel matrix is the largest possible. In practice, to attain such a plane, we can assume, for example, that $\vec{u} = (\cos(\phi)\cos(\theta), \cos(\phi)\sin(\theta), \sin(\phi))$ and $\vec{v} = (\sin(\phi)\cos(\theta), \sin(\phi)\sin(\theta), -\cos(\phi))$ and then take the pair $(\phi, \theta) \in [0, \frac{\pi}{2}] \times [0, 2\pi]$ that realizes the largest gap between the singular values of the Hankel matrix. This issue is discussed numerically in Section 2.4.

2.2.2. General multipolar sources

In this subsection, we consider the source F of the form (2.3) for which we discuss its non-uniqueness giving a suitable counterexample then we present a compatible algebraic algorithm that generalizes the one presented in the previous subsection.

1. Non-uniqueness

As mentioned before, in the general case where $K^\ell \geq 2$, the uniqueness of the sources of form (2.3) is not valid. In fact, it is easy to see that the source $F = \mu\delta_{\mathbf{S}} + \Delta\delta_{\mathbf{S}}$ can not be uniquely determined from a single Cauchy data.

2. Identification Method

The identification method used for multipolar sources reconstruction is a generalization of the one used for monopolar and dipolar sources. Indeed, following the same procedure as in Subsection 2.2.1, multiplying equation (2.1)-(2.3) by v_n^a defined in (2.11), integrating by parts and using Green's formula lead to,

$$\alpha_n^a = \sum_{\ell=1}^{L}\sum_{j=1}^{N^\ell}\sum_{\alpha=0}^{K^\ell} \eta_{j,\ell}^{\{\alpha_1,\alpha_2,\alpha_3\}}(\alpha_1+\alpha_2)!\tbinom{n}{\alpha_1+\alpha_2}(P_j^{\ell,a})^{n-(\alpha_1+\alpha_2)} \qquad \forall n \in \mathbb{N}$$

where

$$\alpha_n^a = \mathcal{R}(v_n^a, f, g), \quad \mathcal{R} \text{ is the operator defined in (2.9)},$$

$$\binom{k}{j} = \begin{cases} \frac{k!}{j!(k-j)!} & \text{if } \ k \geq j \\ 0 & \text{if } \ k < j \end{cases}, \quad P_j^{\ell,a} = x_j^\ell + iy_j^\ell, \quad \alpha = \alpha_1+\alpha_2+\alpha_3$$

and

$$\eta_{j,\ell}^{\{\alpha_1,\alpha_2,\alpha_3\}} = (-1)^\alpha (i)^{\alpha_2}(k)^{\alpha_3}\lambda_{j,\ell}^{\{\alpha_1,\alpha_2,\alpha_3\}}e^{kz_j^\ell}.$$

Therefore,

$$\alpha_n^a = \sum_{\ell=1}^{L}\sum_{j=1}^{N^\ell}\sum_{\beta=0}^{K^\ell}\left(\sum_{\alpha_1+\alpha_2=\beta}\sum_{\alpha=\beta}^{K^\ell}\eta_{j,\ell}^{\{\alpha_1,\alpha_2,\alpha-\beta\}}\right)\beta!\tbinom{n}{\beta}(P_j^{\ell,a})^{n-\beta} \qquad \forall n \in \mathbb{N}$$

where $\beta = \alpha_1+\alpha_2$. This gives the following relationships

$$\alpha_n^a = \sum_{\ell=1}^{L}\sum_{j=1}^{N^\ell}\sum_{\beta=0}^{K^\ell}\nu_{j,\ell}^{\beta,a}\tbinom{n}{\beta}(P_j^{\ell,a})^{n-\beta} \qquad \forall n \in \mathbb{N} \tag{2.29}$$

where, for all $\ell = 1, \cdots, L$ and $\beta = 0, \cdots, K^\ell$, we note

$$\nu_{j,\ell}^{\beta,a} = \beta! \sum_{\alpha_1+\alpha_2=\beta} \sum_{\alpha=\beta}^{K^\ell} \eta_{j,\ell}^{\{\alpha_1,\alpha_2,\alpha-\beta\}}.$$

Moreover, multiplying equation (2.1)-(2.3) by the following test functions

$$v_n^b = (y+iz)^n e^{kx} \quad \text{and} \quad v_n^c = (x+iz)^n e^{ky},$$

we get, as in (2.29), the following relationships

$$\alpha_n^r = \sum_{\ell=1}^{L} \sum_{j=1}^{N^\ell} \sum_{\beta=0}^{K^\ell} \nu_{j,\ell}^{\beta,r} \tbinom{n}{\beta} (P_j^{\ell,r})^{n-\beta} \quad \text{for} \quad r = a, b, c \tag{2.30}$$

where $P_j^{\ell,b}$ and $P_j^{\ell,c}$ are the projections of points $\mathbf{S}_j^\ell$ onto the yz- and xz-complex planes respectively

$$\nu_{j,\ell}^{\beta,b} = \beta! \sum_{\alpha_2+\alpha_3=\beta} \sum_{\alpha=\beta}^{K^\ell} \zeta_{j,\ell}^{\{\alpha-\beta,\alpha_2,\alpha_3\}}$$

with

$$\zeta_{j,\ell}^{\{\alpha_1,\alpha_2,\alpha_3\}} = (-1)^\alpha (i)^{\alpha_3} (k)^{\alpha_1} \lambda_{j,\ell}^{\{\alpha_1,\alpha_2,\alpha_3\}} e^{kx_j^\ell},$$

$$\nu_{j,\ell}^{\beta,c} = \beta! \sum_{\alpha_1+\alpha_3=\beta} \sum_{\alpha=\beta}^{K^\ell} \tau_{j,\ell}^{\{\alpha_1,\alpha-\beta,\alpha_3\}}$$

with

$$\tau_{j,\ell}^{\{\alpha_1,\alpha_2,\alpha_3\}} = (-1)^\alpha (i)^{\alpha_3} (k)^{\alpha_2} \lambda_{j,\ell}^{\{\alpha_1,\alpha_2,\alpha_3\}} e^{ky_j^\ell}.$$

The main objective of the following consists in establishing a general algebraic method for solving equations (2.30), allowing us to generalize Theorem 4 and Theorem 5. Indeed, assume that we know an upper bound $\bar{J}$ for the number

$$J = \sum_{\ell=1}^{L} (K^\ell + 1) N^\ell.$$

Define the complex vectors

$$\xi_n^r = (\alpha_n^r, \cdots, \alpha_{\bar{J}+n-1}^r)^t, \quad \Lambda^r = (\bar{\nu}_1^r, ..., \bar{\nu}_L^r)^t$$

where, for all $\ell = 1, \cdots, L$, we have

$$\bar{\nu}_\ell^r = (\bar{\nu}_\ell^{0,r}, ..., \bar{\nu}_\ell^{K^\ell,r}) \quad \text{with} \quad \bar{\nu}_\ell^{\beta,r} = (\nu_{1,\ell}^{\beta,r}, \cdots, \nu_{N^\ell,\ell}^{\beta,r}) \quad \text{for all} \quad \beta = 0, \cdots, K^\ell,$$

and consider, for all $n \in \mathbb{N}$, the complex matrices A_n^r, of size $\bar{J} \times J$

$$A_n^r = (V_{n,1}^r, \cdots, V_{n,L}^r) \tag{2.31}$$

with

$$V_{n,\ell}^r = (U_{n,\ell}^{0,r}, \cdots, U_{n,\ell}^{K^\ell,r})$$

where, for $\beta = 0, \cdots, K^\ell$, $U_{n,\ell}^{\beta,r}$ are the confluent $\bar{J} \times N^\ell$ Vandermonde matrices

$$U_{n,\ell}^\beta = \begin{pmatrix} \binom{n}{\beta}(P_1^{\ell,r})^{n-\beta} & \cdots & \binom{n}{\beta}(P_{N^\ell}^{\ell,r})^{n-\beta} \\ \binom{n+1}{\beta}(P_1^{\ell,r})^{n-j+1} & \cdots & \binom{n+1}{\beta}(P_{N^\ell}^{\ell,r})^{n-j+1} \\ \vdots & \ddots & \vdots \\ \binom{\bar{J}+n-1}{\beta}(P_1^{\ell,r})^{n-\beta+\bar{J}-1} & \cdots & \binom{\bar{J}+n-1}{\beta}(P_{N^\ell}^{\ell,r})^{n-\beta+\bar{J}-1} \end{pmatrix}.$$

Let us, now, introduce, the Hankel matrix

$$H_{\bar{J}}^r = \begin{pmatrix} \alpha_0^r & \alpha_1^r & \cdots & \alpha_{\bar{J}-1}^r \\ \alpha_1^r & \alpha_2^r & \cdots & \alpha_{\bar{J}}^r \\ \vdots & \vdots & \vdots & \vdots \\ \alpha_{\bar{J}-1}^r & \alpha_{\bar{J}}^r & \cdots & \alpha_{2\bar{J}-2}^r \end{pmatrix} \tag{2.32}$$

and the following multi-diagonal matrices

$$\bar{I}_\ell^r = \begin{pmatrix} \nu_\ell^{0,r} & \nu_\ell^{1,r} & \cdots & \nu_\ell^{K^\ell,r} \\ \vdots & \vdots & \iddots & \vdots \\ \nu_\ell^{K^\ell-1,r} & \nu_\ell^{K^\ell,r} & \cdots & 0 \\ \nu_\ell^{K^\ell,r} & 0 & \cdots & 0 \end{pmatrix} \quad \text{for} \quad \ell = 1, \cdots, L \tag{2.33}$$

where

$$\nu_\ell^{\beta,r} = diag(\nu_{1,\ell}^{\beta,r}, \cdots, \nu_{N^\ell,\ell}^{\beta,r}).$$

As in the previous subsection, we propose an identification processes in three steps.

1. Determination of the number of sources

The first step consists in determining the number of sources by means of the following theorem.

Theorem 6. *Let $H^r_{\bar{J}}$ be the Hankel matrix defined in (2.32) where $\bar{J}$ is a known upper bound of J. Assume that, for $r = a, b, c$, the projected points $P^{\ell,r}_j$ of $\mathbf{S}^\ell_j$ are distinct, then, we have*

$$rank\left(H^r_{\bar{J}}\right) = \sum_{\ell=1}^{L}(K^\ell + 1)N^\ell \quad \textit{if and only if} \quad \nu^{K^\ell,r}_{j,\ell} \neq 0 \quad \textit{for } j = 1, ..., N^\ell \textit{ and } \ell = 1, ..., L.$$

* * *

As before, we need the following decomposition lemma to prove this theorem.

Lemma 2. *Let $H^r_{\bar{J}}$ be the Hankel matrix defined in (2.32), $\bar{I}^r_\ell$ the multi-diagonal matrix defined in (2.33), A^r_0 the Vandermonde matrix defined in (2.31) and $(A^r_0)^t$ its matrix transpose. Then,*

$$H^r_{\bar{J}} = A^r_0 \bar{I}^r (A^r_0)^t. \tag{2.34}$$

Proof: The proof is similar to that of Lemma 1. Indeed, first, from (2.31), we begin by rewriting the algebraic formulae (2.30) in a matrix form as

$$\xi^r_n = A^r_n \Lambda^r, \qquad \forall n \in \mathbb{N}. \tag{2.35}$$

Furthermore, if we denote, for $\ell = 1, \cdots, L$, by T^r_ℓ the block upper triangular complex matrix

$$T^r_\ell = \begin{pmatrix} D^r_{P_\ell} & I & \cdots & 0 \\ 0 & \ddots & \ddots & \vdots \\ \vdots & \ddots & D^r_{P_\ell} & I \\ 0 & \cdots & 0 & D^r_{P_\ell} \end{pmatrix} \tag{2.36}$$

with

$$D^r_{P_\ell} = diag(P^{\ell,r}_1, \cdots, P^{\ell,r}_{N^\ell}) \quad \text{and} \quad I = diag(1, \cdots, 1),$$

one gets, using the Pascal formula $\binom{n}{j-1} + \binom{n}{j} = \binom{n+1}{j}$,

$$V^r_{n+1,\ell} = V^r_{n,\ell} T^r_\ell, \qquad \forall n \in \mathbb{N}.$$

From the definition of A^r_n, we can check that for

$$T^r = diag(T^r_1, \cdots, T^r_L) \tag{2.37}$$

we have

$$A^r_{n+1} = A^r_n T^r = A^r_0 (T^r)^{n+1}, \qquad \forall n \in \mathbb{N}$$

and therefore, from (2.35), one gets

$$\xi^r_n = A^r_0 (T^r)^n \Lambda^r, \qquad \forall n \in \mathbb{N}. \tag{2.38}$$

Now, thanks to (2.38), one can verify by a simple calculation the following relationship

$$H^r_{\bar{J}} = A^r_0 [\Lambda^r, T^r \Lambda^r, ..., (T^r)^{\bar{J}-1} \Lambda^r] = A^r_0 \bar{I}^r (A^r_0)^t$$

which ends the proof of Lemma 2. □

Remark 9. *It is easy to see that*

- $\bar{I}^r_\ell$ *is invertible if and only if* $\nu^{K^\ell,r}_{j,\ell} \neq 0$ *for* $j = 1, ..., N^\ell$ *and* $\ell = 1, ..., L.$
- $rank(A^r_n)^t = J$ *if and only if the projections* $P^{\ell,r}_j, j = 1, \cdots, N^\ell$ *are mutually distinct.*

Proof of Theorem 6. It is similar to the proof of Theorem 4.

2. Reconstruction of the projections $P^{\ell,r}_j$

The second step consists in determining the projections onto the xy-, xz- and yz-complex planes of the points sources.

Henceforth, we replace $\bar{J}$ by J in the quantities defined above. Thus, from (2.38), we can easily derive that

$$\xi^r_{n+1} = B^r \xi^r_n, \qquad \forall n \in \mathbb{N}$$

where we have set

$$B^r = A^r_0 T^r (A^r_0)^{-1}. \tag{2.39}$$

Here, the matrix A^r_0 is invertible since the projected points $P^{\ell,r}_j$ are assumed distinct. Moreover, since $\operatorname{rank}(H^r_J) = J$, the family $(\xi^r_n)_{n=0,...,J-1}$ forms a basis of $\mathbb{C}^J$, so the $J \times J$ complex matrix B^r is given explicitly by

$$B^r = \begin{pmatrix} 0 & 1 & \cdots & 0 & 0 \\ 0 & 0 & 1 & \cdots & 0 \\ \vdots & \vdots & \ddots & \ddots & 0 \\ \vdots & \vdots & \ddots & \ddots & 1 \\ c^r_0 & c^r_1 & \cdots & \cdots & c^r_{J-1} \end{pmatrix} \tag{2.40}$$

where the vector $C^r = (c^r_0, ..., c^r_{J-1})^t$ is obtained by solving the linear system

$$H^r_J C^r = \xi^r_J.$$

Thus, the projection points $P^{\ell,r}_j$ are given by the following theorem, which generalizes theorem 5.

Theorem 7. *Let B^r, for $r = a, b, c$, be the companion matrices defined in (2.40). Assume that the projected points $P^{\ell,r}_j$ of $\boldsymbol{S}^\ell_j$ are distinct and that $\nu^{K^\ell,r}_{j,\ell} \neq 0$ for $j = 1, ..., N^\ell$ and $\ell = 1, ..., L$. Then,*

1. *B^r admits N^ℓ eigenvalues of multiplicity $K^\ell + 1$ for $\ell = 1, ..., L$.*
2. *The N^ℓ eigenvalues of multiplicity $K^\ell + 1$ are the projections $P^{\ell,r}_j$ of the point sources $\boldsymbol{S}^\ell_j$.*

* * *

Proof: The proof of this theorem follows from (2.36), (2.37) and (2.39). □

3. Determination of the vectors Λ^r

In order to determine $\nu_{j,\ell}^{\beta,r}$, it is sufficient, to solve the linear systems

$$A_0^r \Lambda^r = \xi_0^r.$$

Thanks to theorems 6, 7 and using Step 4 detailed in the previous subsection, one can identify the locations $\mathbf{S}_j^\ell$.

Remark 10.

1. *Under conditions $\nu_{j,\ell}^{K^\ell,r} \neq 0$, the projections of source locations are uniquely determined as well as $\nu_{j,\ell}^{\beta,r}$ but not necessarily the intensities $\lambda_{j,\ell}^{\{\alpha_1,\alpha_2,\alpha_3\}}$.*
2. *The hypothesis $\nu_{j,\ell}^{K^\ell,r} \neq 0$, in Theorem 6 and Theorem 7 is not satisfied for the source example $F = \mu\delta_{\mathbf{S}} + \Delta\delta_{\mathbf{S}}$. In fact, it is easy to verify that $\nu_{1,1}^{2,r} = 0$.*
3. *Note that, if $\mu = 0$, it is possible to identify the quantities $\lambda_{j,\ell}^{\{0,0,0\}}$, $\lambda_{j,\ell}^{\{1,0,0\}}$, $\lambda_{j,\ell}^{\{0,1,0\}}$ and $\lambda_{j,\ell}^{\{0,0,1\}}$. In fact, from the definitions of $\nu_{j,\ell}^{\beta,r}$, it is easy to see that*

$$\lambda_{j,\ell}^{\{0,0,0\}} = -\nu_{j,\ell}^{0,a}$$

and

$$\begin{pmatrix} \lambda_{j,\ell}^{\{1,0,0\}} \\ \\ \lambda_{j,\ell}^{\{0,1,0\}} \\ \\ \lambda_{j,\ell}^{\{0,0,1\}} \end{pmatrix} = \begin{pmatrix} 1 & i & 0 \\ 0 & 1 & i \\ 1 & 0 & i \end{pmatrix}^{-1} \begin{pmatrix} -\nu_{j,\ell}^{1,a} \\ \\ -\nu_{j,\ell}^{1,b} \\ \\ -\nu_{j,\ell}^{1,c} \end{pmatrix}.$$

2.3. Some distributed sources

In this section, we consider two classes of distributed sources, sources supported on the hollow/solid balls and sources having compact support within a finite number of subdomains. Then, in Subsection 2.3.3, an application to the problem of identifying general poles of meromorphic function is shown.

2.3.1. Sources supported on the hollow/solid balls and spheres

Let F be the following source term

$$F = \sum_{j=1}^{N} h_j \chi_{D_j} \quad \text{with} \quad D_j = \mathbf{S}_j + B_j \tag{2.41}$$

where we have assumed, here, that h_j are non-null scalar quantities and B_j are hollow or solid balls of center $(0,0,0)$ and radii r_0^j, r_1^j, namely,

$$B_j = \{\mathbf{S} = (x,y,z) \in \mathbb{R}^3 \quad : \quad 0 \leq r_0^j < |\mathbf{S}| \leq r_1^j\}.$$

We say that B_j is a hollow ball if $r_0^j > 0$ and a solid ball if $r_0^j = 0$. In this framework, it is well known that, with a single coefficient μ, both h_j and D_j cannot be uniquely determined from the Cauchy data. However, we show below that the number N, the centers $\mathbf{S}_j$ and some related quantities to h_j can be uniquely determined. For both results, we need the following lemma given in [CH89, Page 288].

Lemma 3. *For every solution of the equation $\Delta u + \mu u = 0$ in Ω, the mean value relation*

$$u(\boldsymbol{S}) \frac{\sin(r\sqrt{\mu})}{r\sqrt{\mu}} = \frac{1}{4\pi r^2} \int_{\Sigma} u d\Sigma \tag{2.42}$$

is valid for any sphere Σ of center $\boldsymbol{S}$ and radius r entirely contained in Ω.

1.Non-uniqueness of source $F = h\chi_D$: (Counter example found in [EBN11a])

Suppose there are two different sources $F_i = h_i \chi_{D_i}$ where D_i are two hollow or solid balls with the same center S and different radii r_0^i, r_1^i, $i = 1, 2$, such that

$$h_1 \int_{r_0^1}^{r_1^1} r \frac{\sin\left(\sqrt{\mu} r\right)}{\sqrt{\mu}} \, dr = h_2 \int_{r_0^2}^{r_1^2} r \frac{\sin\left(\sqrt{\mu} r\right)}{\sqrt{\mu}} \, dr. \tag{2.43}$$

Let u_i, $i = 1, 2$, be 2 functions such that

$$\Delta u_i + \mu u_i = F_i \quad \text{in} \quad \Omega, \qquad u_1 = u_2, \frac{\partial u_1}{\partial \nu} = \frac{\partial u_2}{\partial \nu} \quad \text{on} \quad \Gamma.$$

Define the function w as the solution of

$$\begin{cases} \Delta w + \mu w = F_2 - F_1 & \text{in} \quad \Omega \\ \\ w = 0 & \text{on} \quad \Gamma \end{cases} \tag{2.44}$$

Multiplying equation (2.44) by v, an arbitrary function in $\mathcal{H}_\mu$ as defined in (2.8), and integrating by parts, we get

$$\int_\Gamma \frac{\partial w}{\partial \nu} v\, ds = h_2 \int_{D_2} v(x)\, dx - h_1 \int_{D_1} v(x)\, dx$$

using Lemma 3 and integrating (25) over $[r_0^i, r_1^i]$, one has

$$h_2 \int_{D_2} v(x)\, dx - h_1 \int_{D_1} v(x)\, dx = 4\pi h_2 v(S) \int_{r_0^2}^{r_1^2} r \frac{\sin(\sqrt{\mu} r)}{\sqrt{\mu}}\, dr - 4\pi h_1 v(S) \int_{r_0^1}^{r_1^1} r \frac{\sin(\sqrt{\mu} r)}{\sqrt{\mu}}\, dr.$$

Then, from the imposed condition (2.43) on the sources, one obtains

$$\int_\Gamma \frac{\partial w}{\partial \nu} v\, ds = 0.$$

But, since $H^{\frac{1}{2}}(\Gamma)$ is dense $L^2(\Gamma)$, one has

$$\frac{\partial w}{\partial \nu} = 0 \quad \text{on} \quad \Gamma.$$

Hence, both u_1 and $u_2 = u_1 + w$ are solutions of the problem for the same source F_1. Thus, one confirms the non-uniqueness of the reconstruction of both h_j and D_j by the Cauchy data with a single μ.

2. Identification method

Under the condition

$$\int_{r_0^j}^{r_1^j} \sin(\sqrt{\mu} r)\, dr \neq 0,$$

one can, using the identification method proposed in Subsection 2.2.2, uniquely determine the number N, the projections $P_j^r, r = a, b, c$ of the centers $\mathbf{S}_j$ and the quantities $h_j \int_{r_0^j}^{r_1^j} r \frac{\sin(r\sqrt{\mu})}{\sqrt{\mu}}\, dr$, where we define the square root of μ in the complex meaning if μ is negative.

Indeed, using the functional $\mathcal{R}$ defined in (2.9) and having the sources of the form (2.41), we get, for all v in $\mathcal{H}_\mu$,

$$\mathcal{R}(v,f,g) = \sum_{j=1}^{N} h_j \int_{D_j} v(x)\,dx$$

Thus, from Lemma 3, one has

$$\mathcal{R}(v,f,g) = \sum_{j=1}^{N} 4\pi h_j v(\mathbf{S}_j) \int_{r_0^j}^{r_1^j} r \frac{\sin(\sqrt{\mu} r)}{\sqrt{\mu}}\,dr.$$

Now, denoting

$$p_j = 4\pi h_j \int_{r_0^j}^{r_1^j} r \frac{\sin(\sqrt{\mu} r)}{\sqrt{\mu}}\,dr,$$

and using the test functions defined in (2.11,2.14), we apply the same algebraic algorithm proposed in Subsection 2.2.2 to recover the number of balls N, the projections onto the xy, yz and xz- planes of the centers $\mathbf{S}_j$ and the coefficients p_j related to h_j and the radii r_0^j and r_1^j.

Remark 11. *A similar result to that announced in the previous theorem can be also obtained in the case of source supported on a sphere.*

2.3.2. Identification method for sources of small supports

Now, assume that F represents sources having compact support within a finite number of small subdomains, namely

$$F = \sum_{j=1}^{N} h_j \chi_{D_j} \quad \text{with} \quad D_j = \mathbf{S}_j + \varepsilon B_j \tag{2.45}$$

where $\mathbf{S}_j = (x_j, y_j, z_j)$ and $B_j \subset \mathbb{R}^3$ is a bounded domain containing the origin. The points $\mathbf{S}_j \in \Omega$ are assumed to be mutually distinct, ε is a positive real number strictly less than 1 and the densities h_j are non-null functions belonging to the space $L^1(\Omega)$.

The inverse source problem we are concerned with, here, consists in determining the number N, the centers $\mathbf{S}_j$ and the mass of the domains D_j.

Indeed, as in (2.10), multiplying equation (2.1) by a test function v belonging to $\mathcal{H}_\mu$ and integrating by parts, we get for the source (2.45), the following relationship between the Cauchy data (f,g) and the source F,

$$\mathcal{R}(v,f,g)=\sum_{j=1}^{N}\int_{D_j} h_j(\mathbf{S})v(\mathbf{S})d\mathbf{S},\quad \text{for all}\quad v\in\mathcal{H}_\mu.$$

Here, $\mathcal{R}$ is the operator defined in (2.9) and $\mathbf{S}=(x,y,z)$.

Then, using the change of variables $\mathbf{S}=\mathbf{S}_j+\varepsilon t$ with $t=(t_1,t_2,t_3)$, one obtains

$$\mathcal{R}(v,f,g)=\sum_{j=1}^{N}\varepsilon^3\int_{B_j}\tilde{h}_j(t)v(\mathbf{S}_j+\varepsilon t)dt,\quad \text{for all}\quad v\in\mathcal{H}_\mu, \tag{2.46}$$

where $\tilde{h}_j(t)=h_j(\mathbf{S}_j+\varepsilon t)$.

Now, using in equations (2.46) the test functions v_n^a, defined in (2.11), we get

$$\mathcal{R}(v_n^a,f,g)=\sum_{j=1}^{N}\varepsilon^3 e^{kz_j}\int_{B_j}\tilde{h}_j(t)[(x_j+iy_j)+\varepsilon(t_1+it_2)]^n e^{k\varepsilon t_3}dt,\quad n\in\mathbb{N} \tag{2.47}$$

and consequently since

$$[(x_j+iy_j)+\varepsilon(t_1+it_2)]^n=\sum_{\beta=0}^{n}\binom{n}{\beta}\varepsilon^\beta(t_1+it_2)^\beta(x_j+iy_j)^{n-\beta},$$

we get

$$\mathcal{R}(v_n^a,f,g)=\sum_{j=1}^{N}\sum_{\beta=0}^{n}\nu_j^{\beta,a}\tbinom{n}{\beta}(P_j^a)^{n-\beta},\quad \text{for all}\quad n\in\mathbb{N} \tag{2.48}$$

where

$$\nu_j^{\beta,a}=\varepsilon^{3+\beta}e^{kz_j}\int_{B_j}\tilde{h}_j(t)[t_1+it_2]^\beta e^{k\varepsilon t_3}dt,$$

$$P_j^a = x_j + iy_j$$

and

$$\binom{n}{\beta} = \begin{cases} \frac{n!}{\beta!(n-\beta)!} & \text{if } n \geq \beta \\ 0 & \text{if } n < \beta. \end{cases}$$

Remark 12. *When $k = 0$, $\nu_j^{0,a}$ corresponds to the mass of the domain D_j and $\nu_j^{1,a}$ correspond to the projection of its moments onto the xy-plane.*

Now, observe that the equations (2.48) do not allow us to identify the source F directly because they contain more unknowns than equations. To overcome this difficulty, we will truncate these equations from a small error. First, for a given positive $\varepsilon < 1$, we choose a fixed integer K such that ε^{K+4} is small enough and we set

$$\alpha_n^a = \sum_{j=1}^{N} \sum_{\beta=0}^{K} \nu_j^{\beta,a} \tbinom{n}{\beta} (P_j^a)^{n-\beta}, \quad \text{for all} \quad n \in \mathbb{N}. \tag{2.49}$$

Then, according to (2.48), we can see that, for $n \leq K$

$$\mathcal{R}(v_n^a, f, g) = \sum_{j=1}^{N} \sum_{\beta=0}^{n} \nu_j^{\beta,a} \tbinom{n}{\beta} (P_j^a)^{n-\beta} = \sum_{j=1}^{N} \sum_{\beta=0}^{K} \nu_j^{\beta,a} \tbinom{n}{\beta} (P_j^a)^{n-\beta} = \alpha_n^a$$

and for $n > K$

$$\mathcal{R}(v_n^a, f, g) = \sum_{j=1}^{N} \sum_{\beta=0}^{n} \nu_j^{\beta,a} \tbinom{n}{\beta} (P_j^a)^{n-\beta} = \alpha_n^a + O(\varepsilon^{K+4})$$

where

$$O(\varepsilon^{K+4}) = \sum_{j=1}^{N} \sum_{\beta=K+1}^{n} \nu_j^{\beta,a} \tbinom{n}{\beta} (P_j^a)^{n-\beta}.$$

Finally, we approximate the coefficients α_n^a by $\mathcal{R}(v_n^a, f, g)$ and then we determine the quantities N, P_j^a, $\nu_j^{\beta,a}$ by solving the algebraic equations (2.49) by means of the the algebraic algorithm developed in Subsection 2.2.2. More precisely, we begin by defining the complex Hankel matrix

$$H^a_{\bar{J},K} = \begin{pmatrix} \alpha^a_0 & \alpha^a_1 & \cdots & \alpha^a_{\bar{J}-1} \\ \alpha^a_1 & \alpha^a_2 & \cdots & \alpha^a_{\bar{J}} \\ \vdots & \vdots & \vdots & \vdots \\ \alpha^a_{\bar{J}-1} & \alpha^a_{\bar{J}} & \cdots & \alpha^a_{2\bar{J}-2} \end{pmatrix} \quad \text{for} \quad \bar{J} \in \mathbb{N}^*, \tag{2.50}$$

and we introduce the companion matrix

$$B^a_K = \begin{pmatrix} 0 & 1 & \cdots & 0 & 0 \\ 0 & 0 & 1 & \cdots & 0 \\ \vdots & \vdots & \ddots & \ddots & 0 \\ \vdots & \vdots & \ddots & \ddots & 1 \\ c^a_0 & c^a_1 & \cdots & \cdots & c^a_{J-1} \end{pmatrix} \quad \text{for} \quad J = (K+1)N, \tag{2.51}$$

where the vector $C^a = (c^a_0, ..., c^a_{J-1})^t$ is solution of the linear system

$$H^a_{J,K} C^a = \xi^a_J$$

with $\xi^a_J = (\alpha^a_J, \cdots, \alpha^a_{2J-1})^t$ and then, we obtain from Theorem 6 and Theorem 7 the following corollary.

Corollary 1. *Let K be a non-negative integer, $J = (K+1)N$ and $H^a_{\bar{J},K}$ be the Hankel matrix defined in (2.50). Assume that we know an upper bound $\bar{J}$ for the number J, then*

$$\textit{rank}(H^a_{\bar{J},K}) = (K+1)N \quad \textit{if and only if} \quad \nu^{K,a}_j \neq 0 \quad \textit{for} \quad j = 1, ..., N.$$

Corollary 2. *Let K be a non-negative integer, $J = (K+1)N$ and assume that $\nu^{K,a}_j \neq 0$ for all $j = 1, ..., N$. Then, the companion matrix B^a_K, defined in (2.51), admits N eigenvalues of multiplicity $K+1$. These eigenvalues are the projections P^a_j of points $\boldsymbol{S}_j$ onto the xy complex plane.*

Corollaries 1 and 2 allow us to identify the number N, the projection points P^a_j and the coefficients $\nu^{\beta,a}_j$ as done in Section 2.2.2.

Remark 13. *In practice, for a given positive constant $\varepsilon < 1$, we choose the integer K such that ε^{K+4} is small enough. Then, we estimate the coefficients α^a_n defined in*

(2.49) by $\mathcal{R}(v_n^a, f, g)$. This introduces an accuracy error $O(\varepsilon^{K+4})$ in our identification algorithm, precisely, in determining of the rank of Hankel matrix $H_{J,K}^a$ and the eigenvalues of companion matrix B_K^a (see [Ste73a, p. 321-322] for estimating result on SVD). Therefore, through corollaries 1 and 2 respectively, we can find, modulo a small error, the number of sources and the projections (onto the xy complex plane) of their positions. To determine the position of the point sources, we proceed as in Subsection 2.2.1 and we repeat the same algorithm by making projections onto the $xz-$ and $yz-$complex planes, considering the test functions v_n^b and v_n^c defined in (2.14).

2.3.3. Remark on the problem of identifying general poles of meromorphic functions

In here, our aim is to show that our algorithm can be applied to the interesting problem of computing the poles of a meromorphic function f with a finite number of poles in a disc $\{|z| < R\}$

$$f(z) = \sum_{\ell=1}^{L}\sum_{j=1}^{N^\ell}\sum_{\beta=0}^{K^\ell} \frac{\nu_{j,\ell}^\beta}{(z - P_j^\ell)^{\beta+1}} + g(z), \quad |z| < R,$$

where g is an analytic function with no zero in the disc $\{|z| < R\}$. The inverse problem consists in identifying the locations P_j^ℓ, the coefficients $\nu_{j,\ell}^\beta$ and the number N^ℓ, by means of the value $f(z)$ on a circle $|z| = R$ enclosing all the general poles P_j^ℓ of the function f. Problems with less general functions have been considered by many other authors. We cite only the recent papers [CKC12; HR11; Nar12] where one can find all references dealing with this question. In fact, this question amounts to solve the algebraic relationships (2.30). Indeed, multiplying $f(z)$ by z^n and integrating on the circle $|z| = R$, we obtain the Laurent coefficients α_n of $f(z)$ around zero and using the residue theorem, we obtain

$$\alpha_n = \sum_{\ell=1}^{L}\sum_{j=1}^{N^\ell}\sum_{\beta=0}^{K^\ell} \nu_{j,\ell}^\beta \tbinom{n}{\beta} (P_j^\ell)^{n-\beta} \tag{2.52}$$

where

$$\alpha_n = \frac{1}{2\pi i}\int_{|z|=R} z^n f(z)dz.$$

Then, it is sufficient to solve the algebraic equations (2.52) using the method presented in Subsection 2.2.2.

Note that the presented algorithm employed to solve (2.52) can be seen as a interesting application of the much older Pade machinery used over inverse source problems.

2.4. Numerical simulations

In this section, we study numerically the robustness of the algebraic algorithm with respect to the different parameters interfering in the reconstruction process bringing out, in the case of monopoles and dipoles, the theoretical stability estimates obtained in [EBEH13] and recalled in (2.6) and (2.7).

From (2.6) and (2.7), one can see that several factors such as the number of sensors, the separability coefficient, the noise and the coefficient μ have an important effect on the stability of the identification process. In the following subsections, the impact of all these parameters is studied numerically.

Here, we focus on the identification of the number and the positions of the sources from the Cauchy data (f, g). The moments and the intensities can be calculated easily solving the linear system $A_0^r \Lambda^r = \xi_0^r$. It is rather interesting to note that the most essential part in the whole identification process is the reconstruction of the number of sources as to be seen later.

Indeed, the algebraic algorithm proposed in Subsection 2.2.1 is verified numerically in this subsection on dipole sources (the case of (2.5) with $p_j = q_j = 0$) with fixed moments at $\mathbf{r}_j = (1, 1, 1)$, on combinations of monopolar and dipolar sources (the case of (2.5) with $q_j = 0$) at fixed intensities $p_j = 1$ and fixed moments $\mathbf{r}_j = (1, 1, 1)$ and later on sources with small compact support (2.41). The numerical tests will be held over both Helmholtz equation firstly and then over the BLT problem. The case of monopole sources has been already considered in paper [EBN11a] for Helmholtz equation and later revisited in [AEBEH14c] for BLT problem. In this numerical study, the boundary Γ is assumed to be a unit sphere whose center is the origin O. The Cauchy data (f, g) on the boundary Γ are obtained by means of the fundamental solution of equation (2.1) in $\mathbb{R}^3$. In fact, f and g are respectively the trace and the normal trace of w on Γ, where w is the fundamental solution corresponding to F, defined in the free space as:

$$w(\mathbf{S}) = \sum_{j=1}^{N^1} p_j w_0(\mathbf{S} - \mathbf{S}_j^1) + \sum_{j=1}^{N^2} \mathbf{r}_j \cdot \nabla w_0(\mathbf{S} - \mathbf{S}_j^2)$$

where

$$w_0(\mathbf{S}) = \frac{-1}{4\pi}\frac{e^{k\rho}}{\rho}$$

with

$$\mu + k^2 = 0 \quad \text{and} \quad \rho = \sqrt{x^2+y^2+z^2}.$$

Moreover, the coefficients α_n^r are numerically computed using spherical coordinates over a uniform meshing of distributed points on the unit sphere.

Particular attention will be devoted to determining the number of sources. As mentioned before, theoretically their number is the rank of the Hankel matrices $H_{\bar{J}}^r$ which is numerically determined using the SVD method with an appropriate threshold. However, this is not always an easy matter since $H_{\bar{J}}^r$ is an ill-conditioned matrix. As a matter of fact, the $(J+1)$th singular value, σ_{J+1}, of $H_{\bar{J}}^r$ is theoretically zero, whereas when the perturbed $H_{\bar{J}}^r + \delta H_{\bar{J}}^r$ is given, one obtains a non zero σ_{J+1}. Therefore, in our study, due to the classical estimate,[Han98],

$$|\sigma_{J+1}| \leq \|\delta H_{\bar{J}}\|_F, \tag{2.53}$$

we truncate beyond a threshold inferior to $\|\delta H_{\bar{J}}\|_F$. Here, $\|\cdot\|_F$ is the corresponding Frobenius norm and $\delta H_{\bar{J}}$ is the perturbation of $H_{\bar{J}}$ that originates from the noise in data as well as from the numerical quadrature error using a finite number of sensors on Γ. This leads us then to study also the impact of the upper bound of sources, $\bar{J}$ since this latter increases the size de matrix $\delta H_{\bar{J}}^r$ and consequently its norm $\|\delta H_{\bar{J}}^r\|_F$.

Remark 14. *We draw the attention of the reader to the fact that in the case of M^2 sensors, the numerical error can be seen as noise equivalent to $(2\pi^2/M^2)$ perturbation. That is why, apart from the Subsection 2.5.1 dedicated to study the noise effect, we use the Cauchy data as non-noisy ones to see the identification process in an approximately ideal framework.*

Remark 15. *The calculation of $\|\delta H_{\bar{J}}\|_F$ is related to the numerical quadrature error. In here, this computation is not exact since we take into consideration just the numerical error $(2\pi^2/M^2)$ which is an approximate value. Nevertheless, in reality, $\delta H_{\bar{J}}$ depends also on the points $\mathbf{S}_j^\ell$ and on κ and consequently,*

$$\|\delta H_{\bar{J}}\|_F \simeq \bar{J}\frac{\sqrt{2}\pi}{M}\beta(\kappa, sources)$$

where β is the error related to the wave number and to the source positions. Therefore, *in the following, we aren't reasonably capable of using the truncation threshold $\|\delta H_{\bar{J}}\|_F$ in the analysis of the impacts of the wave number and the closeness of the sources over the identification process, unless we have a precise knowledge of β. Consequently, it is used uniquely in the analysis of the impact of the number of sensors and the number upper bound $\bar{J}$.*

2.5. Numerical results for Helmholtz equation

In this section, our choice is focused on the Helmholtz case and the wavenumber $\kappa = \sqrt{\mu}$ is fixed at $\kappa = 1.85\ m^{-1}$ (when assuming the sound source with the sound velocity of $340\ ms^{-1}$, the temporal frequency 100 Hz gives this wave number with the wavelength $3.4\ m$), except in the case where we study its influence on the localization accuracy in Subsubsection 2.5.1(f).

2.5.1. Determining number and position of dipole sources

In the following subsection, unless mentioned otherwise, we fix the number of dipoles at 3 at fixed moments $\mathbf{r}_j = (1, 1, 1)$, whose positions are taken as in Table 2.1 and we consider the projection on the xy plane.

j (location $\sharp$)	1	2	3
$\mathbf{S}_j^2$	(0.6,-0.3,0.1)	(-0.6,-0.4,0.0)	(0.5,0.5,0.2)

Table 2.1.: *The dipole positions.*

a. The impact of the number of sensors

The choice of the number of sensors is an important issue in the recovery of the number and the position of the sources. Refining more the mesh (here 25^2 to 100^2 sensors), as seen in Figure 2.2, permits us to approach better the true number of sources. Indeed, the gap between the 7^{th} and the 6^{th} singular value increases with respect to the number of sensors and the localization error decreases with higher mesh level. Respecting their corresponding $\|\delta H_{\bar{J}}^a\|_F$ (Table 2.2), we note that the number of sources can't be recovered with less than 50^2 sensors. Therefore, we conclude that this identification process necessitates the use of 50^2 sensors so that the number of dipoles and consequently their positions are well-approximated. For a better clarification, we present the numerical results explicitly in Table 2.3. As seen in Table 2.3, we observe that when imposing the rank of $H^a_{\bar{J}}$ as 6, with 25^2 sensors one obtains 6 eigenvalues that aren't even doubles while for a higher number of sensors, one obtains 3 double eigenvalues.

Number of sensors	25^2	35^2	50^2	100^2
$\|\delta H^a_8\|_F \simeq$	1.42	1.02	0.71	0.36

Table 2.2.: *The Frobenius norm of δH^a_8 with respect to the sensors.*

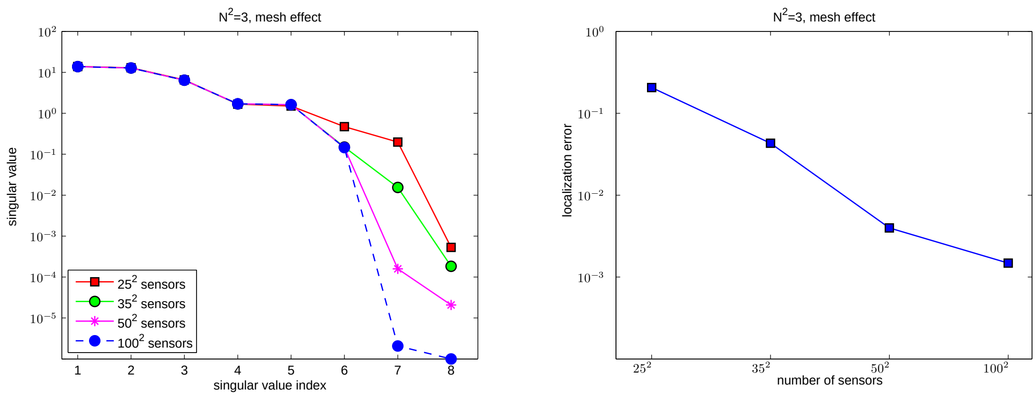

Figure 2.2.: *Singular value of H^a_8 (left) and the localization error (right) projected on the xy plane for $N^2 = 3$ with respect to the number of sensors.*

Number of sensors	Estimated 2D Positions	Localization Error level
25^2	-0.6824 - 0.5123i 0.6688 - 0.3713i -0.4997 - 0.1008i 0.5774 + 0.5467i 0.3924 + 0.2611i 0.0233 + 0.0676i	0.6436
35^2	-0.6025 - 0.3972i 0.5022 + 0.4907i 0.5710 - 0.3005i	0.063
50^2	-0.6000 - 0.4000i 0.5000 + 0.5000i 0.5998 - 0.3001i	0.006
100^2	-0.6000 - 0.4000i 0.5000 + 0.5000i 0.6000 - 0.2999i	0.002

Table 2.3.: *The calculated $xy-$ source positions and their error for $N^2 = 3$ varying the number of sensors.*

Remark 16. *Note that 50^2 sensors represent a suitable framework for the recovery of 3 dipoles. For a higher number of dipoles, one must provide their specific suitable framework also. For instance, one can even reconstruct precisely the position of 7 dipoles using 100^2 sensors (see Figure 2.3). Thus, as we have tested, meshing more finely leads also to identify much more dipoles. However, an even higher number of sensors becomes "unrealistic" since we are limited by the number of observations. Besides, for the instant the tests were done in a perfect non-noisy background. Whereas in the presence of noise, one can't improve the numerical results even with a higher discterization since the noise would dominate, beyond a certain level, the mesh error. The noise impact on the reconstruction method is taken into consideration and is analyzed in subsubsection g.*

From now on, we fix our study to 50^2 sensors that enable us to recover precisely the number and the location of up to 3 dipoles.

b. The impact of the upper bound $\bar{J}$

Our aim, in this subsubsection, is to discuss the effect of the supposed upper bound $\bar{J}$ on the identification of the number of the dipoles, J. Indeed, as seen in Figure

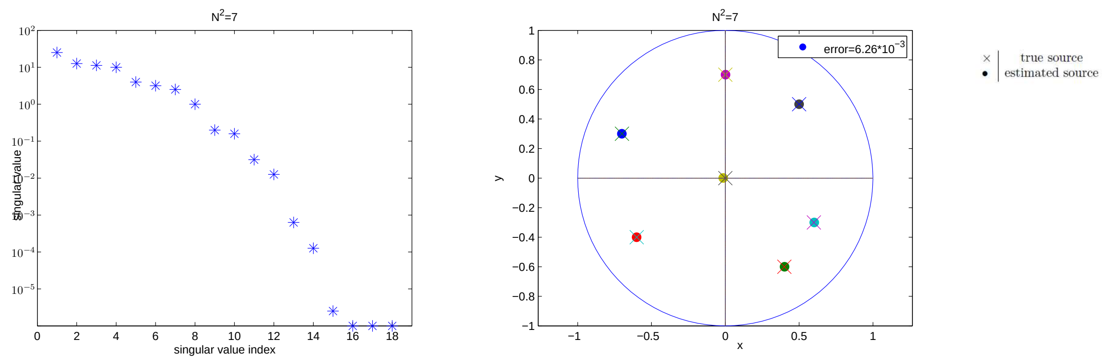

Figure 2.3.: *Singular values of H^a_{18} and the localization results projected on the xy plane for $N^2 = 7$ with 100^2 sensors.*

2.4, as $\bar{J}$ increases, the gap between the J^{th} and the $(J+1)^{th}$ singular values of $H^a_{\bar{J}}$ decreases. This is obvious since we know that the theoretical rank is fixed at J for whatever value of $\bar{J}$ and so increasing $\bar{J}$ accumulates more and more error on the corresponding Hankel matrix causing it to become more and more ill-conditioned. Moreover, since the calculation of the numerical rank of $H^a_{\bar{J}}$ is done by the means of the truncation threshold (2.53) based on the Frobenius norm of the perturbation $\delta H^a_{\bar{J}}$, presented in Table 2.4, we observe that exceeding a certain $\bar{J}$ ($\bar{J} = 11$ as seen in Figure 2.4), we aren't capable of estimating the theoretical rank J due to the high ill-conditionement of $H^a_{\bar{J}}$. Therefore, it is crucial to have an upper bound which isn't so far than the exact needed number of sources to accomplish a better identification process.

$\bar{J}$	7	9	11	13	15	17	19
$\|\delta H^a_{\bar{J}}\|_F \simeq$	0.6220	0.7997	0.9774	1.1551	1.3329	1.5106	1.6883

Table 2.4.: *The Frobenius norm of $\delta H^a_{\bar{J}}$ with respect to $\bar{J}$.*

c. What happens when the number is wrongly-estimated?

Suppose that due to a bad estimation of the rank of the Hankel matrix, we have cut the singular values either over or under the desired value. Doing that, we have noticed, as seen in Table 2.5 that truncating more than needed gives the real values of the locations and other additional disperse points (representing imaginary monopoles). However, truncating for a number less than desired, one obtains a combination of positions which aren't even related to the desired sources, as shown in

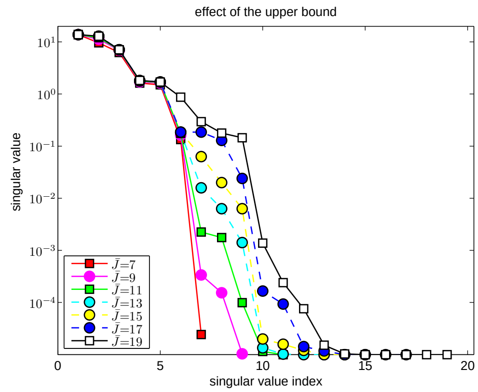

Figure 2.4.: *The localization error (right) for $N^2 = 3$ and 50^2 sensors with respect to $\bar{J}$.*

Table 2.5. This shows the importance of a good truncation threshold and consequently the essentiality of obtaining the right number of sources from the rank of the Hankel matrix.

truncation level	Estimated 2D Positions
8	0.808 + 1.082i -1.161 - 0.783i -0.5995 - 0.400i 0.500 + 0.500i 0.6000 - 0.3000i
5	-0.689 - 0.418i f-0.461 - 0.409i 0.685 - 0.410i 0.499 + 0.652i 0.727 + 0.312i

Table 2.5.: *The calculated $xy-$ source positions and their error for $N^2 = 3$ when truncating wrongly.*

d. Effect of the separability between dipoles

The separability between the sources plays a great role in the dipoles reconstruction and counts even more than the number of the sources themselves. To study its effect, we take 2 dipoles placed at $(\pm d, 0, 0)$ where d varies from 0.05 to 0.5 m and a fixed dipole S_3 (Table 2.1). One observes that if the distance between the 2 dipoles is really small, the dipoles could not be well-approximated where neither their number nor their position is well-reconstructed. On the other hand, as they become farther (remaining far from the boundary), we note a better numerical estimation of the rank of H_8^a, due to the larger gap between the 6^{th} and the 7^{th} singular values, as well as a better relative localization error as shown in Figure 2.5. This is explained by the decomposition of the Hankel matrix $H_{\bar{J}}^r$ given in Lemma 1. Indeed, due to (2.21), one can see that the conditionment of the Hankel matrix $H_{\bar{J}}^r$ depends on that of the Vandermonde matrix A_0^r. Moreover, since the condition number of A_0^r is analytically calculated as the multiplication of the separability between the source projections $P_j^{2,r}$, then the numerical rank estimation of the Hankel matrix becomes worse as the sources become closer.

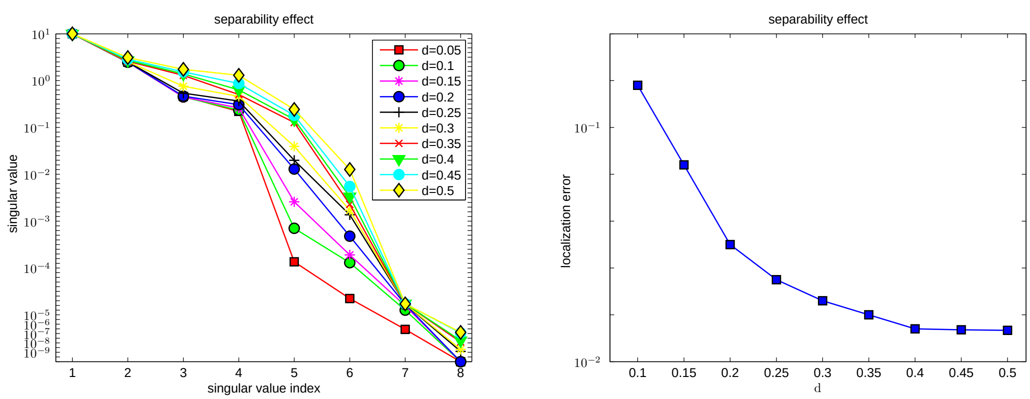

Figure 2.5.: *Singular values of H_8^a (left) and the localization errors (right), projected on the xy plane with 50^2 sensors, with respect to the position of the sources.*

As seen just above, the reconstruction of the sources depends on the separability coefficient between the projected locations. Therefore, an important factor in the identification process is the choice of the projection plane that would yield to a good separability between the sources and consequently a more precise localization. To do so, in a practical point of view, a strategy that could be utilized is that mentioned previously in Remark 8. More precisely, for a $m_1 \times m_2$ discretization points (ϕ_i, θ_j) over the box $[0, \frac{\pi}{2}] \times [0, 2\pi]$, we consider the corresponding orthonormal basis $(\vec{u_{ij}}, \vec{v_{ij}}, \vec{u_{ij}} \wedge \vec{v_{ij}})$ where $\vec{u_{ij}} = (\cos(\phi_i)\cos(\theta_j), \cos(\phi_i)\sin(\theta_j), \sin(\phi_i))$ and $\vec{v_{ij}} = (\sin(\phi_i)\cos(\theta_j), \sin(\phi_i)\sin(\theta_j), -\cos(\phi_i))$. Then, for each basis, we calculate, for all $1 \leq i \leq m_1$, $1 \leq j \leq m_2$, the numerical rank of the three Hankel matrices $(H^r_{\bar{J}})_{ij}$, $r = a, b, c$ (which represent the three plane projections in the considered basis), always respecting the truncation threshold (2.53). Consequently, the number of sources is obtained as the maximum between these three ranks. Now, to recover most precisely the projected sources locations, few steps should be done. First, one should choose only the space frames having $rank((H^r_{\bar{J}})_{ij}) = J$ for $r = a, b, c$. The existence of such a basis is possible due to the natural hypothesis that these sources are well-separated. Next, we calculate the condition numbers a_{ij}, b_{ij} and c_{ij} of the corresponding Hankel matrices $(H^r_J)_{ij}$. Finally, to obtain the basis $(u_{ij}, v_{ij}, u_{ij} \wedge v_{ij})$ with the best location estimation, we choose the frame with the best conditionement of $(H^r_J)_{ij}$ which corresponds, as mentioned before, to the best conditionement of $(A^r_0)_{ij}$ and consequently the highest separability coefficient. Technically, the basis containing the matrices $(H^r_J)_{ij}$ with the best condition numbers is obtained in the sense of having the smallest Euclidean distance between (a_{ij}, b_{ij}, c_{ij}) and the vector $(1, 1, 1)$.

Remark 17. *Note that the precision quality of the number and the location of the sources depends also on the augmentation of the number of sources that affects the separability coefficient between the projected points. Indeed, the reason behind the fact that adding more sources leads to less precision in the identification process is due to the diminishment of their separability coefficient, considering a size-fixed domain.*

e. Obtaining the 3D coordinates and the effect of the separability coefficient

To obtain the 3D coordinates of the sources, we use consequently the projections on the xy, yz and xz planes in the case of 3 dipoles as shown in Figure 2.6 and Figure 2.7. Note that, theoretically according to hypothesis **(H)** the number of sources must be the same whatever the complex plane onto which the projections are performed. However, numerically the situation may be different since the number depends also on the separability of these projections. In fact, to recover their number, we consider the numerical rank of the three Hankel matrices $H^r_{\bar{J}}$, $r = a, b, c$, obtained respecting the truncation threshold upper bounded by $\|\delta H^r_8\|_F \simeq 0.71$ and then take the maximum between them as shown in Figure 2.6. Note that this is validated by the example given in Figure 2.6 and Figure 2.7 which reflect the largest gap between the 6th and the 7th singular value of H^r_8 in the xy plane which has the highest separability coefficient between the projections.

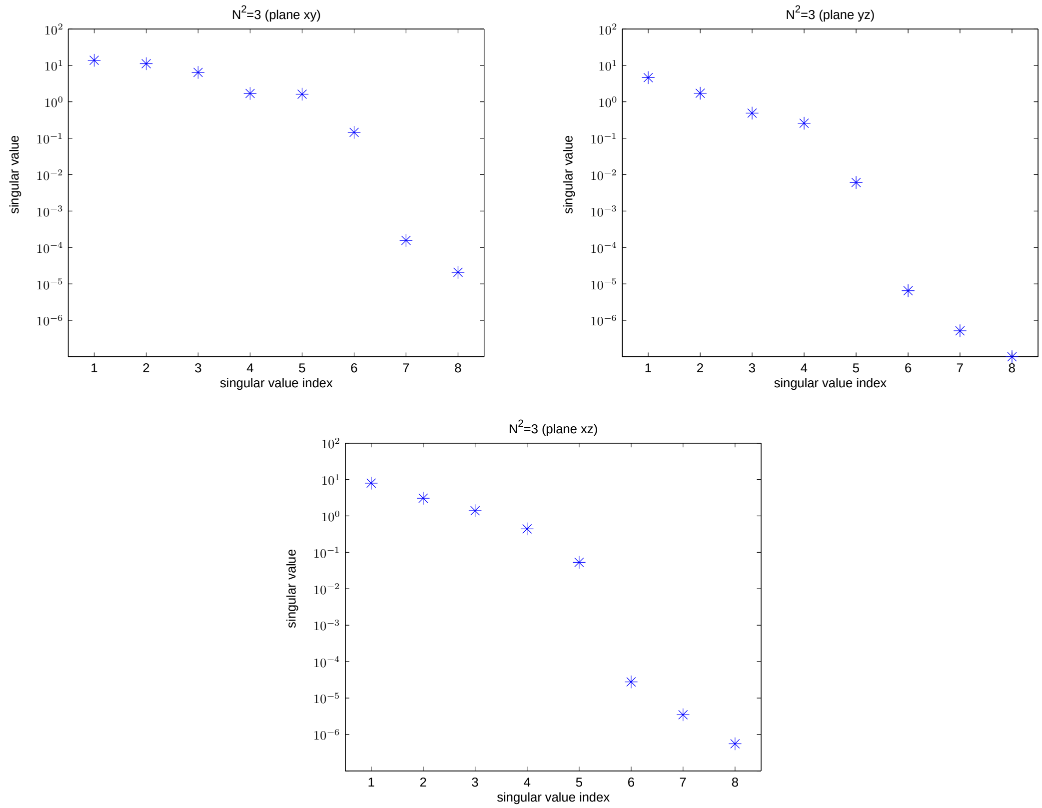

Figure 2.6.: *Singular values of* H_8^r *for* $N^2 = 3$ *where* $r = a, b, c$.

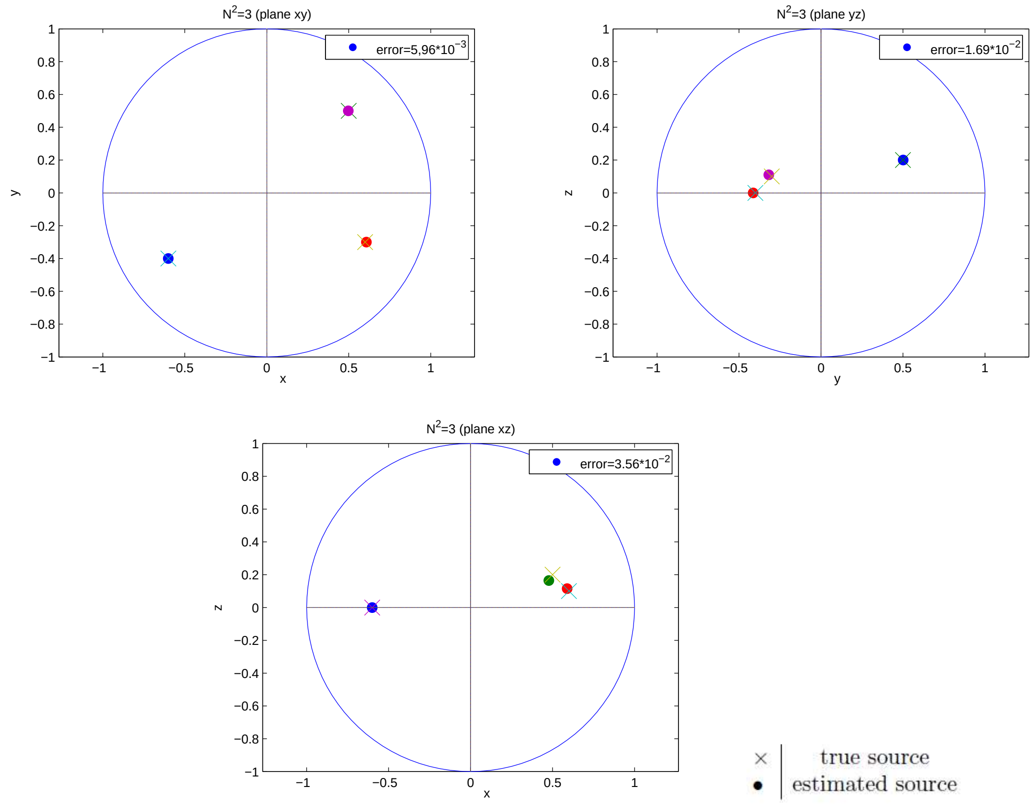

Figure 2.7.: *Estimation results projected on the xy,yz and $xz-$ planes when $N^2 = 3$.*

f. Impact of the wavenumber

The left and the right panels of Figure 2.8 show the singular values of H_8^a and the localization error when changing κ. We note that the gap between the 6^{th} and the 7^{th} singular value of H_8^a decreases and the position accuracy increases minorly with respect to κ which means the deterioration of the results with the increase of the wavenumber coefficient. This result could be explained since the number of points per wavelength defined by

$$p \approx \frac{\sqrt{\pi}}{\kappa} \times \sqrt{number of sensors}$$

decreases as κ augments. In fact, when taking $\kappa = 2$, the number of points touched by the wavelength are about 44 points. However, this number is limited to approximately 12 points when $\kappa = 7$.

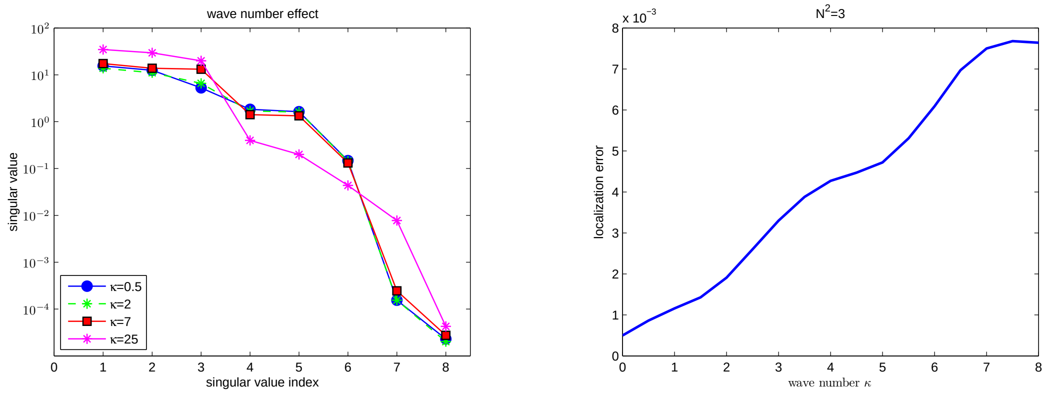

Figure 2.8.: *Singular values of H_8^a (left) and the localization error (right)when $N^2 = 3$ with 50^2 sensors with respect to the wavenumber.*

g. Impact of the noise

Reconstruction stability on the xy projections with respect to the noise level is examined in this subsubsection. In fact, Gaussian noise is added to f (and g) where the noise standard deviation added varies from 10^{-2} to 10^0 % (see Figure 2.9). We have noted studying the SVD of the Hankel matrix $H_{\bar{J}}^a$ and using the truncation threshold 2.53, with $\|\delta H_8^a\|_F$, computed in Table 2.6, that the number of dipoles is well estimated when the percentage of noise doesn't exceed $10^0\%$. Beyond that, their number is not well determined anymore. Moreover, we note that the localization error increases as the percentage of the noise added increases.

Noise percentage	$10^{-2}\%$	$10^{-1}\%$	$10^{0}\%$	$10^{1}\%$
$\|\delta H_8^a\|_F \simeq$	0.71	0.71	0.72	0.81

Table 2.6.: *The Frobenius norm of δH_8^a with respect to the noise.*

Remark 18. *Let us mention that we have, also, as to be seen in Section 2.6, studied the case of a negative number μ, the case of diffusion instead of propagation.*

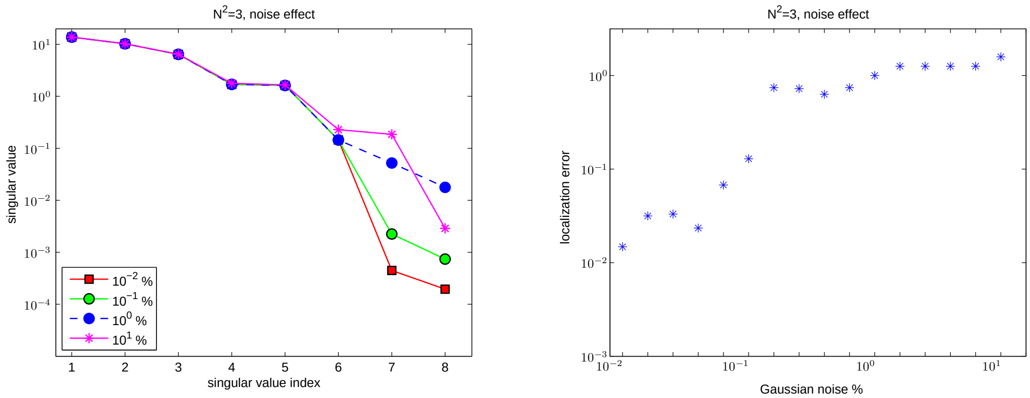

Figure 2.9.: *Singular values of δH_8^a (left) and the localization errors (right) projected on the xy plane for $N^2 = 3$ with 50^2 sensors with respect to the noise.*

2.5.2. Determining the number and the position of a combination of monopoles and dipoles

Now, we aim to reconstruct a combination of monopoles and dipoles. Applying the same methodology utilized over the dipoles, one can observe that the same phenomena can be noted regarding the different parameters over the number of sources and their localization. Indeed, for instance in Figure 2.10, we study the effect of the mesh level on the identification process for 2 monopoles (defined in Table 2.7) with the former 3 dipoles in the xy projection plane. We note the same results as before, for both, the variation of the singular values of H_{10}^a and the localization precision. Moreover, based on $\|\delta H_{10}^a\|_F$ computed in Table 2.8, 100^2 sensors are needed for the number identification. We have decided not to present the impact of $\bar{J}$, the separability coefficient, the projection plane, the wave number and the noise since they are similar to those presented just before.

For a better clarification, the numerical results are presented in Table 2.9.

j (location $\sharp$)	1	2
$\mathbf{S}_j^1$	(-0.7,0.3,-0.2)	(0.0,0.7,0.1)

Table 2.7.: *The source positions.*

Number of sensors	25^2	35^2	50^2	100^2
$\|\delta H_{10}^a\|_F \simeq$	1.78	1.27	0.89	0.44

Table 2.8.: *The Frobenius norm of δH_{10}^a with respect to the sensors.*

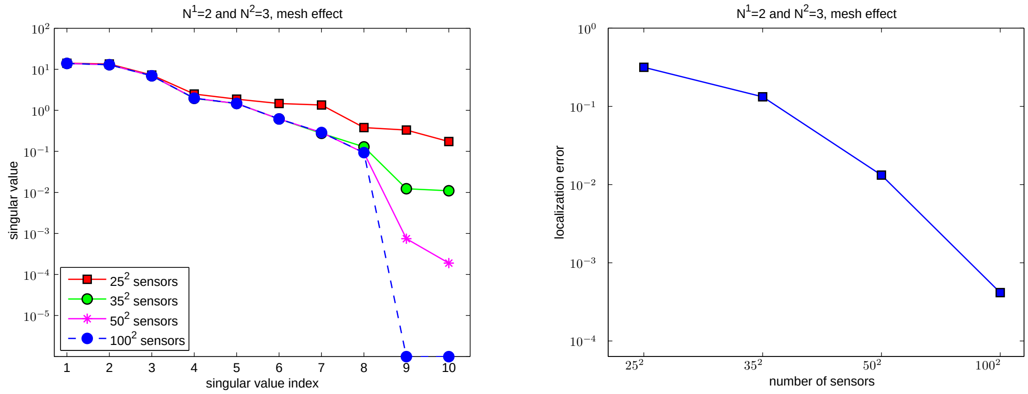

Figure 2.10.: *Singular values of δH_{10}^a (left) and the localization errors (right) projected on the xy plane for $N^1 = 2$ with $N^2 = 3$.*

2.5.3. Comparison between monopole and dipole sources

In this subsection, we perform a comparison of the proposed reconstruction method on the monopoles (sources of form (2.3) with $L = 1$ and $K^1 = 0$) and the dipoles. We consider the monopoles as defined in Table 2.10 and we focus on the impact of the number of sensors and the noise of this type of sources to establish the differences.

a. The impact of the number of sensors

Consider Figure 2.2 and Figure 2.11 related to the dipoles and the monopoles respectively with respect to the number of sensors. Comparing these figures, we observe that a less number of sensors are required for the reconstruction of monopoles than dipole sources. Indeed, based on $\|\delta H_8^a\|_F$ calculated in Table 2.2 and on Figure 2.11, we note that, for 6 monopoles, 35^2 sensors are sufficient for the sources number determination. Whereas, 50^2 sensors are needed for the dipoles number reconstruction. Moreover, the localization accuracy is much better comparing the right panels of the corresponding figures. Note that this result was expected.

Number of sensors	Estimated eigenvalues	Localization Error level
25^2	-1.9705 - 1.2132i 0.1176 + 0.9867i 0.6764 + 0.5779i 0.9129 - 0.1711i 0.6647 - 0.4600i -0.6927 + 0.3868i -0.7091 - 0.5103i -0.2095 - 0.4154i	0.5010
35^2	-0.7467 + 0.2863i -0.6568 - 0.4532i -0.4552 - 0.3448i -0.1603 + 0.5526i 0.2901+ 0.6508i 0.5924 + 0.5139i 0.6482 - 0.3059i 0.5145 - 0.3146i	0.1233
50^2	-0.7002 + 0.2994i -0.6064 - 0.4094i -0.5929 - 0.3898i 0.0002 +0.6975i 0.6105 - 0.3002i 0.5885 - 0.3008i 0.5201 + 0.5076i 0.4751 + 0.4914i	0.0121
100^2	-0.7000 + 0.2999i 1.7545e-06 + 0.6999i 0.6005 - 0.2995i 0.5995 -0.3006i -0.5996 - 0.4001i -0.6004 - 0.3999i 0.5009 + 0.5009i 0.4991 + 0.4990i	6.2e-04

Table 2.9.: *The calculated $xy-$ source positions and their error for $N^1 = 2$ with $N^2 = 3$ varying the number of sensors.*

b. Impact of the noise

Figure 2.12 represents the noise effect on the 6 monopoles in the same framework as in Figure 2.9. Comparing these 2 figures, we remark that the error caused by the

j	1	2	3	4	5	6
$\mathbf{S}_j^1$	(-0.7,0.3,-0.2)	(0.6,-0.3,0.1)	(0.5,0.5,0.2)	(-0.6,-0.4,0.0)	(-0.1,-0.6,0.4)	(-0.2,0.7,0.5)

Table 2.10.: *The monopoles positions.*

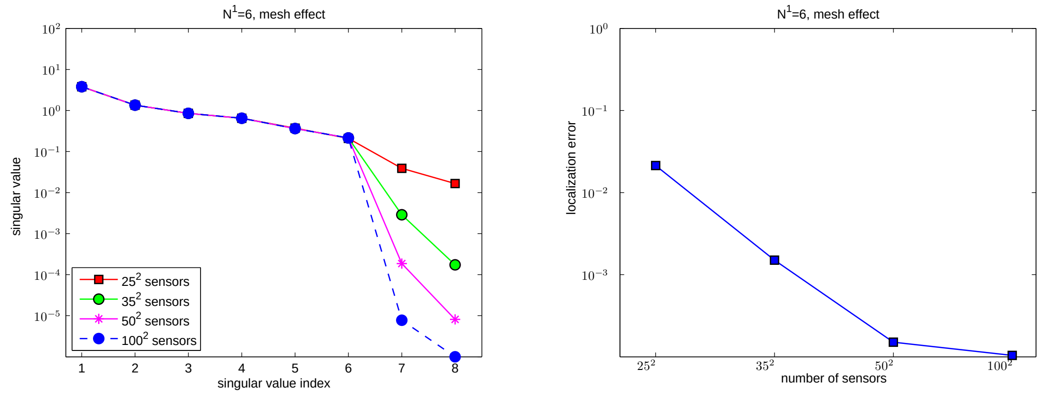

Figure 2.11.: *Singular value of H_8^a (left) and the localization error (right) projected on the xy plane for $N^1 = 6$ with respect to the number of sensors.*

noise on monopoles is much less than that on dipoles. This means that monopoles are more persistent with respect to the noise which is consistent with the stability estimates (2.6) and (2.7).

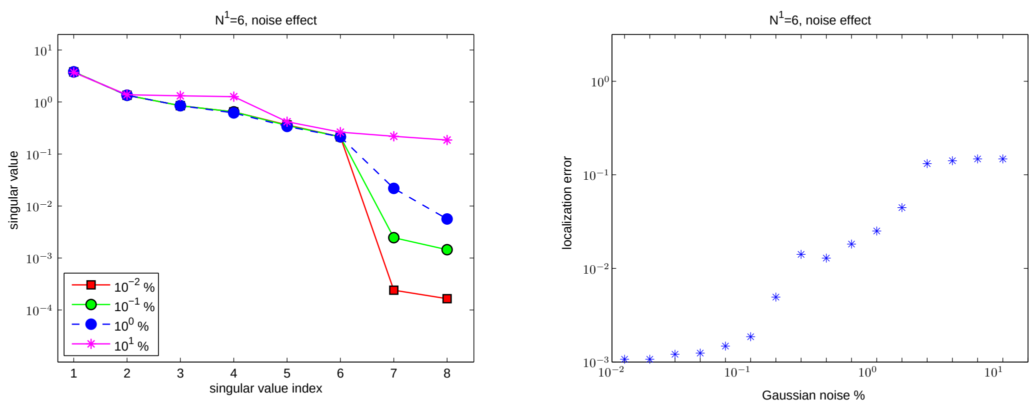

Figure 2.12.: *Singular values of H_8^a (left) and the localization errors (right), projected on the xy plane with 50^2 sensors, for $N^1 = 6$ with respect to the noise.*

2.5.4. Determining number, position and radius of sources supported on solid balls

In here, we aim to recover sources with solid balls support. To do so, we consider sources supported over balls of the form (2.41). As shown in Subsection 2.3.1,

$$\mathcal{R}(v) = \sum_{j=1}^{N} p_j v(\mathbf{S}_j)$$

where

$$p_j = 4\pi h_j \int_{r_0^j}^{r_1^j} r \frac{\sin\left(\sqrt{\mu} r\right)}{\sqrt{\mu}}\, dr$$

and $\mathbf{S}_j$ represent the centers of the N balls. Using the test functions v_n^a defined in (2.11) and considering 5 small balls with equal intensities $h_j = 1, j = 1, .., 5$, one observes, as shown in Figure 2.13, that the number, the center and the radius (taking equal radii R) of the balls are well-reconstructed. In fact, the radius R can be computed using the calculated coefficients p_j given by

$$p_j = 4\pi \int_{0}^{R} r \frac{\sin\left(\sqrt{\mu} r\right)}{\sqrt{\mu}}\, dr.$$

Indeed, integrating this integral over $(0, R)$, we obtain the equation

$$-\kappa R \cos \kappa R + \sin \kappa R = \frac{\kappa^3 p_1}{4\pi},$$

which is needed to recover the radius R over the interval $(0, 1)$ (since the circles belongs to the domain).

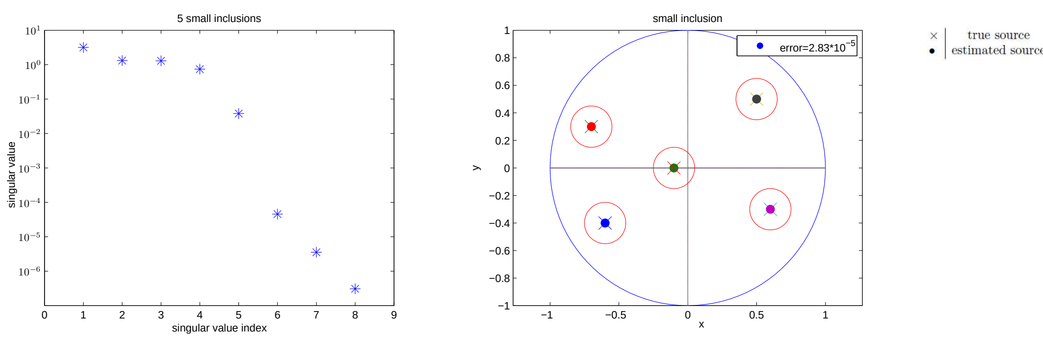

Figure 2.13.: Singular values of H_8, and the localization results projected on the xy plane for 5 balls with 50^2 sensors.

2.6. Numerical results in the BLT case

In this section, our choice focuses on the BLT case for which the absorption coefficient will be fixed at $\mu = -0.35\ mm^{-1}$ (supposing that the source is in the lungs, the absorption coefficient of this organ is normally of value $-0.35\ mm^{-1}$, [Wan+06b]). Our basic aim in this section is to preform the same tests as done in the previous subsection in order to establish the difference between these cases belonging to the different signs of μ.

2.6.1. Determining number and position of dipole sources

In the following subsection, we fix the same 3 dipoles considered in the Helmholtz case whose moments are fixed at $\mathbf{r}_j = (1, 1, 1)$ and positions are also taken as in Table 2.1. Although that we have noticed that the results are similar, we show, for later comparison, the numerical simulations showing the impact of the parameters interfering in the reconstruction process. Here, the values of $\|\delta H_{\bar{J}}\|_F$ are taken as in Table 2.2 for the impact of sensors and as in Table 2.4 for the impact of $\bar{J}$.

a. The impact of the number of sensors

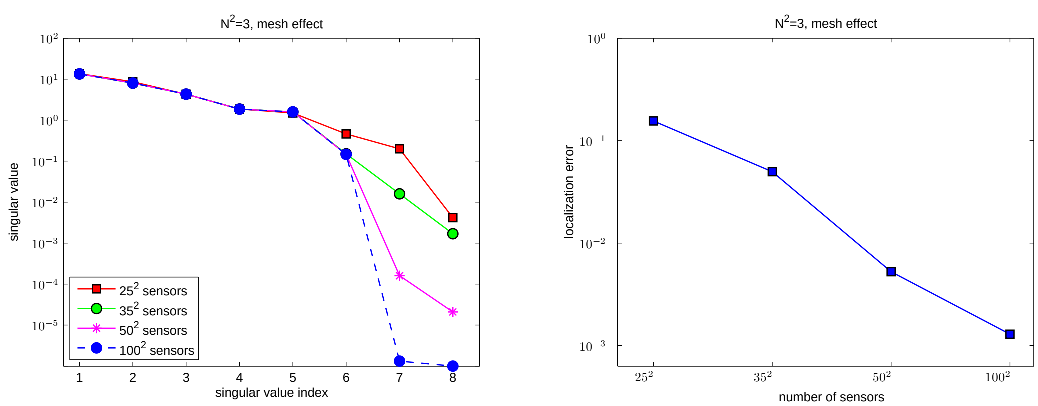

Figure 2.14.: *Singular value of H_8^a (left) and the localization error (right) projected on the xy plane for $N^2 = 3$ with respect to the number of sensors ($\mu < 0$).*

The numerical results are presented explicitly in Table 2.11.

Number of sensors	Estimated 2D Positions	Localization Error level
25^2	-0.6891 - 0.5113i -0.6175 - 0.1422i 0.6840 - 0.3796i 0.5458 + 0.5149i 0.4707 + 0.3962i 0.1311 - 0.2157i	0.1915
35^2	-0.6096 - 0.4418i -0.5988 - 0.3532i 0.6646 - 0.3346i 0.4798 - 0.2766i 0.4971 + 0.5519i 0.5098 + 0.4207i	0.070
50^2	-0.6001 - 0.4000i 0.5997 - 0.3002i 0.5001 + 0.4999i	0.0072
100^2	-0.6000 - 0.4000i 0.6000 - 0.3000i 0.5000 + 0.500i	0.0011

Table 2.11.: *The calculated $xy-$ source positions and their error for $N^2 = 3$ varying the number of sensors ($\mu < 0$).*

b. Number of sources obtained using 100^2 sensors

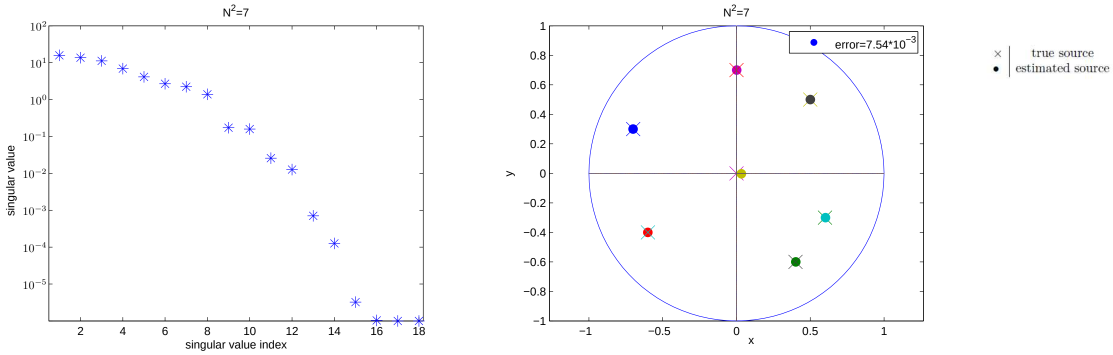

Figure 2.15.: *Singular values of* H^a_{18} *and the localization results projected on the* xy *plane for* $N^2 = 7$ *with* 100^2 *sensors* ($\mu < 0$).

c. The impact of the upper bound $\bar{J}$

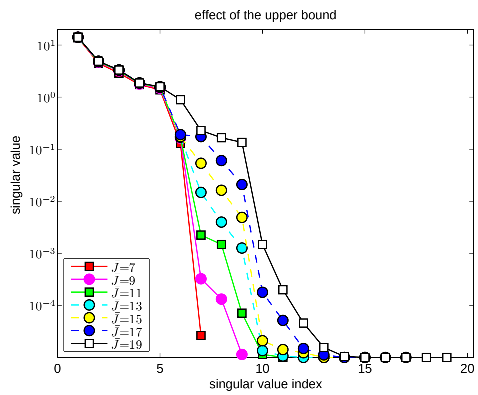

Figure 2.16.: *Singular value of* $H^a_{\bar{J}}$ *for* $N^2 = 3$ *and* 50^2 *sensors with respect to* $\bar{J}$ ($\mu < 0$).

d. Effect of the separability between dipoles

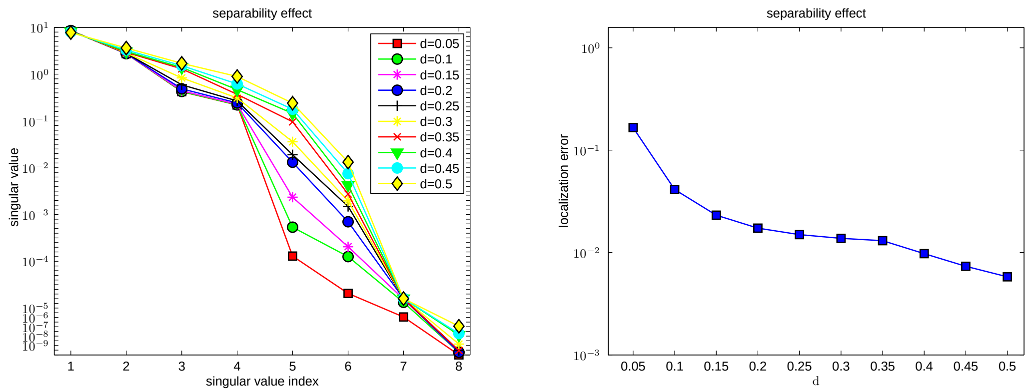

Figure 2.17.: *Singular values of H_8^a (left) and the localization errors (right) projected on the xy plane with 50^2 sensors($\mu < 0$).*

e. Obtaining the 3D coordinates and the effect of the separability coefficient

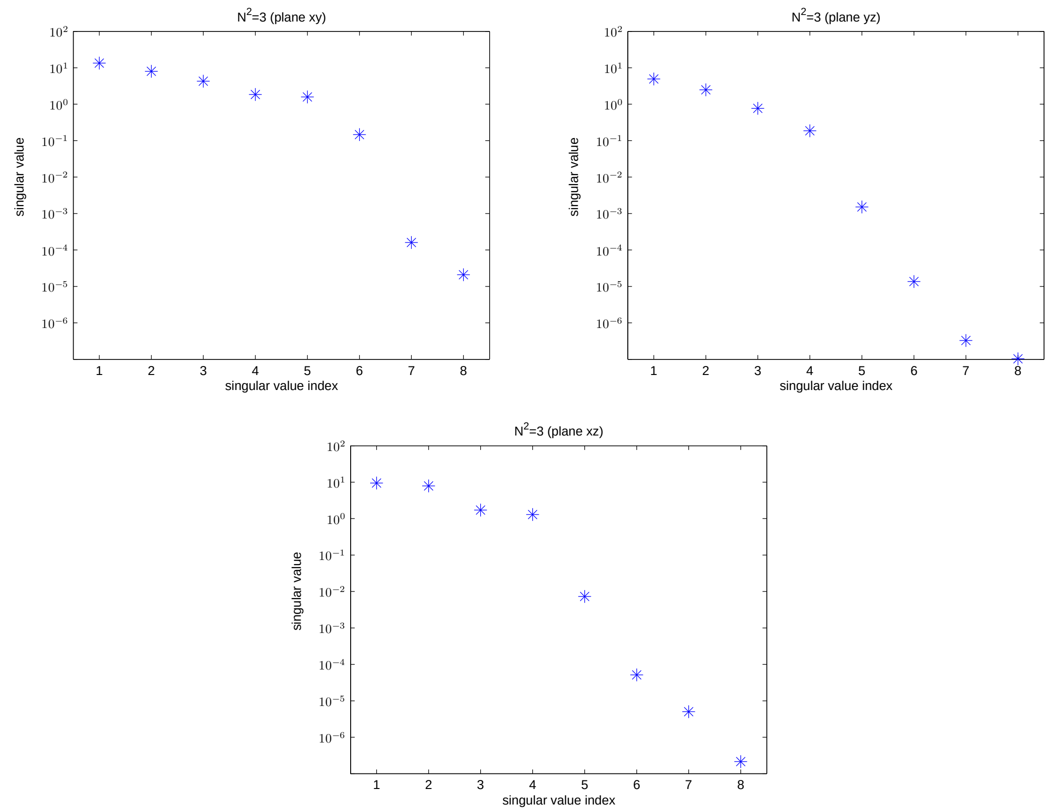

Figure 2.18.: *Singular values of H_8^r for $N^2 = 3$ where $r = a, b, c$ ($\mu < 0$).*

Examining Figure 2.14 till Figure 2.19, one observes that the use of a positive μ is better in the identification process. This is normal since the diffusion phenomenon causes more errors than the propagation one represented by Helmholtz equation. This confirms the fact that the constant c in (2.7) is equal to 1 in the Helmholtz case. However, numerically, we notice, as shown in the figures above, that the difference between these 2 cases is minor. Indeed, the difference in the position reconstruction is of an order less than 10^{-1}. The reason behind this difference is due to the change in the coefficients of the Hankel matrix $H_{\bar{J}}^r$ where the test functions and the Cauchy data are introduced depending on the value of μ. To illustrate this difference, we present below the singular values of a Hankel matrix for $\mu = \pm 3.42$ consecutively. We note, as seen in Table 2.12, that the gap is found at the same singular value with a minor difference in their values.

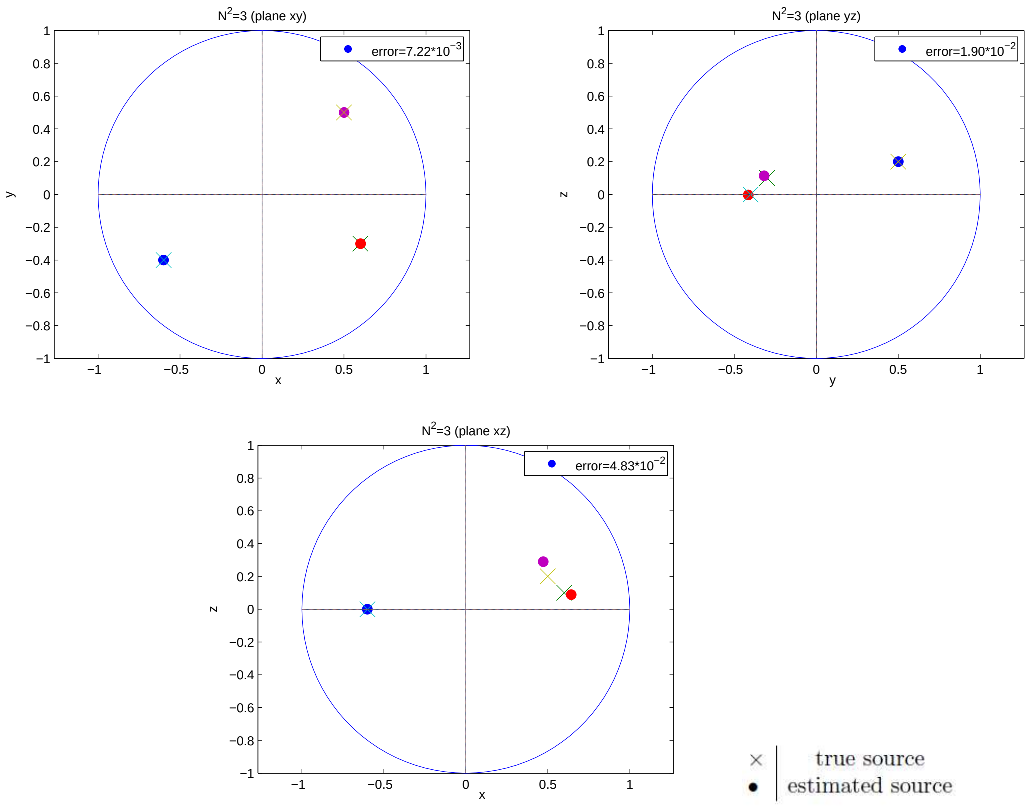

Figure 2.19.: *Estimation results projected on the $xy-$,$yz-$ and $xz-$ planes when $N^2 = 3$ ($\mu < 0$).*

value of μ	singular values of H_8^a
3.42	13.9724
	10.4820
	8.0744
	2.3002
	2.0874
	0.1612
	1.9e-4
	3.2e-5
-3.42	15.0532
	6.6709
	4.8376
	2.5005
	1.7188
	0.1445
	2.0e-4
	3.2e-5

Table 2.12.: *The singular values of H_8^a using 3 dipoles with 50^2 sensors with positive and negative μ.*

CHAPTER 3

2D Stationary Inverse Source Problem

"Obvious" is the most dangerous word in mathematics.

(Eric Temple Bell)

The object of this chapter is to solve an inverse source problem over the same elliptic equation (1.10) from boundary measurements in the two-dimensional space domain. First, we use a fixed frequency and then with multi-frequencies.

Section 3.1 states the main inverse problem we are concerned with and the form of the sources to be considered in this chapter.

Section 3.2 considers the case using a single fixed wavenumber. It is consecrated to elaborate the algebraic relationships between the monopolar sources and the Cauchy data using the passage to a three-dimensional space and then explains the identification method to be followed using a wavenumber greater than 1.

Section 3.3 discusses the case of sources having small compact supports.

Section 3.4 studies the case with multiple frequencies and the relevant algebraic algorithm used to reconstruct monopolar sources using several frequencies. Then, extensions to multipolar sources and sources with small support are shown.

Section 3.5 shows some numerical experiments performed to illustrate our identification method using multiple frequencies and studies the effect of several factors on the reconstruction process.

3.1. Inverse problem statement

The algebraic method proposed in the previous chapter is valid only in the 3D case. Therefore, to solve the 2D case, we need to establish some transformations and developments that enable us in certain frameworks to attain a full resolution method. Therefore, in this chapter, we consider the problem of recovering the source F in the 2D Helmholtz equation

$$\Delta u + \kappa^2 u = F \quad \text{in} \quad \Omega \tag{3.1}$$

where Ω is an open bounded in $\mathbb{R}^2$ and κ is a given real number.

As mentioned before, one of difficulties of the inverse source problem from boundary measurements concerns the source uniqueness issue. We can expect a well-posed inverse source problem only if *a priori* information is available. Usually this information takes the form of certain conditions on admissible sources depending on the underlying physical problem. Here, we consider two type of sources:

1. Sources as a linear combination of monopolar point sources given by,

$$F = \sum_{j=1}^{m} \lambda_j \delta_{\mathbf{S}_j} \qquad \mathbf{S}_j \in \Omega, \quad \lambda_j \neq 0, \tag{3.2}$$

where $\delta_{\mathbf{S}}$ stands for the Dirac distribution at point $\mathbf{S}$, m is a nonnegative integer and $\lambda_j \neq 0$ are scalar quantities.

2. Sources having compact support within a finite number of small subdomains, namely,

$$F = \sum_{j=1}^{m} h_j \chi_{D_j} \quad \text{with} \quad D_j = \mathbf{S}_j + \varepsilon B_j, \tag{3.3}$$

where $\mathbf{S}_j = (a_j, b_j)$, $B_j \subset \mathbb{R}^2$ is a bounded domain containing the origin, the densities h_j are non-null functions belonging to the space $L^1(\Omega)$ and ε is a positive real number small enough compared to the domain. In the following, we focus our work only on the case $0 < \varepsilon < 1$, which amounts to consider a domain of a size smaller than 1. However, this does not restrict the generality since we can always be brought back to this framework by using a suitable rescaling argument.

Furthermore, in both cases, the points $\mathbf{S}_j \equiv (a_j, b_j)$ are assumed to be mutually distinct.

Our aim is to reconstruct the source term F from the Cauchy data $(f, g) := (u_{|\Gamma}, \frac{\partial u}{\partial \nu}_{|\Gamma})$

prescribed on a sufficiently regular boundary Γ of Ω. Here, ν denotes the outward unit normal to Γ.

For this Helmholtz problem, 2 approaches are considered firstly having a single fixed wavenumber κ and then using multiple wavenumbers.

To be more precise, first we begin by defining, for all F satisfying (3.2) or (3.3), the following application in $H^{\frac{1}{2}}(\Gamma) \times H^{-\frac{1}{2}}(\Gamma)$

$$\Lambda : F \to (u_{|\Gamma}, \frac{\partial u}{\partial \nu}|_\Gamma).$$

Then, our inverse problem is formulated as follows:

$$\text{Given } (f, g) \in H^{\frac{1}{2}}(\Gamma) \times H^{-\frac{1}{2}}(\Gamma), \text{ determine } F \text{ such that } \Lambda(F) = (f, g). \tag{3.4}$$

Remark 19.

1. *For monopolar sources (3.2) the uniqueness issue is trivial. It can be obtained by means of Holmgren's theorem and the regularity of the direct problem, that is,* $u \in H^{1-s}(\Omega)$*, with* $s > 0$ *as it was done in the 3D case [EBN11a].*
2. *In the case of sources having compact support (3.3), the uniqueness is not guaranteed as it is shown in the example given in [Subsection 5.1,[EBN11a]] with* $F = h\chi_D$*.*

In here, we focus on the recovering process of the sources by seeking to establish an effective algebraic reconstruction method for the source parameters. The basic idea, standing behind our work, is the transformation of a 2D Helmholtz equation into a 3D Helmholtz equation leading to changes in the source term. Using the developments obtained in Chapter 2, we derive new relationships between the transformed source and the Cauchy data pair (f, g). These relationships would lead to algebraic equations that we solve later using the same techniques proposed in Chapter 2.

3.2. Pointwise sources identification using a single wavenumber $\kappa > 1$

In this section, our aim is to solve the inverse problem (3.4) associated to equation (3.1) having the source term of the form (3.2). More precisely, it consists in identifying the number m, the intensities λ_j and the locations $\mathbf{S}_j$ from the Cauchy data

(f, g). This section is divided into three subsections. First, in Subsection 3.2.1, we extend, by mean of a change of variables, the 2D Helmholtz equation (3.1) to a new three-dimensional Helmholtz equation defined in $\Omega \times \mathbb{R}$. Then, Subsection 3.2.2 is devoted to establish the new relationships between the Cauchy data (f, g) and the sources parameters $(m, \lambda_j, \mathbf{S}_j)$. Finally, Subsection 3.2.3 presents the identification method employed to reconstruct these sources using the obtained algebraic relations.

3.2.1. Transformation of the 2D Helmholtz equation

Due to the complexity of the 2D Helmholtz equation and the absence of a direct method for the source reconstruction in such a case, our basic idea is to prolong the 2D problem into an equivalent 3D Helmholtz problem via a suitable change of variable, which we are capable of solving algebraically using the tools employed in the previous chapter. Before doing so, we need to introduce the following notations:

For all $\omega \in \mathbb{R}$ and $\eta > 0$, set

$$\rho = \sqrt{\omega^2 + \kappa^2} \tag{3.5}$$

and, as seen in Figure 3.1, we denote

$$\overline{\Gamma} = \Gamma \times [-\eta, \eta], \quad \Gamma^+ = \Omega \times \{\eta\}, \quad \Gamma^- = \Omega \times \{-\eta\}. \tag{3.6}$$

Then, using the change of variables,

$$v(x, y, z) = u(x, y)e^{-i\omega z}, \qquad i^2 = -1 \quad \text{and} \quad z \in [-\eta, \eta], \tag{3.7}$$

the function v satisfies the system

$$\begin{array}{rcll} \Delta v + \rho^2 v & = & e^{-i\omega z} \sum\limits_{j=1}^{m} \lambda_j \delta_{S_j} & \text{in} \quad \Omega \times]-\eta, \eta[\\ (v, \frac{\partial v}{\partial \overline{\nu}}) & = & (fe^{-i\omega z}, ge^{-i\omega z}) & \text{on} \quad \overline{\Gamma} \\ (v, \frac{\partial v}{\partial z}) & = & (ue^{-i\omega z}, -i\omega u e^{-i\omega z}) & \text{on} \quad \Gamma^+ \cup \Gamma^- \end{array} \tag{3.8}$$

where $\overline{\nu} = (\nu, 0)$ is the outward unit normal to $\Gamma \times \mathbb{R}$ with ν being the outward unit normal to Γ. Thus, the problem now is to establish relationships between the Cauchy data pair (f, g) and the source parameters (m, λ_j, S_j) for equation (3.8).

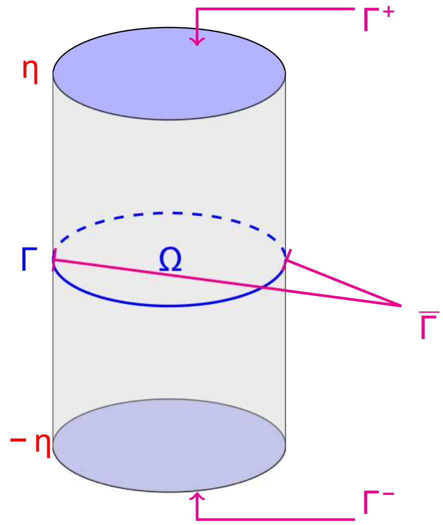

Figure 3.1.: *The new 3D domain.*

3.2.2. Reciprocity gap formulae

Before establishing our reciprocity gap formulae, we start by defining, for all $n \in \mathbb{N}$, the following operator:

$$\begin{aligned}\mathcal{R}(n,f,g) &= \sum_{\alpha=0}^{n}\binom{n}{\alpha}(-1)^\alpha \int_\Gamma y^{n-\alpha} g\left(\int_{\mathbb{R}} e^{-ix\sqrt{\omega^2+\kappa^2}}\delta^{(\alpha)}(\omega)d\omega\right) ds \\ &+i\sum_{\alpha=0}^{n}\binom{n}{\alpha}(-1)^\alpha \int_\Gamma \nu_1 y^{n-\alpha} f\left(\int_{\mathbb{R}} \sqrt{\omega^2+\kappa^2}\, e^{-ix\sqrt{\omega^2+\kappa^2}}\delta^{(\alpha)}(\omega)d\omega\right) ds \\ &-n\sum_{\alpha=0}^{n-1}\binom{n-1}{\alpha}(-1)^\alpha \int_\Gamma \nu_2 y^{n-1-\alpha} f\left(\int_{\mathbb{R}} e^{-ix\sqrt{\omega^2+\kappa^2}}\delta^{(\alpha)}(\omega)d\omega\right) ds\end{aligned} \tag{3.9}$$

where $\delta^{(\alpha)}$ indicates the αth derivative of Dirac delta function,

$$\nu = (\nu_1(x,y), \nu_2(x,y)) := (\nu_1, \nu_2) \qquad \text{and} \qquad \binom{n}{\alpha} = \begin{cases} \frac{n!}{\alpha!(n-\alpha)!} & \text{if } n \geq \alpha \\ 0 & \text{if } n < \alpha \end{cases}.$$

Thus, the reciprocity gap formulae, behind our algebraic identification method, are stated as follows.

Theorem 8. *Let $(f,g) \in H^{\frac{1}{2}}(\Gamma) \times H^{-\frac{1}{2}}(\Gamma)$ and u be the corresponding solution of (3.1). Then,*

$$\mathcal{R}(n,f,g) = \sum_{j=1}^{m} \sum_{\alpha=0}^{n} \binom{n}{\alpha} (-1)^{\alpha} \lambda_j b_j^{n-\alpha} \int_{\mathbb{R}} e^{-ia_j\sqrt{\omega^2+\kappa^2}} \delta^{(\alpha)}(\omega) d\omega, \quad \forall n \in \mathbb{N}.$$

* * *

Note that, in this theorem and also in formula (3.9), the integrals with respect to ω are to be understood in the duality sense.

Proof. The proof of Theorem 8 is to de done in two steps. In the first step, we establish an algebraic relationship satisfied only on the interval $[-\eta, \eta]$ and then we prove the mentioned relationship by passing to the limit $\eta \to +\infty$.

Step 1. Considering, for all $n \in \mathbb{N}$, the test functions

$$\varphi_\omega^n(x,y,z) = (y+iz)^n e^{-ix\rho} \tag{3.10}$$

satisfying the homogenous equation

$$\Delta v + \rho^2 v = 0 \quad \text{in} \quad \Omega \times \mathbb{R} \tag{3.11}$$

and then multiplying (3.8) by φ_ω^n, integration by parts and using Green's formula, we can verify that

$$\mathcal{R}^\eta(\varphi_\omega^n, f, g) = \sum_{j=1}^{m} \lambda_j \int_{-\eta}^{\eta} \varphi_\omega^n(a_j, b_j, z) e^{-i\omega z}\, dz \tag{3.12}$$

where $\mathcal{R}^\eta$ is the operator defined by

$$\begin{aligned} \mathcal{R}^\eta(\varphi_\omega^n, f, g) &= \int_\Gamma \int_{-\eta}^{\eta} \left(g\, \varphi_\omega^n - f\, \frac{\partial \varphi_\omega^n}{\partial \overline{\nu}} \right) e^{-i\omega z} dz ds \\ &- \int_\Omega \left(i\omega u\, \varphi_\omega^n + u\, \frac{\partial \varphi_\omega^n}{\partial z} \right)_{|z=\eta} e^{-i\omega\eta} dx dy \\ &+ \int_\Omega \left(i\omega u\, \varphi_\omega^n + u\, \frac{\partial \varphi_\omega^n}{\partial z} \right)_{|z=-\eta} e^{i\omega\eta} dx dy. \end{aligned} \tag{3.13}$$

Let $\theta \in C^\infty(\mathbb{R})$ be a function with compact support (i.e. $\theta \in C_c^\infty(\mathbb{R})$) such that $\theta(\omega) = 1$ over $\left[-\frac{\eta}{2}, \frac{\eta}{2}\right]$. Then, multiplying (3.12) by $\theta(\omega)$ and integrating, with respect to ω, over $\mathbb{R}$ lead to

$$\int_{\mathbb{R}} \theta(\omega)\mathcal{R}^{\eta}(\varphi_\omega^n, f, g)d\omega = \sum_{j=1}^{m} \lambda_j \int_{\mathbb{R}} \int_{-\eta}^{\eta} \theta(\omega)\varphi_\omega^n(a_j, b_j, z)e^{-i\omega z}dz\, d\omega. \tag{3.14}$$

Now, we desire to get the reciprocity gap formulae, given in Theorem 8, by passing to the limit $\eta \to +\infty$ in the previous equation. This will be the object of the following step.

Step 2. To justify the passage to the limit in (3.14), it is sufficient to examine the convergence, when $\eta \to +\infty$, of all the terms involved, denoted by

$$\begin{aligned}
I_1^\eta &= \int_{\mathbb{R}}\int_{\Gamma}\int_{-\eta}^{\eta} \theta(\omega)\left(g\,\varphi_\omega^n - f\,\frac{\partial \varphi_\omega^n}{\partial \overline{\nu}}\right) e^{-i\omega z}dzdsd\omega,\\
I_2^\eta &= \int_{-\eta}^{\eta}\int_{\mathbb{R}} \theta(\omega)\varphi_\omega^n(a_j, b_j, z)e^{-i\omega z}\, d\omega\, dz,\\
I_+^\eta &= \int_{\mathbb{R}}\int_{\Omega} \theta(\omega)\left(i\omega u\,\varphi_\omega^n + u\,\frac{\partial \varphi_\omega^n}{\partial z}\right)_{|z=\eta} e^{-i\omega\eta}dxdyd\omega,\\
I_-^\eta &= \int_{\mathbb{R}}\int_{\Omega} \theta(\omega)\left(i\omega u\,\varphi_\omega^n + u\,\frac{\partial \varphi_\omega^n}{\partial z}\right)_{|z=-\eta} e^{i\omega\eta}dxdyd\omega.
\end{aligned}$$

Indeed, using the definition of φ_ω^n in (3.10) and the binomial formula, we can show, using a simple calculation, that

$$\begin{aligned}
g\,\varphi_\omega^n - f\,\frac{\partial \varphi_\omega^n}{\partial \overline{\nu}} &= g e^{-ix\rho}\left(\sum_{\alpha=0}^{n}\binom{n}{\alpha} y^{n-\alpha}(iz)^\alpha\right)\\
&+ if\,\rho\, e^{-ix\delta}\left(\sum_{\alpha=0}^{n}\binom{n}{\alpha} y^{n-\alpha}(iz)^\alpha\right)\nu_1\\
&- nfe^{-ix\rho}\left(\sum_{\alpha=0}^{n-1}\binom{n-1}{\alpha} y^{n-1-\alpha}(iz)^\alpha\right)\nu_2.
\end{aligned}$$

Moreover, since the Fourier transform $\displaystyle\int_{\mathbb{R}} \mathbf{1}_{[-\eta,\eta]}(iz)^\alpha e^{-i\omega z}dz$, where $\mathbf{1}_{[-\eta,\eta]}$ is characteristic function of $[-\eta, \eta]$, converges, in the distribution sense, to $2\pi(-1)^\alpha\delta^{(\alpha)}$ when

$\eta \to +\infty$, then, according to the expression of I_1^η, we can prove that

$$\lim_{\eta\to+\infty} I_1^\eta = \quad 2\pi \sum_{\alpha=0}^{n} \binom{n}{\alpha} (-1)^\alpha \int_\Gamma y^{n-\alpha} g \left(\int_{\mathbb{R}} e^{-ix\sqrt{\omega^2+\kappa^2}} \delta^{(\alpha)}(\omega) d\omega \right) ds$$

$$+2\pi i \sum_{\alpha=0}^{n} \binom{n}{\alpha} (-1)^\alpha \int_\Gamma \nu_1 y^{n-\alpha} f \left(\int_{\mathbb{R}} \sqrt{\omega^2+\kappa^2}\, e^{-ix\sqrt{\omega^2+\kappa^2}} \delta^{(\alpha)}(\omega) d\omega \right) ds$$

$$-2\pi n \sum_{\alpha=0}^{n-1} \binom{n-1}{\alpha} (-1)^\alpha \int_\Gamma \nu_2 y^{n-1-\alpha} f \left(\int_{\mathbb{R}} e^{-ix\sqrt{\omega^2+\kappa^2}} \delta^{(\alpha)}(\omega) d\omega \right) ds \tag{3.15}$$

Using a similar calculation, we obtain

$$\lim_{\eta\to+\infty} I_2^\eta = 2\pi \sum_{\alpha=0}^{n} \binom{n}{\alpha} (-1)^\alpha b_j^{n-\alpha} \int_{\mathbb{R}} e^{-ia_j\sqrt{\omega^2+\kappa^2}} \delta^{(\alpha)}(\omega) d\omega. \tag{3.16}$$

To achieve the proof of this theorem, it remains to prove that

$$\lim_{\eta\to+\infty} I_\pm^\eta = 0. \tag{3.17}$$

We only show the result for I_+^η, the case of I_-^η is proved analogously. First, we can see that

$$\left(i\omega u\, \varphi_\omega^n + u\, \frac{\partial \varphi_\omega^n}{\partial z} \right)_{|z=\eta} = iue^{-ix\sqrt{\omega^2+\kappa^2}} \left[\omega \sum_{\alpha=0}^{n} \binom{n}{\alpha} y^{n-\alpha} (i\eta)^\alpha + n \sum_{\alpha=0}^{n-1} \binom{n-1}{\alpha} y^{n-1-\alpha} (i\eta)^\alpha \right].$$

This implies that

$$I_+^\eta \quad = \quad \sum_{\alpha=0}^{n} \int_\Omega \int_{\mathbb{R}} \theta(\omega) f_\alpha(x,y,\omega) (i\eta)^\alpha e^{-i\omega\eta} d\omega dx dy$$

$$+ \quad \sum_{\alpha=0}^{n-1} \int_\Omega \int_{\mathbb{R}} \theta(\omega) g_\alpha(x,y,\omega) (i\eta)^\alpha e^{-i\omega\eta} d\omega dx dy$$

with

$$f_\alpha(x,y,\eta,\omega) = i\omega u e^{-ix\sqrt{\omega^2+\kappa^2}}\binom{n}{\alpha}y^{n-\alpha} \quad \text{and} \quad g_\alpha(x,y,\eta,\omega) = inue^{-ix\sqrt{\omega^2+\kappa^2}}\binom{n-1}{\alpha}y^{n-1-\alpha}.$$

Furthermore, since $\theta f_\alpha, \theta g_\alpha \in C_c^\infty(\mathbb{R})$ with respect to ω, then using Fourier transform properties, one has

$$\int_{\mathbb{R}} \theta(\omega) f_\alpha(x,y,\omega)(i\eta)^\alpha e^{-i\omega\eta} d\omega = \widehat{(\theta f_\alpha)}^{(\alpha)}(\eta)$$

$$\int_{\mathbb{R}} \theta(\omega) g_\alpha(x,y,\omega)(i\eta)^\alpha e^{-i\omega\eta} d\omega = \widehat{(\theta g_\alpha)}^{(\alpha)}(\eta).$$

By Riemann-Lebesgue lemma and Lebesgue dominated convergence theorem, we get $\lim\limits_{\eta\to+\infty} I_+^\eta = 0$. Finally, passing to the limit $\eta \to +\infty$ in (3.14) and using (3.15), (3.16), (3.17), we obtain the desired result. □

Remark 20. *Note that, we can get a similar result to that of Theorem 8 in the case when κ^2 is replaced by $-\kappa^2$. To obtain this result, it is necessary ,only, to replace in (3.5) the parameter ρ by $\sqrt{\kappa^2-\omega^2}$ and in (3.10) the test function φ_ω^n by $(y+iz)^n e^{-x\rho}$. Then, we repeat the same procedure as in Step 1, but here we multiply equation (3.12) by $\gamma^\varsigma(\omega)$ instead of $\theta(\omega)$, where γ^ς is a function belonging in $C_c^\infty(\mathbb{R})$ such that $\gamma^\varsigma(\omega) = 1$ over $[-\kappa+\varsigma, \kappa-\varsigma]$, with small enough constant ς. By doing this, we can then pass to the limit $\eta \to +\infty$, in the same way as in Step 2 and show the corresponding results.*

The relationships, which are behind the identification algorithm, given in Theorem 8 can then be written as

$$\mathcal{R}(n,f,g) = \sum_{j=1}^{m}\sum_{\alpha=0}^{n} \mu_j^\alpha \binom{n}{\alpha} b_j^{n-\alpha} \tag{3.18}$$

where

$$\mu_j^\alpha = \lambda_j I_{\alpha,j} \quad \text{with} \quad I_{\alpha,j} = (-1)^\alpha \int_{\mathbb{R}} e^{-ia_j\sqrt{\omega^2+\kappa^2}} \delta^{(\alpha)}(\omega)\, d\omega.$$

Here, the quantities $I_{\alpha,j}$ are calculated explicitly as

$$I_{0,j} = e^{-ia_j\kappa}$$

and for $\alpha = 1, \cdots, n$

$$I_{\alpha,j} = \begin{cases} (-1)^\ell \frac{ia_j\beta_\ell}{\kappa^{2\ell-1}}\theta_{\ell-1}(ia_j\kappa)e^{-a_j\kappa} & \text{if} \qquad \alpha = 2\ell \\ \\ 0 & \text{if} \qquad \alpha = 2\ell+1 \end{cases} \tag{3.19}$$

where $\theta_\ell(\xi) = \displaystyle\sum_{j=0}^{\ell} \frac{(2\ell-j)!}{(\ell-j)!j!}\frac{\xi^j}{2^{\ell-j}}$ is the ℓ^{th} degree reverse Bessel polynomial and β_ℓ is a constant defined recursively by

$$\begin{cases} \beta_1 = 1 \\ \beta_\ell = (2\ell-1)\beta_{\ell-1}. \end{cases}$$

3.2.3. Identification Method

The main objective of the following is to establish an efficient identification method for solving equations (3.18) in order to determine the parameters (m, λ_j, a_j, b_j). Since the number of unknowns is greater than the number of equations, then the algebraic equations (3.18) can't be solved for whatever value of n. Thus, we need to truncate the equations (3.18) from a non-negative integer constant K. Namely, we set

$$c_n := \sum_{j=1}^{m}\sum_{\alpha=0}^{K} \mu_j^\alpha \tbinom{n}{\alpha} b_j^{n-\alpha}, \qquad \forall n \in \mathbb{N}. \tag{3.20}$$

Then, according to (3.18), we can see that, for $n \le K$

$$\mathcal{R}(n,f,g) = \sum_{j=1}^{m}\sum_{\alpha=0}^{n} \mu_j^\alpha \tbinom{n}{\alpha} b_j^{n-\alpha} = \sum_{j=1}^{m}\sum_{\alpha=0}^{K} \mu_j^\alpha \tbinom{n}{\alpha} b_j^{n-\alpha} = c_n.$$

Moreover, since we have $I_{\alpha,j} = O\left(\frac{1}{\kappa^\ell}\right)$ when $\alpha = 2\ell$ and κ is large enough, we can check that, for $n > K$,

$$\mathcal{R}(n,f,g) = \sum_{j=1}^{m}\sum_{\alpha=0}^{n} \mu_j^\alpha \tbinom{n}{\alpha} b_j^{n-\alpha} = c_n + O\left(\frac{1}{\kappa^s}\right)$$

where

$$O\left(\frac{1}{\kappa^s}\right) = \sum_{j=1}^{m} \sum_{\alpha=K+1}^{n} \mu_j^\alpha \binom{n}{\alpha} b_j^{n-\alpha}, \quad \text{with} \quad s = \begin{cases} \frac{K+2}{2} & \text{if} \quad K \quad \text{is} \quad \text{even} \\ \\ \frac{K+1}{2} & \text{if} \quad K \quad \text{is} \quad \text{odd}. \end{cases} \tag{3.21}$$

Therefore, for a κ greater than 1, we choose a fixed non-negative integer K such that $\frac{1}{\kappa^s}$ is small enough. Thanks to that, we approximate the coefficients c_n by $\mathcal{R}(n, f, g)$ and then we determine the quantities m, b_j and μ_j^α by solving the algebraic equations (3.20) by means of the identification algorithm developed in the previous chapter.

More precisely, if $H_{\bar{J},K}$ is the complex Hankel matrix, defined as

$$H_{\bar{J},K} = \begin{pmatrix} c_0 & c_1 & \cdots & c_{\bar{J}-1} \\ c_1 & c_2 & \cdots & c_{\bar{J}} \\ \vdots & \vdots & \vdots & \vdots \\ c_{\bar{J}-1} & c_{\bar{J}} & \cdots & c_{2\bar{J}-2} \end{pmatrix} \quad \text{for} \quad \bar{J} \in \mathbb{N}^*, \tag{3.22}$$

then, we have the following result.

Theorem 9. *Let K be a given non-negative integer and $H_{\bar{J},K}$ be the Hankel matrix defined in (3.22), where $\bar{J}$ is a known upper bound of*

$$J = \begin{cases} (K+1)m & \textit{if} \quad K \quad \textit{is} \quad \textit{even} \\ \\ Km & \textit{if} \quad K \quad \textit{is} \quad \textit{odd}. \end{cases} \tag{3.23}$$

Assume that the ordinate points b_j of $\mathbf{S}_j$ are distinct, then, we have

$$\textit{rank}(H_{\bar{J},K}) = J.$$

* * *

Proof. As seen in, [Theorem 4, Chapter 2], the Hankel matrix $H_{\bar{J},K}$ can be decomposed as

$$H_{\bar{J},K} = A_0 \bar{I} (A_0)^t$$

with A_0 is the complex matrix of size $\bar{J} \times J$ given by

$$A_0 = (U^0, \cdots, U^K),$$

where, for $\beta = 0, \cdots, K$, U^β are the confluent $\bar{J} \times m$ Vandermonde matrices

$$U^\beta = \begin{pmatrix} \binom{0}{\beta}(b_1)^{-\beta} & \cdots & \binom{0}{\beta}(b_m)^{-\beta} \\ \binom{1}{\beta}(b_1)^{-\beta+1} & \cdots & \binom{1}{\beta}(b_m)^{-\beta+1} \\ \vdots & \ddots & \vdots \\ \binom{\bar{J}-1}{\beta}(b_1)^{-\beta+\bar{J}-1} & \cdots & \binom{\bar{J}-1}{\beta}(b_m)^{-\beta+\bar{J}-1} \end{pmatrix},$$

$(A_0)^t$ its transpose matrix and $\bar{I}$ is the multi-diagonal matrix

$$\bar{I} = \begin{pmatrix} \mu^0 & \mu^1 & \cdots & \mu^K \\ \vdots & \vdots & \iddots & \vdots \\ \mu^{K-1} & \mu^K & \cdots & 0 \\ \mu^K & 0 & \cdots & 0 \end{pmatrix}$$

where

$$\mu^\alpha = diag(\mu_1^\alpha, \cdots, \mu_m^\alpha) \quad \text{for} \quad \alpha = 0, \cdots, K.$$

Therefore, the rank of the Hankel matrix $H_{\bar{J},K}$ is the same as that of A_0 since $\bar{I}$ is nonsingular and $(A_0)^t$ is surjective.

Nevertheless, if K is even, from (3.19), we know that $\mu_j^K = \lambda_j I_{K,j} \neq 0$, for all $j = 1, \cdots, m$, and so rank$(\bar{I}) = (K+1)m$ and consequently rank$(H_{\bar{J},K}) = (K+1)m$. However, if K is odd, we have $\mu_j^K = \lambda_j I_{K,j} = 0$, for all $j = 1, \cdots, m$, implying that rank$(H_{\bar{J},K}) = Km$. $\square$

Now, we introduce the companion matrix

$$B_K = \begin{pmatrix} 0 & 1 & \cdots & 0 & 0 \\ 0 & 0 & 1 & \cdots & 0 \\ \vdots & \vdots & \ddots & \ddots & 0 \\ \vdots & \vdots & \ddots & \ddots & 1 \\ d_0 & d_1 & \cdots & \cdots & d_{J-1} \end{pmatrix} \tag{3.24}$$

where J is defined in (3.23) and $D = (d_0, ..., d_{J-1})^t$, is the vector solution to the linear system $H_{J,K}D = \xi_J$ with $\xi_J = (c_J, \cdots, c_{2J-1})^t$. Then, one has the following theorem.

Theorem 10. *Let K be a given non-negative integer, $L = \frac{J}{m}$, and B_K be the companion matrices defined in (3.24). Assume that, the ordinate points b_j of $\boldsymbol{S}_j$ are distinct. Then,*

1. *B_K admits m eigenvalues of multiplicity L.*
2. *The m eigenvalues of multiplicity L are the ordinate points b_j of $\boldsymbol{S}_j$.*

* * *

The proof of this theorem is very similar to that of [Theorem 5, Chapter 2].

Remark 21. *In practice, for given a positive constant $\kappa > 1$, we choose the integer K such that $\frac{1}{\kappa^s}$ is small enough, where s is defined in (3.21). Then, we estimate the coefficients c_n defined in (3.20) by $\mathcal{R}(n, f, g)$. This introduces an accuracy error $O\left(\frac{1}{\kappa^s}\right)$ in our identification algorithm, precisely, in determining of the rank of Hankel matrix $H_{\bar{J},K}$ and the eigenvalues of companion matrix B_K (see [Ste73b, p. 321-322] for estimating result on SVD). Therefore, through Theorem 9 and Theorem 10 respectively, we can find, modulo a small error, the number of sources and the ordinates of their positions. To determine the position of the point sources, in particular the coordinate a_j, we proceed in the same way, considering the test functions*

$$\psi_\omega^n(x, y, z) = (x + iz)^n e^{-iy\sqrt{\omega^2+\kappa^2}}.$$

Remark 22. *In the previous theorems we have assumed that, the projected points onto the x- and the y-axis of the point sources $\boldsymbol{S}_j$ are distinct. Henceforth, we were able to identify the points $\boldsymbol{S}_j$ through these projection points. However, if by bad luck one of the projected points onto x- or y-axis coincide, we can do the same thing by choosing another basis in the xy-plane, where the projected points are distinct. This is possible, since, for all orthonormal basis $(\vec{u}, \vec{v})$ in the xy-plane, the following functions*

$$\left.\begin{aligned} \varphi_\omega^n(\boldsymbol{S}) &= (\vec{v}.\boldsymbol{S} + iz)^n e^{-i\vec{u}.\boldsymbol{S}\sqrt{\omega^2+\kappa^2}} \\ \psi_\omega^n(\boldsymbol{S}) &= (\vec{u}.\boldsymbol{S} + iz)^n e^{-i\vec{v}.\boldsymbol{S}\sqrt{\omega^2+\kappa^2}} \end{aligned}\right| \quad \textit{with} \quad \boldsymbol{S} = (x, y, z)$$

remain solutions of equation (3.11), for all $n \in \mathbb{N}$. Let us mention that, to reach a better identification of the point sources, it is desirable to project the point sources in a basis $(\vec{u}, \vec{v})$ where the absolute gap between the singular values of the corresponding Hankel matrix is the largest possible. In practice, to attain such a basis, we can assume, for example, that $\vec{u} = (\cos(\theta), \sin(\theta), 0)$, $\vec{v} = (-\sin(\theta), \cos(\theta), 0)$ and then take the angle $\theta \in [0, 2\pi]$ that realizes the largest gap between the singular values of the Hankel matrix (3.22).

3.3. Sources of small supports using a single wavenumber $\kappa > 1$

In this subsection, we consider the case where the source term F is assumed to represent sources having compact support within a finite number of small subdomains, given by (3.3). The aim objective of this subsection consists in establishing relationships between the source F and the Cauchy data (f, g) in order to identify, using a single fixed wavenumber κ, the number m, the points $\mathbf{S}_j$ and some characteristics of the domains D_j, for example, their masses and their centers of gravity. To do so, we proceed in the same way as in the case of pointwise source. We begin by taking (as in Subsection 3.2.1) the change of variables v defined in (3.7) and therefore we show that v satisfies the following 3D equation

$$\Delta v + \delta^2 v = e^{-i\omega z} \sum_{j=1}^{m} h_j \chi_{D_j} \quad \text{in} \quad \Omega\times]-\eta, \eta[\tag{3.25}$$

as well as the boundary conditions

$$\begin{aligned}
(v, \tfrac{\partial v}{\partial \overline{\nu}}) &= (f e^{-i\omega z}, g e^{-i\omega z}) && \text{on} \quad \overline{\Gamma} \\
(v, \tfrac{\partial v}{\partial z}) &= (u e^{-i\omega\eta}, -i\omega u e^{-i\omega\eta}) && \text{on} \quad \Gamma^{+} \\
(v, -\tfrac{\partial v}{\partial z}) &= (u e^{i\omega\eta}, i\omega u e^{i\omega\eta}) && \text{on} \quad \Gamma^{-}.
\end{aligned}$$

where $\overline{\Gamma}$ and $\Gamma^{\pm}$ are defined in (3.6). Then, we obtain as in Theorem 8, the following reciprocity gap formulae.

Theorem 11. *Let $(f, g) \in H^{\frac{1}{2}}(\Gamma) \times H^{-\frac{1}{2}}(\Gamma)$ and u be the corresponding solution of (3.1) with F given by (3.3). Then,*

$$\mathcal{R}(n, f, g) = \varepsilon^2 \sum_{j=1}^{m} \sum_{\alpha=0}^{n} \binom{n}{\alpha} b_j^{n-\alpha} \sum_{\beta=0}^{\alpha} (-1)^{\beta} \int_{B_j} \int_{\mathbb{R}} \Phi_j(\alpha, \beta, \omega, t) \delta^{(\beta)}(\omega)\, d\omega dt,$$

where $\mathcal{R}$ is defined in (3.9) and Φ_j is the function

$$\Phi_j(\alpha, \beta, \omega, t) = \binom{\alpha}{\beta} \varepsilon^{\alpha-\beta} h_j(\boldsymbol{S}_j + \varepsilon t) t_2^{\alpha-\beta} e^{-i(a_j + \varepsilon t_1)\sqrt{\omega^2+\kappa^2}} \quad \textit{with} \quad t = (t_1, t_2). \tag{3.26}$$

* * *

Proof. To prove this theorem, we proceed as in Step 1 of the proof of Theorem 8. Multiplying equation (3.25) by the test functions φ_ω^n, defined in (3.10), and integrating by parts, we get

$$\mathcal{R}^\eta(\varphi_\omega^n, f, g) = \sum_{j=1}^m \int_{-\eta}^{\eta}\int_{D_j} h_j(x,y)\varphi_\omega^n(x,y,z)e^{-i\omega z}dxdydz, \quad \text{for all } \; n \in \mathbb{N} \; \text{ and } \; \omega \in \mathbb{R}$$

where $\mathcal{R}^\eta$ is defined in (3.13). Then, using the change of variables $(x,y) = \mathbf{S}_j + \varepsilon t$ with $t = (t_1, t_2)$, one obtains

$$\mathcal{R}^\eta(\varphi_\omega^n, f, g) = \sum_{j=1}^m \varepsilon^2 \int_{-\eta}^{\eta}\int_{B_j} \tilde{h}_j(t)\varphi_\omega^n(\mathbf{S}_j + \varepsilon t, z)e^{-i\omega z}dtdz \tag{3.27}$$

where $\tilde{h}_j(t) = h_j(\mathbf{S}_j + \varepsilon t)$.

Now, substituting, in equations (3.27), the test functions φ_ω^n by their values leads to

$$\mathcal{R}^\eta(\varphi_\omega^n, f, g) = \varepsilon^2 \sum_{j=1}^m \int_{-\eta}^{\eta}\int_{B_j} \tilde{h}_j(t)(b_j + \varepsilon t_2 + iz)^n e^{-i(a_j+\varepsilon t_1)\sqrt{\omega^2+\kappa^2}} e^{-i\omega z}\, dtdz$$

and consequently, since

$$\begin{aligned}
[b_j + (\varepsilon t_2 + iz)]^n &= \sum_{\alpha=0}^{n} \binom{n}{\alpha} (b_j)^{n-\alpha}(\varepsilon t_2 + iz)^\alpha \\
&= \sum_{\alpha=0}^{n} \binom{n}{\alpha} (b_j)^{n-\alpha} \left(\sum_{\beta=0}^{\alpha} \binom{\alpha}{\beta} \varepsilon^{\alpha-\beta} t_2^{\alpha-\beta} (iz)^\beta \right),
\end{aligned}$$

we deduce that

$$\mathcal{R}^\eta(\varphi_\omega^n, f, g) = \varepsilon^2 \sum_{j=1}^m \sum_{\alpha=0}^n \binom{n}{\alpha} b_j^{n-\alpha} \sum_{\beta=0}^{\alpha} \int_{B_j} \Phi_j(\alpha,\beta,\omega,t) \int_{-\eta}^{\eta} (iz)^\beta e^{-i\omega z}\, dzdt \tag{3.28}$$

where Φ_j is the function defined in (3.26). To complete the proof, we proceed exactly as in Step 2 of the proof of Theorem 8, we, first, multiply equation (3.28) by a function $\theta(\omega)$ belonging to $C_c^\infty(\mathbb{R})$ such that $\theta(\omega) = 1$ over $\left[-\frac{\eta}{2}, \frac{\eta}{2}\right]$, then integrate with respect to ω and finally pass to the limit $\eta \to +\infty$ to conclude. □

The relationships given in the Theorem 11 can, then, be written as

$$\mathcal{R}(n, f, g) = \sum_{j=1}^{m} \sum_{\alpha=0}^{n} \nu_j^\alpha \binom{n}{\alpha} b_j^{n-\alpha} \quad \forall n \in \mathbb{N} \tag{3.29}$$

where

$$\nu_j^\alpha = \varepsilon^2 \sum_{\beta=0}^{\alpha} \binom{\alpha}{\beta} \varepsilon^{\alpha-\beta} \int_{B_j} \tilde{h}_j(t) t_2^{\alpha-\beta} I_{\beta,j}^t dt \tag{3.30}$$

with

$$I_{\beta,j}^t = (-1)^\beta \int_{\mathbb{R}} e^{-i(a_j+\varepsilon t_1)\sqrt{\omega^2+\kappa^2}} \delta^{(\beta)}(\omega)\, d\omega.$$

To solve equations (3.29), as in Subsection 3.2.3, we truncate them beyond a non-negative integer constant K. First, we set

$$c_n := \sum_{j=1}^{m} \sum_{\alpha=0}^{K} \nu_j^\alpha \tbinom{n}{\alpha} b_j^{n-\alpha}, \qquad \forall n \in \mathbb{N}. \tag{3.31}$$

According to (3.29), we can see that, for $n \leq K$

$$\mathcal{R}(n, f, g) = \sum_{j=1}^{m} \sum_{\alpha=0}^{n} \nu_j^\alpha \tbinom{n}{\alpha} b_j^{n-\alpha} = \sum_{j=1}^{m} \sum_{\alpha=0}^{K} \nu_j^\alpha \tbinom{n}{\alpha} b_j^{n-\alpha} = c_n.$$

Moreover, by a simple calculation done as in (3.19) replacing a_j by $a_j + \varepsilon t_1$, we can prove that, for κ large enough, $I_{\beta,j}^t = 0$ when $\beta = 2\ell + 1$ and $I_{\beta,j}^t = O\left(\frac{1}{\kappa^\ell}\right)$ when $\beta = 2\ell$. From this and the definition of ν_j^α in (3.30), we can check that, if τ is the parameter defined by

$$\tau = \max\left(\varepsilon, \frac{1}{\sqrt{\kappa}}\right),$$

then, for $K > n$,

$$\mathcal{R}(n, f, g) = \sum_{j=1}^{m} \sum_{\alpha=0}^{n} \nu_j^\alpha \tbinom{n}{\alpha} b_j^{n-\alpha} = c_n + O\left(\tau^r\right)$$

where

$$O\left(\tau^{r}\right)=\sum_{j=1}^{m}\sum_{\alpha=K+1}^{n}\nu_j^{\alpha}\binom{n}{\alpha}b_j^{n-\alpha},\quad \text{with}\quad r=\begin{cases}K+4 & \text{if} \quad K \quad \text{is} \quad \text{even}\\ K+3 & \text{if} \quad K \quad \text{is} \quad \text{odd.}\end{cases}$$

Finally, for $\kappa > 1$, $\varepsilon < 1$, choosing an integer K such that τ^r is small enough, we approximate the coefficients c_n by $\mathcal{R}(n, f, g)$. Then, we determine the quantities m, b_j, ν_j^{α} by solving the algebraic equations (3.31), by means of the identification algorithm developed in Chapter 2 and recalled in Subsection 3.2.3.

3.4. Multi-Frequencial case

In this section, we consider the case having the possibility of using multiple frequencies in order to resolve the inverse problem, the sources reconstruction in (3.1). In other words, our goal is to identify F in (3.1) by varying the wavenumber κ, from a single corresponding Cauchy data $(f_\kappa, g_\kappa) := (u_{\kappa|_\Gamma}, \frac{\partial u_\kappa}{\partial \nu}_{|_\Gamma})$. In such a case, to reconstruct the source parameters using the algebraic method, the resolution is direct where one needs neither to transform the equation under study (3.1) nor to pass to the three-dimensional space.

This sections is divided into five subsections. After presenting the principle of the method in Subsection 3.4.1, we treat, in Subsection 3.4.2, the case with monopolar sources (3.2) and then propose an algebraic algorithm in Subsection 3.4.3. Later, in Subsection 3.4.4, we present the identification method over the possible extension to multipolar sources(3.46). Finally, Subsection 3.4.5 deals with the case of sources with small supports (3.3).

3.4.1. Statement of the inverse problem

Let $\mathcal{K}$ be the set of M wavenumbers given by

$$\mathcal{K}=\{\kappa_1,\kappa_2,\cdots,\kappa_M\},\qquad M\in\mathbb{N}^*.$$

For $n = 1, \cdots, M$, we consider the elliptic problem

$$\Delta u_{\kappa_n} + \kappa_n^2 u_{\kappa_n} = F \tag{3.32}$$

and we define the operators

$$\Lambda_{\kappa_n}(F) = (u_{\kappa_n|\Gamma}, \frac{\partial u_{\kappa_n}}{\partial \nu}_{|\Gamma}).$$

Then, the inverse source problem considered is formulated as:

Given M Cauchy data $(f_{\kappa_n}, g_{\kappa_n}) \in H^{\frac{1}{2}}(\Gamma) \times H^{-\frac{1}{2}}(\Gamma)$, determine F such that

$$\Lambda_{\kappa_n}(F) = (f_{\kappa_n}, g_{\kappa_n}) \quad \text{for all} \quad n = 1, \cdots, M.$$

In the following, based on the former work [EBN11b] and the methodology used in Chapter 2, we propose an algebraic method allowing to solve this inverse problem in the case of monopolar sources, multipolar sources and sources with small supports.

3.4.2. Pointwise sources

First, we begin by establishing an algebraic relationship between $(m, \lambda_j, \mathbf{S}_j)$ and the Cauchy data. For this, we need to introduce, for any real $\kappa \geq 0$, the following space

$$\mathcal{H}_\kappa = \{v \in H^1(\Omega) : \Delta v + \kappa^2 v = 0\}$$

and define, for all $(f, g) \in H^{\frac{1}{2}}(\Gamma) \times H^{-\frac{1}{2}}(\Gamma)$ and $v \in \mathcal{H}_\kappa$, the operator $\mathcal{R}$ as follows

$$\mathcal{R}(v, f, g) = \int_\Gamma \left(gv - f\frac{\partial v}{\partial \nu} \right) ds. \tag{3.33}$$

Multiplying equation (3.32)-(3.2) by v, element of $\mathcal{H}_\kappa$, integrating by parts and using Green's formula lead to

$$\mathcal{R}(v, f_\kappa, g_\kappa) = \sum_{j=1}^{m} \lambda_j v(\mathbf{S}_j) \quad \text{for all} \quad v \in \mathcal{H}_\kappa. \tag{3.34}$$

Here, (f_κ, g_κ) presents the corresponding Cauchy data of u_κ the solution of (3.32).

Now, for each $\kappa \in \mathcal{K}$, we consider, the function

$$v_\kappa^d(x, y) = e^{i\kappa d \cdot X} \tag{3.35}$$

where

$$X = (x, y), \quad d = (d_1, d_2) \quad \text{with} \quad d_1^2 + d_2^2 = 1.$$

Replacing v by v_κ^d in (3.34), one obtains

$$\mathcal{R}(v_\kappa, f_\kappa, g_\kappa) = \sum_{j=1}^{m} \lambda_j e^{i\kappa d.\mathbf{S}_j} \qquad \forall \kappa \in \mathcal{K}. \tag{3.36}$$

This equation can be solved in order to determine m, λ_j and $\mathbf{S}_j$. To do so, we fix a real number $\kappa_0 > 0$, choose the variable wavenumbers in $\mathcal{K}$ as

$$\kappa_n = n\kappa_0, \qquad n = 1, \cdots, M$$

and take the number M as

$$M = 2\bar{m}, \quad \bar{m} \text{ being a known upper bound of the number of sources.}$$

Under these assumptions, equation (3.36) is written as

$$c_n := \mathcal{R}(v_{\kappa_n}^d, f_{\kappa_n}, g_{\kappa_n}) = \sum_{j=1}^{m} \lambda_j (e^{i\kappa_0 d.\mathbf{S}_j})^n \quad \text{for} \quad n = 1, \cdots, 2\bar{m}. \tag{3.37}$$

Therefore, the identification process is attained in two steps.

The first step consists in determining the number of source, through the rank of the following Hankel matrix:

$$H_{\bar{m}}^d = \begin{pmatrix} c_1 & c_2 & \cdots & c_{\bar{m}} \\ c_2 & c_3 & \cdots & c_{\bar{m}+1} \\ \vdots & \vdots & \vdots & \vdots \\ c_{\bar{m}} & c_{\bar{m}+1} & \cdots & c_{2\bar{m}-1} \end{pmatrix}. \tag{3.38}$$

More precisely, if we assume that the points $e^{i\kappa_0 d.\mathbf{S}_j}$, for $j = 1, \cdots, M$, are mutually distinct, namely the direction $d = (d_1, d_2)$ satisfies

$$\textbf{(H2)} \qquad d \cdot (\mathbf{S}_j - \mathbf{S}_l) \neq \tfrac{2q\pi}{\kappa_0}, \qquad \forall\, j \neq l,\ q \in \mathbb{Z}$$

then, we have the following result.

Theorem 12. *Let $H^d_{\bar{m}}$ be the Hankel matrix defined in (3.38) where $\bar{m}$ is a known upper bound of m. Under hypothesis **(H2)**, we have*

$$\textit{rank}\left(H^d_{\bar{m}}\right) = m.$$

* * *

Proof. The proof is similar to that done in [Theorem 4, Chapter 2]. First, we rewrite the algebraic formulae (3.37) in the matrix form

$$\xi_n = A_n\Lambda, \quad \text{for all} \quad n = 1, \cdots, \bar{m},$$

where

$$\xi_n = (c_n, \cdots, c_{\bar{m}+n-1})^t, \qquad \Lambda = (\lambda_1, \cdots, \lambda_m)^t, \tag{3.39}$$

and for all $n \in \mathbb{N}$, A_n is the following $\bar{m} \times m$ Vandermonde matrices

$$A_n = \begin{pmatrix} (e^{i\kappa_0 d.\mathbf{S}_1})^n & \cdots & (e^{i\kappa_0 d.\mathbf{S}_m})^n \\ (e^{i\kappa_0 d.\mathbf{S}_1})^{n+1} & \cdots & (e^{i\kappa_0 d.\mathbf{S}_m})^{n+1} \\ \vdots & \ddots & \vdots \\ (e^{i\kappa_0 d.\mathbf{S}_1})^{\bar{m}+n-1} & \cdots & (e^{i\kappa_0 d.\mathbf{S}_m})^{\bar{m}+n-1} \end{pmatrix}. \tag{3.40}$$

On the other hand, if we denote by D the diagonal matrix

$$D = diag(e^{i\kappa_0 d.\mathbf{S}_1}, \cdots, e^{i\kappa_0 d.\mathbf{S}_m}) \tag{3.41}$$

one gets, for all $n \in \mathbb{N}$,

$$A_{n+1} = A_n D = A_1 D^n$$

and therefore

$$\xi_n = A_1 D^{n-1}\Lambda \quad \text{for all} \quad n = 1, \cdots, \bar{m}. \tag{3.42}$$

Then, using (3.42), one can rewrite the Hankel matrix $H^d_{\bar{m}}$ as

$$H^d_{\bar{m}} = A_1[\Lambda, D\Lambda, ..., D^{\bar{m}-1}\Lambda] = A_1 T (A_0)^t$$

where $(A_0)^t$ is the transpose matrix of A_0 and $T = diag(\lambda_1, \cdots, \lambda_m)$. From **(H2)** and the fact that $\lambda_j \neq 0$, for $j = 1, \cdots, m$, we can check that rank$(A_0)^t = m$ and that the matrix T is nonsingular. This implies that $T(A_0)^t$ is surjective and therefore we have rank$(A_1 T(A_0)^t) =$ rank(A_1). Finally, using the fact rank$(A_1) = m$, we obtain the desired result. $\square$

The second step consists in determining the position of the monopolar sources, by means of the eigenvalues of the companion matrix:

$$B^d = \begin{pmatrix} 0 & 1 & \cdots & 0 & 0 \\ 0 & 0 & 1 & \cdots & 0 \\ \vdots & \vdots & \ddots & \ddots & 0 \\ \vdots & \vdots & \ddots & \ddots & 1 \\ q_1 & q_2 & \cdots & \cdots & q_m \end{pmatrix}, \tag{3.43}$$

where the vector $Q = (q_1, ..., q_m)^t$ is obtained by solving the linear system $H^d_m Q = \xi_{m+1}$, with ξ_{m+1} defined as in (3.39) replacing $\bar{m}$ by m. More precisely, we have the following theorem.

Theorem 13. *Let B^d be the companion matrix defined in (3.43). Assume that the hypothesis* ***(H2)*** *is satisfied, then B^d admits m simple eigenvalues represented by $e^{i\kappa_0(d_1 a_j + d_2 b_j)}$, for $j = 1, \cdots, m$, where a_j and b_j are the coordinates of the positions $\boldsymbol{S}_j$.*

* * *

Proof. Since as we have shown in Theorem 12 that the rank of $H^d_{\bar{m}}$ is m, we replace in ξ_n and A_n (defined in (3.39) and (3.40)) $\bar{m}$ by m. Then, from (3.42), we can easily derive the following relations:

$$\begin{aligned}\xi_{n+1} &= A_1 D^n \Lambda \\ &= A_1 D (A_1)^{-1} A_1 D^{n-1} \Lambda \\ &= B^d \xi_n\end{aligned}$$

where we have set

$$B^d = A_1 D (A_1)^{-1}.$$

Here, the matrix A_1 is invertible since $e^{i\kappa_0 d.\mathbf{S}_j}$ are assumed distinct (respecting **(H2)**). Moreover, since $\operatorname{rank}(H^d_m) = m$, the family $(\xi_k)_{k=1,\ldots,m}$ forms a basis of $\mathbb{C}^m$ and consequently the $m \times m$ complex matrix B^d is given explicitly by (3.43) and its eigenvalues are those of the diagonal matrix D defined in (3.41). $\square$

Remark 23. *Note that, in order to obtain the* $2D$ *location of the monopoles, we use the previous theorem, taking consecutively in (3.35) the direction* d *as* $d = (1, 0)$ *and* $d = (0, 1)$ *that give us the* $x-$ *and the* $y-$*coordinates of* $\boldsymbol{S}_j$*. In the case where these two directions do not verify **(H2)**, we can choose two other directions, denoted* $d = (d_1, d_2)$ *and* $e = (e_1, e_2)$*, to determine the source positions, by solving the corresponding system of* $2m$ *equations with* $2m$ *unknowns* a_j *and* b_j*.*

Theorems 12 and 13 suggest that if an upper bound $\bar{m}$ of m is known, one can establish an algorithm to identify, the coefficients m and $e^{i\kappa_0 d.\mathbf{S}_j}$, for $j = 1, \cdots, m$. Moreover, λ_j can be determined by solving the linear systems $A_1\Lambda = \xi_1$. This allows us to obtain the coefficients m, a_j, b_j and λ_j, as suggested in the following algorithm.

3.4.3. Algebraic algorithm

Step 1. Let $\bar{m}$ be an upper bound of the number of sources and consider a fixed wavenumber κ. For each wavenumber $\kappa_n = n\kappa_0, n = 1, \cdots, 2\bar{m}$, we use a single given Cauchy data $(f_{\kappa_n}, g_{\kappa_n})$ on the boundary Γ and we compute c_1, $c_2, \cdots, c_{2\bar{m}}$ taking the direction d consecutively as $d_1 = (1, 0)$ and $d_2 = (0, 1)$. Then, the number m can be determined as the rank of one of the two Hankel matrices $H^{d_i}_{\bar{m}}$ related to $d_i, i = 1, 2$. This rank is estimated using the Singular Value Decomposition method with an appropriate threshold, following [Han98], see Section 3.5 for more details concerning the choice of the threshold.

Step 2. Solve the linear system $H_m^d Q = \xi_m$. The coordinates a_j and b_j of the m monopolar sources are obtained as

$$a_j = \frac{1}{i\kappa_0} \ln(\beta_{j,1}) + \frac{2q\pi}{\kappa_0}, \qquad q \in \mathbb{Z} \tag{3.44}$$

and

$$b_j = \frac{1}{i\kappa_0} \ln(\beta_{j,2}) + \frac{2q\pi}{\kappa_0}, \qquad q \in \mathbb{Z} \tag{3.45}$$

where $\beta_{j,1}$ and $\beta_{j,2}$, $j = 1, \cdots, m$ represent the m simple eigenvalues of the matrix B with $d = (1,0)$ and $d = (0,1)$ respectively.

Step 3. The vector Λ is, then, easily obtained by solving the system $A_1 \Lambda = \xi_1$.

Remark 24. *Note that, in Step 2, the eigenvalues of the matrix B^{d_r}, $r = a, b$, allow us to identify only the mesh points*

$$\left(\frac{1}{i\kappa_0} \log(\beta_{j,a}) + \frac{2p\pi}{\kappa_0}, \frac{1}{i\kappa_0} \log(\beta_{j,b}) + \frac{2q\pi}{\kappa_0} \right), \qquad (p,q) \in \mathbb{Z}^2.$$

To find the parameters q_a, q_b, satisfying the equalities (3.44) and (3.45), we, first, choose the mesh points belonging in Ω and then select, among those, the ones verifying the $2m$ underlying equations satisfied by a_j and b_j considering other directions of d.

3.4.4. Extension to multipolar sources

The proposed algorithm developed in the previous subsection can be extended even over multipolar sources of the form

$$F = \sum_{\ell=1}^{L} \sum_{j=1}^{N^\ell} \sum_{\alpha=0}^{K^\ell} \lambda_{j,\ell}^{\{\alpha_1,\alpha_2\}} \frac{\partial^\alpha}{\partial_x^{\alpha_1} \partial_y^{\alpha_2}} \delta_{\mathbf{S}_j^\ell} \tag{3.46}$$

where $\delta_{\mathbf{S}}$ stands for the Dirac distribution at the point $\mathbf{S}$, the quantities L, N^ℓ, K^ℓ are integers, the coefficients $\lambda_{j,\ell}^{\{\alpha_1,\alpha_2\}}$ are scalar quantities and $\alpha = \alpha_1 + \alpha_2$ with $(\alpha_1, \alpha_2) \in \mathbb{N}^2$. The points $\mathbf{S}_j^\ell = (a_j^\ell, b_j^\ell) \in \Omega$ and the orders of derivation K^ℓ are, respectively, assumed to be mutually distinct.

In this case, these sources could be recovered using the techniques employed in Subsection 3.4.2. Indeed, multiplying (3.32)-(3.46) by the test functions v_κ (defined in (3.35)) and assuming that $\kappa_n = n\kappa_0$, for $n = 1, \cdots, 2\bar{J}$, where κ_0 is a fixed positive wavenumber and $\bar{J}$ is a positive integer, we get the following algebraic relationships:

$$c_n := \mathcal{R}(v_{\kappa_n}, f_{\kappa_n}, g_{\kappa_n}) = \sum_{\ell=1}^{L}\sum_{j=1}^{N^\ell}\sum_{\alpha=0}^{K^\ell} \nu_{j,\ell}^{\alpha} n^\alpha (\mathbf{P}_j^\ell)^n \tag{3.47}$$

where $\mathcal{R}$ is the operator defined in (3.33),

$$\nu_{j,\ell}^{\alpha} = (-1)^\alpha (i\kappa)^\alpha \sum_{\alpha=\alpha_1+\alpha_2} d_1^{\alpha_1} d_2^{\alpha_2} \lambda_{j,\ell}^{\{\alpha_1,\alpha_2\}} \quad \text{and} \quad \mathbf{P}_j^\ell = e^{i\kappa_0 d.\mathbf{S}_j^\ell}.$$

The main objective of the following consists in establishing a general algebraic method for solving equations (3.47), allowing us to generalize Theorem 12 and Theorem 13. Indeed, assume that we know an upper bound $\bar{J}$ for the number

$$J = \sum_{\ell=1}^{L} (K^\ell + 1) N^\ell.$$

Define, for $n = 1, \cdots, \bar{J}$, the complex vectors

$$\xi_n = (c_n, \cdots, c_{\bar{J}+n-1})^t, \quad \Lambda = (\bar{\nu}_1, ..., \bar{\nu}_L)^t$$

where, for all $\ell = 1, \cdots, L$, we have

$$\bar{\nu}_\ell = (\bar{\nu}_\ell^0, ..., \bar{\nu}_\ell^{K^\ell}) \quad \text{with} \quad \bar{\nu}_\ell^\alpha = (\nu_{1,\ell}^\alpha, \cdots, \nu_{N^\ell,\ell}^\alpha) \quad \text{for all} \quad \alpha = 0, \cdots, K^\ell,$$

and consider, for all $n \in \mathbb{N}$, the complex matrices A_n, of size $\bar{J} \times J$

$$A_n = (V_{n,1}, \cdots, V_{n,L}) \tag{3.48}$$

with $V_{n,\ell} = (U_{n,\ell}^0, \cdots, U_{n,\ell}^{K^\ell})$, where, for $\alpha = 0, \cdots, K^\ell$, $U_{n,\ell}^\alpha$ are the confluent $\bar{J} \times N^\ell$ Vandermonde matrices

$$U_{n,\ell}^{\alpha} = \begin{pmatrix} n^{\alpha}(\mathbf{P}_1^{\ell})^n & \cdots & n^{\alpha}(\mathbf{P}_{N^{\ell}}^{\ell})^n \\ (n+1)^{\alpha}(\mathbf{P}_1^{\ell})^{n+1} & \cdots & (n+1)^{\alpha}(\mathbf{P}_{N^{\ell}}^{\ell})^{n+1} \\ \vdots & \ddots & \vdots \\ (\bar{J}+n-1)^{\alpha}(\mathbf{P}_1^{\ell})^{n+\bar{J}-1} & \cdots & (\bar{J}+n-1)^{\alpha}(\mathbf{P}_{N^{\ell}}^{\ell})^{n+\bar{J}-1} \end{pmatrix}.$$

Let c_n be the coefficients defined in (3.47) and introduce the Hankel matrix

$$H_{\bar{J}} = \begin{pmatrix} c_1 & c_2 & \cdots & c_{\bar{J}} \\ c_2 & c_3 & \cdots & c_{\bar{J}+1} \\ \vdots & \vdots & \vdots & \vdots \\ c_{\bar{J}} & c_{\bar{J}+1} & \cdots & c_{2\bar{J}-1} \end{pmatrix} \tag{3.49}$$

and the following multi-diagonal matrices

$$\bar{I}_{\ell} = \begin{pmatrix} \binom{0}{0}\nu_{\ell}^{0} & \binom{1}{0}\nu_{\ell}^{1} & \cdots & \binom{K^{\ell}}{0}\nu_{\ell}^{K^{\ell}} \\ \binom{1}{1}\nu_{\ell}^{1} & \binom{2}{1}\nu_{\ell}^{1} & \ldots \ \binom{K^{\ell}}{1}\nu_{\ell}^{K^{\ell}} & 0 \\ \vdots & \vdots & .\cdot^{\cdot} & \vdots \\ \binom{K^{\ell}-1}{K^{\ell}-1}\nu_{\ell}^{K^{\ell}-1} & \binom{K^{\ell}}{K^{\ell}-1}\nu_{\ell}^{K^{\ell}} & \cdots & 0 \\ \binom{K^{\ell}}{K^{\ell}}\nu_{\ell}^{K^{\ell}} & 0 & \cdots & 0 \end{pmatrix} \quad \text{for} \quad \ell = 1, \cdots, L \tag{3.50}$$

where, for $\alpha = 0, \cdots, K^{\ell}$,

$$\nu_{\ell}^{\alpha} = diag(\nu_{1,\ell}^{\alpha}, \cdots, \nu_{N^{\ell},\ell}^{\alpha}).$$

As in Subection 3.4.2, we propose an identification processes in two steps.

The first step consists in determining the number of sources by means of the following theorem.

Theorem 14. *Let $H_{\bar{J}}$ be the Hankel matrix defined in (3.49) where $\bar{J}$ is a known upper bound of J. Assume **(H2)** is verified, then, we have*

$$rank\,(H_{\bar{J}}) = \sum_{\ell=1}^{L}(K^{\ell}+1)N^{\ell} \quad \textit{if and only if} \quad \nu_{j,\ell}^{K^{\ell}} \neq 0 \quad \textit{for} \quad j = 1, ..., N^{\ell}, \quad \ell = 1, ..., L.$$

* * *

Proof. The proof is similar to that of Theorem 12. Indeed, first, from (3.48), we begin by rewriting the algebraic formulae (3.47) in a matrix form

$$\xi_n = A_n \Lambda, \quad \text{for} \quad n = 1, \cdots, \bar{J}. \tag{3.51}$$

Furthermore, if we denote, for $\ell = 1, \cdots, L$, by T_ℓ the block upper triangular complex matrix

$$T_\ell = \begin{pmatrix} \binom{0}{0} D_{P_\ell} & \binom{1}{0} D_{P_\ell} & \binom{2}{0} D_{P_\ell} & \cdots & \binom{K^\ell}{0} D_{P_\ell} \\ 0 & \binom{1}{1} D_{P_\ell} & \binom{2}{1} D_{P_\ell} & \cdots & \binom{K^\ell}{1} D_{P_\ell} \\ 0 & 0 & \ddots & \ddots & \vdots \\ \vdots & \ddots & \ddots & \binom{K^\ell - 1}{K^\ell - 1} D_{P_\ell} & \binom{K^\ell}{K^\ell - 1} D_{P_\ell} \\ 0 & 0 & \cdots & 0 & \binom{K^\ell}{K^\ell} D_{P_\ell} \end{pmatrix} \tag{3.52}$$

with

$$D_{P_\ell} = diag(\mathbf{P}_1^\ell, \cdots, \mathbf{P}_{N^\ell}^\ell),$$

one gets, using the following binomial formula $\sum_{j=0}^{\alpha} \binom{\alpha}{j} n^j = (n+1)^\alpha$, that

$$V_{n+1,\ell} = V_{n,\ell} T_\ell, \qquad \forall n \in \mathbb{N}.$$

From the definition of A_n (see (3.48)), we can check that for

$$T = diag(T_1, \cdots, T_L) \tag{3.53}$$

we have

$$A_{n+1} = A_n T = A_1 T^n, \qquad \forall n \in \mathbb{N}$$

and therefore, from (3.51), one gets

$$\xi_n = A_1 T^{n-1} \Lambda, \quad \text{for} \quad n = 1, \cdots, \bar{J}. \tag{3.54}$$

Now, thanks to (3.54), one can verify, by a simple calculation, that

$$H_{\bar{J}} = A_1[\Lambda, T\Lambda, ..., T^{\bar{J}-1}\Lambda] = A_1\bar{I}(A_0)^t$$

with $(A_0)^t$ the matrix transpose of A_0 and

$$\bar{I} = diag(\bar{I}_1, \cdots, \bar{I}_L)$$

where $\bar{I}_\alpha$, for $\alpha = 0, \cdots, K^\ell$, are defined in (3.50). The rest of the proof is done as in the end of the proof of Theorem 12. □

The second step consists in determining the location of the point sources. Henceforth, we replace $\bar{J}$ by J in the quantities defined above. Thus, from (3.54), we can easily derive the relations:

$$\xi_{n+1} = B\xi_n \quad \text{for} \quad n = 1, \cdots, \bar{J},$$

where we have set

$$B = A_1 T (A_1)^{-1}. \tag{3.55}$$

Here, the matrix A_1 is invertible, thanks to the assumption **(H2)**. Moreover, since rank$(H_J) = J$, the family $(\xi_n)_{n=1,...,J}$ forms a basis of $\mathbb{C}^J$, so the $J \times J$ complex matrix B is given explicitly by

$$B = \begin{pmatrix} 0 & 1 & \cdots & 0 & 0 \\ 0 & 0 & 1 & \cdots & 0 \\ \vdots & \vdots & \ddots & \ddots & 0 \\ \vdots & \vdots & \ddots & \ddots & 1 \\ q_1 & q_2 & \cdots & \cdots & q_J \end{pmatrix} \tag{3.56}$$

where the vector $Q = (q_1, ..., q_J)^t$ is obtained by solving the linear system $H_J Q = \xi_{J+1}$. Thus, the points $\mathbf{P}_j^\ell$ are given by the following theorem, which generalizes Theorem 13.

Theorem 15. *Let B, be the companion matrices defined in (3.56). Assume **(H2)** and that $\nu_{j,\ell}^{K^\ell} \neq 0$ for $j = 1, ..., N^\ell$ and $\ell = 1, ..., L$. Then*

1. *B admits N^ℓ eigenvalues of multiplicity $K^\ell + 1$ for $\ell = 1, ..., L$.*
2. *The N^ℓ eigenvalues of multiplicity $K^\ell + 1$ are the points $\mathbf{P}_j^\ell$.*

* * *

Proof. The proof of this theorem follows from (3.52), (3.53) and (3.55).

Thanks to Theorem 14, Theorem 15 and using the same algorithm detailed in the Subsection 3.4.3, we can identify the locations $\mathbf{S}_j^\ell$. Moreover, in order to determine $\nu_{j,\ell}^\alpha$, it is sufficient, for example, to solve the linear systems $A_1\Lambda = \xi_1$.

3.4.5. Sources with small support

In this subsection, we focus on the reconstruction of sources having compact support within a finite number of small subdomains of form (3.3), using multiple frequencies. The method proposed allows to solve the inverse source problem stated in Subsection 3.4.1 and particularly finding the number m, the points $\mathbf{S}_j$ and some characteristics of the domains D_j.

We proceed as in Subsection 3.4.2, we begin by multiplying equation (3.32)-(3.3) by the test functions v_κ (defined in (3.35)), integrating by parts and using Green's formula, we get

$$\mathcal{R}(v_\kappa, f_\kappa, g_\kappa) = \sum_{j=1}^{m} \int_{D_j} h_j(X) e^{i\kappa d.X} \, dX.$$

where $X = (x, y)$ and $\mathcal{R}$ is the operator defined in (3.33). Then, using the change of variable $X = \mathbf{S}_j + \varepsilon t$, with $t = (t_1, t_2)$, leads to

$$\mathcal{R}(v_\kappa, f_\kappa, g_\kappa) = \sum_{j=1}^{m} \mu_j^{\varepsilon,\kappa} e^{i\kappa d.\mathbf{S}_j}$$

where

$$\mu_j^{\varepsilon,\kappa} = \varepsilon^2 \int_{B_j} \tilde{h}_j(t) e^{i\varepsilon\kappa d.t} \, dt \qquad \text{with} \qquad \tilde{h}_j(t) = h_j(\mathbf{S}_j + \varepsilon t).$$

As in Subsection 3.4.4, replacing κ by κ_n, where $\kappa_n = n\kappa_0$, for $n = 1, \cdots, 2\bar{J}$, with κ_0 is a fixed positive constante and $\bar{J}$ is a positive integer, we obtain the algebraic relationships related to these source parameters and the Cauchy data

$$\mathcal{R}(v_{\kappa_n}, f_{\kappa_n}, g_{\kappa_n}) = \sum_{j=1}^{m} \mu_j^{\varepsilon,\kappa_n} \left(e^{i\kappa_0 d.\mathbf{S}_j}\right)^n. \tag{3.57}$$

Using the Taylor development of the exponential with respect to ε, we know that for $0 < \varepsilon < 1$ and non-negative integer K, we have

$$\mu_j^{\varepsilon,\kappa_n} = \sum_{\alpha=0}^{K} \nu_j^\alpha n^\alpha + O(\varepsilon^{K+3})$$

where

$$\nu_j^\alpha = \varepsilon^{2+\alpha} \frac{(i\kappa_0)^\alpha}{\alpha!} \int_{B_j} (d.t)^\alpha \tilde{h}_j(t)\, dt.$$

Replacing $\mu_j^{\varepsilon,\kappa_n}$ by its Taylor development in (3.57), we get

$$\mathcal{R}(v_{\kappa_n}, f_{\kappa_n}, g_{\kappa_n}) = \sum_{j=1}^{m} \sum_{\alpha=0}^{K} \nu_j^\alpha n^\alpha \left(e^{i\kappa_0 d.\mathbf{S}_j}\right)^n + O(\varepsilon^{K+3}).$$

Now, for a given positive $\varepsilon < 1$, we choose a fixed integer K such that ε^{K+3} is small enough and we assume that we know an upper bound $\bar{J}$ of $(m+1)K$. Then, we approximate the coefficients

$$c_n = \sum_{j=1}^{m} \sum_{\alpha=0}^{K} \nu_j^\alpha n^\alpha \left(e^{i\kappa_0 d.\mathbf{S}_j}\right)^n \quad \text{for} \quad n = 1, \cdots, 2\bar{J} \tag{3.58}$$

by $\mathcal{R}(v_{\kappa_n}, f_{\kappa_n}, g_{\kappa_n})$. Finally, we solve the algebraic relationships (3.58) using the same algorithm developed in the previous subsection to recover m, $\mathbf{S}_j$ and ν_j^α.

Note that, the coefficients ν_j^α are capable of giving some information over the domain B_j. Thus, one can obtain, up to a certain ε, for instance, certain quantities related to the mass or the moment of B_j.

Remark 25. *In the particular case where $D_j = \mathbf{S}_j + B_j$, with the domains B_j are hollow or solid balls of center $(0,0)$ and radii r_0^j, r_1^j, namely*

$$B_j = \{(x,y) \in \mathbb{R}^2 \quad : \quad 0 \leq r_0^j < \sqrt{x^2+y^2} \leq r_1^j\}$$

and taking the terms h_j as scalars, the points $\boldsymbol{S}_j$, their number and quantities related to h_j are easily recovered. This is done as in [EBN11b, Theorem 2], using the following mean value relation given in [CH89, Page 289], valid on all functions v solution of $\Delta v + \mu v = 0$ in Ω

$$v(\boldsymbol{S}_0)J_0(r\sqrt{\mu}) = \frac{1}{2\pi r^2}\int_C v dC$$

where $J_v(x)$ is the vth Bessel function, and C is the circle of center $\boldsymbol{S}_0$ and radius r entirely contained in Ω.

Using this theorem, these sources are reconstructed using algebraic relations of form (3.34).

3.5. Numerical simulations

This section studies numerically the robustness of the algebraic algorithm in the multi-frequential case with respect to the different parameters interfering in the reconstruction process. In this numerical study, the base wave coefficient κ_0 is fixed at $1.85\ m^{-1}$ and Γ is assumed to be a unit circle whose center is the origin O. The Cauchy data $(f_{\kappa_n}, g_{\kappa_n})$ on the boundary Γ are obtained by means of the fundamental solution of Helmholtz equation in $\mathbb{R}^2$. In fact, f_{κ_n} and g_{κ_n} are respectively the trace and the normal trace of w_{κ_n} on Γ, where w_{κ_n} is the fundamental solution corresponding to F (given by (3.2)), defined in the free space as:

$$w_{\kappa_n}(X) = \sum_{j=1}^{m} \lambda_j w^0_{\kappa_n}(X - \mathbf{S}_j), \qquad n = 1, ..., \bar{m}$$

where

$$w^0_\kappa(X) = \frac{1}{4i} H_0^{(1)}(\kappa\rho) \quad \text{and} \quad X = (x, y)$$

with $H_0^{(1)}$ is the Hankel function of first kind of order zero and $\rho = \sqrt{x^2 + y^2}$. Moreover, the coefficients c_r, defined in (3.36), are numerically computed using polar coordinates over a uniform meshing of distributed points on the unit circle.

The reconstruction of the number of sources is the major step in the identification process. Theoretically, their number is the rank of the Hankel matrices $H^d_{\bar{m}}$ which is numerically determined using SVD method with an appropriate threshold. However, since $H^d_{\bar{m}}$ is an ill-conditioned matrix, a regularization approach is employed. In fact, the $(m+1)$th singular value, σ_{m+1}, of $H^d_{\bar{m}}$ is theoretically zero, whereas when the perturbed $H^d_{\bar{m}} + \delta H^d_{\bar{m}}$ is given, one obtains a non zero σ_{m+1}. Therefore, based on the classical estimate,[Han98],

$$|\sigma_{m+1}| \leq \|\delta H^d_{\bar{m}}\|_F, \tag{3.59}$$

we truncate beyond a threshold inferior to $\|\delta H^d_{\bar{m}}\|_F$. Here, $\|\cdot\|_F$ is the corresponding Frobenius norm and $\delta H^d_{\bar{m}}$ is the related perturbation matrix of $H^d_{\bar{m}}$ that originates from the noise in data as well as from the numerical quadrature error using a finite number of sensors on Γ.

Remark 26. *We draw the attention of the reader to the fact that in the case of M sensors, the numerical error can be seen as noise equivalent to $(2\pi/M)$ perturbation. That is why, apart from the Subsection 3.5.1 dedicated to study the noise effect, we use the Cauchy data as non-noisy ones to see the identification process in an approximately ideal framework.*

Remark 27. *The calculation of $\|\delta H_{\bar{J}}\|_F$ is related to the numerical quadrature error. In here and as mentioned in the previous chapter this computation is not exact since we take into consideration just the numerical error $(2\pi/M)$. Nevertheless, in reality, $\delta H_{\bar{J}}$ is computed as*

$$\|\delta H_{\bar{J}}\|_F \simeq \bar{J}\sqrt{\frac{2\pi}{M}}\beta(\kappa_0, sources)$$

where β is the error related to the wavenumber and to the source positions. Therefore, in the following, we aren't reasonably capable of using the truncation threshold $\|\delta H_{\bar{J}}\|_F$ in the analysis of the impact of the wavenumber and the closeness of the sources over the identification process, unless we have a precise knowledge of β. Consequently, it will be used uniquely in the analysis of the impact of the number of sensors.

3.5.1. Determining number and position of monopole sources

In the following subsection, unless mentioned otherwise, we fix the number of monopoles at 5 having fixed intensities $\lambda_j = 1$ with positions taken as in Table 3.1.

j (location $\sharp$)	1	2	3	4	5
$\mathbf{S}_j$	(-0.7,0.3)	(0.6,-0.3)	(0.3,0.5)	(-0.5,-0.4)	(-0.1,0.0)

Table 3.1.: *The source positions*

a. Impact of the number of sensors

The mesh level represented by the number of sensors on the boundary has a great impact on the identification process. Increasing the sensors gives more accessibility to the Cauchy data pair and thus more specificity in the reconstruction process. Indeed, varying the number of sensors from 25 to 100 sensors, we note that, as seen in Figure 3.2 and Figure 3.3, their increase ameliorates the identification of both the number and the position of the monopoles. Moreover, we remark, based on that $\|\delta H_8^{d_i}\|_F$ (see Table 3.2) used for SVD truncation, that 5 monopoles can't be reconstructed with less than 50 sensors.

In addition to that, when projecting to the $x-$axis and the $y-$axis, we see that numerically, as noticed in the previous chapter and seen in the left and right panels of Figure 3.2, the number of sources is not the same on whatever axes where the projection is performed. This is due to the fact that the separability coefficient plays a role in the identification process as studied in the following subsubsection. Indeed, even with 100 sensors, the number of sources is ill-estimated in the y-projection, Figure 3.2 (right), since the sources projections are close. Therefore, to recover their number, we consider the numerical rank of the two Hankel matrices $H_{\tilde{m}}^{d_i}$, $i = 1, 2$, obtained respecting the truncation threshold defined in (3.59) and then we take the maximum of these ranks as the desired number of sources.

Number of sensors	25	35	50	100
$\|\delta H_8^{d_i}\|_F \simeq$	4.01	3.39	2.84	2.01

Table 3.2.: *The Frobenius norm of $\delta H_8^{d_1}$ with respect to the number of sensors*

For a better clarification, we present the numerical results explicitly in Table 3.3.

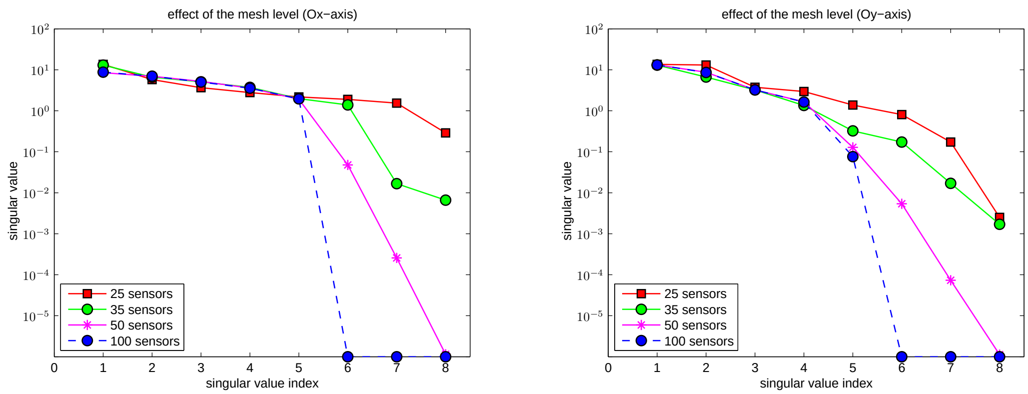

Figure 3.2.: *Singular value of $H_8^{d_i}$ on the $x-$ and $y-$ axis respectively for $m = 5$ with respect to the number of sensors.*

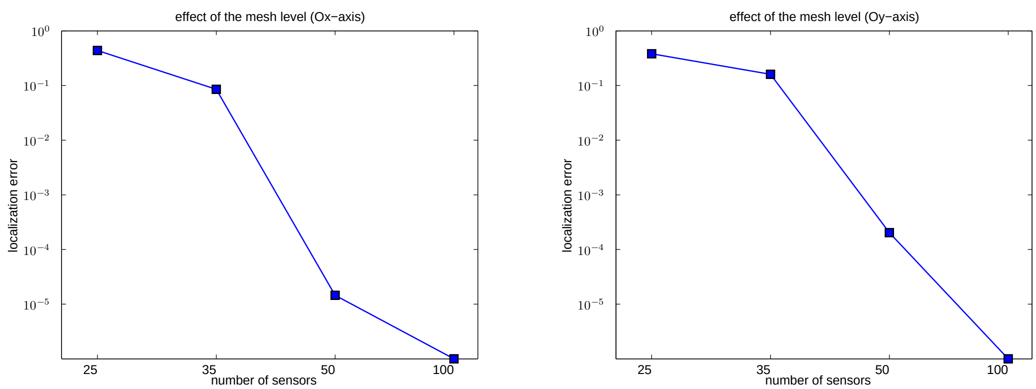

Figure 3.3.: *The localization error projected on the $x-$ and $y-$ axis respectively for $m = 5$ with respect to the number of sensors.*

From now on, we fix our study to 50 sensors that enable us to recover precisely the number and the location of up to 5 monopoles.

Number of sensors	Estimated x-projection	Estimated y-projection	Localization Error level
25	1.5603 - 0.4287i -0.1684 - 0.2029i -0.6806 + 0.0837i 0.8598 - 0.1819i 0.5905 + 0.2216i	1.3052 - 0.3423i 1.4591 - 0.2254i 0.4472 + 0.0772i -0.0631 + 0.0047i -0.3615 + 0.0183i	0.6145
35	-0.7044 - 0.0971i -0.6225 +0.0383i -0.0183 - 0.0899i 0.6141 - 0.0072i 0.2739 + 0.1010i	-1.2070 - 1.4298i 0.2916 - 0.2491i -0.3756 + 0.0178i 0.0665 + 0.1417i 0.4867 + 0.0251i	0.1485
50	0.6000 + 9.1e-07i 0.3000 + 4.6e-06i -0.1000 + 1.8e-05i -0.7000 + 1.0e-05i -0.5000 - 3.2e-05i	0.4999 + 1.9e-05i 0.2999 - 0.0004i 0.0004 + 0.0004i -0.4001 - 0.0003i -0.3009 - 0.0003i	1.6e-4
100	0.6000 - 7.1e-13i 0.3000 + 5.0e-12i -0.1000 - 3.2e-12i -0.7000 - 8.3e-12i -0.5000 - 1.1e-11i	0.5000 + 9.1e-12i 0.3000 - 2.0e-11i 7.1e-11 - 3.3e-11i -0.4000 - 1.8e-12i -0.3000 +7.8e-11i	2.9e-11

Table 3.3.: *The calculated $xy-$ source positions and their error for $m = 5$ when varying the number of sensors*

b. Impact of the base wavenumber

The left and right panels of Figure 3.4 show singular values of $H_8^{d_1}$ and the localization error when changing the base wavenumber κ_0. We observe that when as we enlarge the base wavenumber, the number is wrongly-estimated and the localization error increases. This result could be explained since we use $\bar{m} \times \kappa_0$ wavelengthes and the number of points per wavelength defined by

$$p \approx \frac{\text{number of sensors}}{\kappa_0}$$

decreases as κ_0 increases. We observe that when κ_0 is higher than $3\,m^{-1}$, we don't obtain the desired results anymore. Above this value, the exact truncation becomes impossible.

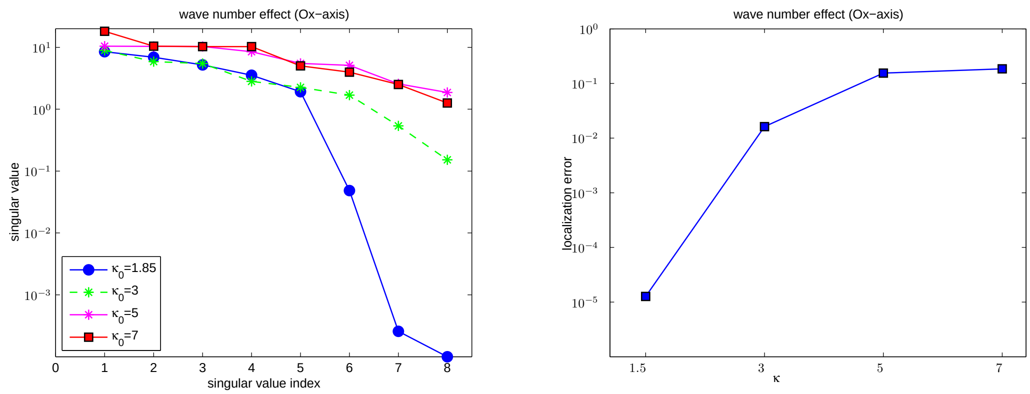

Figure 3.4.: *Singular values of* $H_8^{d_1}$ *(left) and the localization errors (right) projected on the* $x-axis$ *for* $m = 5$ *with* 50 *sensors.*

c. Impact of the noise

Reconstruction stability on the $x - axis$ projection with respect to the noise level is examined in this subsubsection. In fact, Gaussian noise is added to f (and g) with a standard deviation that varies from 10^{-2} to 10^{0} % (see Figure 3.5). We have noted studying the SVD of the Hankel matrix $H_{\tilde{m}}^{d_1}$ that the number of monopoles are badly-estimated when the percentage of noise exceeds $10^{0}\%$. Moreover, we note that the localization error increases gradually as the percentage of the noise added increases. Indeed, the error is of order 10^{-1} whereas in a noise free framework, we had an error of order 10^{-4}.

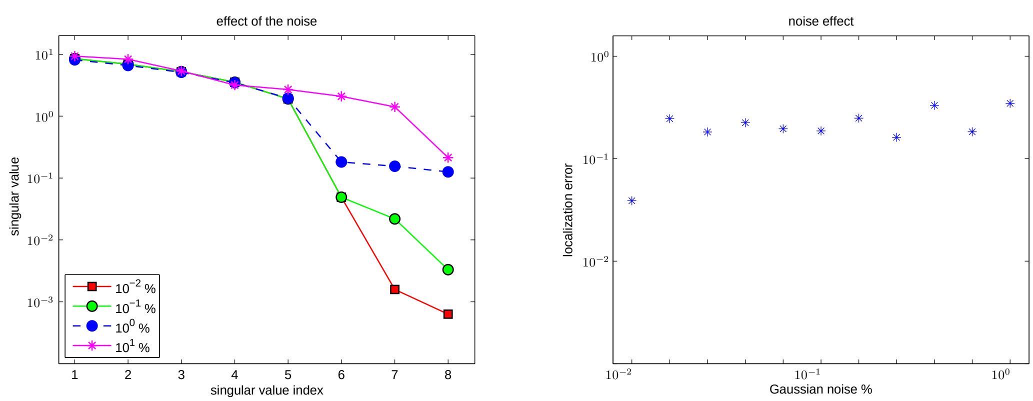

Figure 3.5.: *Singular values of* $H_8^{d_1}$ *(left) and the localization errors (right) projected on the* $x-axis$ *with* 50 *sensors.*

Chapter 4

Non-Stationary BLT Source Problem

One reason why mathematics enjoys special esteem, above all other sciences, is that its laws are absolutely certain and indisputable, while those of other sciences are to some extent debatable and in constant danger of being overthrown by newly discovered facts.

(Albert Einstein)

The object of this chapter is to study an inverse source problem over the parabolic equation (1.11) where the source term is a non-stationary one. Particulary, we consider monopoles having time-dependant intensities.

Section 4.1 states the inverse problem of the parabolic equation we are concerned with. Then, we present briefly the different source identification techniques used previously in the literature. Finally, we specify the type of sources to be considered in this chapter.

Section 4.2 presents the forward problem regularity in such a case in order to specify the space of the boundary measurement.

Section 4.3 is intended to prove the uniqueness of the inverse problem with the specified source form.

Section 4.4 states the principle of the identification method to be used.

Section 4.5 deals with the algebraic method used to determine the number and the position of the sources.

Section 4.6 proposes an optimization method to reconstruct the sources variable intensities based on a Kohn-Vogelius functional and calculates the needed gradient using the adjoint state method.

Section 4.7 presents the identification method based on both previous sections. We also pass by the resolution of a forward one-dimensional parabolic system used in the test functions of the algebraic algorithm.

Section 4.8 is consecrated to show the numerical results for the reconstruction of non-stationary monopoles. Other effects are considered, especially a comparison is done with the stationary case considered in Chapter 2.

4.1. Problem Statement

In this chapter, we aim to solve an inverse source problem to recover a source F in the parabolic equation (1.11). Since, in the BLT study, the intensity of the bioluminescent source varies [MV+12], it is more natural to consider the case where the source term has a time-variable moment "intensity" (variable orientation and amplitude) with a time-fixed position. Moreover, another important application related to this diffusion problem is that related to the identification of the pollution sources in a contaminant [OL01]. In fact, this chapter forms a revisit of the work [EBHD02], motivated by the latter application, where, in here, our objective is to provide a more complete study in particular by developing a new algebraic algorithm and by resolving the needed optimization problem.

Indeed, consider the region of study $\Omega \subset \mathbb{R}^3$, an open bounded domain with a sufficiently smooth boundary Γ and a fixed time $T > 0$. Let $\mathcal{Q}_T$ be the space-time domain $\Omega \times (0, T)$ and Σ_T the lateral boundary $\Gamma \times (0, T)$. The inverse problem, we are concerned with, is the problem of determining a source $\widetilde{F}(\mathbf{X}, t), \mathbf{X} = (x, y, z)$, in the equation (1.4) satisfied by $\widetilde{u}$ over $\mathcal{Q}_T$ given the boundary condition g^- and the measurement g.

Remark 28. *Note that the general case having a non-null g^- can be employed. However, due to the absence of an entering light source in the BLT study, the boundary condition g^- will be taken identically null, without loss of generality.*

Simplified Form

For reasons to explain later in Section 4.5, we simplify equation (1.4) using a convenient transformation. In fact, applying the following change of variable over $\widetilde{u}$, the solution of (1.4),

$$u(\mathbf{X}, t) = \widetilde{u}(\mathbf{X}, t)e^{c\mu_a t}, \tag{4.1}$$

the equation (1.4) can be simplified into the parabolic equation

$$\begin{cases} \frac{1}{c}\frac{\partial u}{\partial t}(\mathbf{X}, t) - \sigma\Delta u(\mathbf{X}, t) & = & F(\mathbf{X}, t) & \text{in} & \mathcal{Q}_T \\ u(\mathbf{X}, 0) & = & 0 & \text{in} & \Omega \\ u(\mathbf{X}, t) + 2\sigma\frac{\partial u}{\partial \nu}(\mathbf{X}, t) & = & 0 & \text{on} & \Sigma_T \end{cases} \tag{4.2}$$

where

$$F(\mathbf{X}, t) = \widetilde{F}(\mathbf{X}, t) e^{c\mu_a t}.$$

Here, the coefficient σ is supposed to be a fixed known constant and ν is the outward normal unit vector to Γ. The problem becomes thus the problem of determining the source F in the parabolic problem (4.2) from the measurement $f := u_{|\Sigma_T}$ prescribed on the boundary Σ_T of Q_T.

More precisely, we begin by defining, for all F in (4.2) the application

$$\Lambda : F \to u_{|\Sigma_T}.$$

The inverse problem is formulated as:

$$\text{given} \quad f \in L^2(\Sigma_T) \qquad \text{find} \quad F \quad \text{such that} \qquad \Lambda(F) = f.$$

The choice of the space $L^2(\Sigma_T)$ will be justified according to the nature of the considered sources.

As mentioned previously, one of the major difficulties of inverse source problems from boundary measurements is the problem of uniqueness. To overcome this difficulty, one must assume some *a priori* information on the sources, depending on the underlying physical problem.

4.1.1. Different identification Techniques

Time independent sources $F(\mathbf{X}, t) = f(\mathbf{X})$ were treated by Cannon in [Can68] using the spectral theory and by H. Engl,O.Scherzer and M. Yamamoto [ESY94] using the approximated controllability of the heat equation and generalized by Yamamoto [Yam93; Yam94] to the sources of the form $F(\mathbf{X}, t) = \alpha(t) f(\mathbf{X}), f \in \mathbb{L}^2$, where $\alpha \in \mathcal{C}^1[0, T]$ is known with $\alpha(0) \neq 0$. Only time dependant sources $F = F(t)$ were studied in [FL06]. A moving source whose spatial support is contained within a ball with a given radius is treated by Kusiak and Weatherwax [KW08] where they make use of an array of distributed observations in the space available at various instants in time. Hettlich and Rundell [HR01] considered a 2D problem for the heat equation with the sources $F(\mathbf{X}, t) = \chi_D(\mathbf{X})$, where D is a subset of a disk. Moreover, the fundamental solution method for reconstruction of certain source structures were considered in[Lin+06; YFY08]. For pointwise sources, an optimization method was applied in [EBHDH05; ABEB11] to get non-stationary monopoles and an algebraic method was utilized in [EBHD02] to recover stationary monpolar sources with time-varying intensities. In the latter papers, the authors used a method based on the assumption that the sources become inactive after a given time $T^* < T$ and the use of the null contrability approach.

4.1.2. Source form

In here, as in [EBHD02], we assume that the source F is a finite linear combination of monopolar sources having each a time-varying intensity. In fact, this source form may represent the early stage of a tumor development and thus helps in the early diagnosis of a cancer in the BLT method. Therefore, it is characterized by

$$F = \sum_{j=1}^{m} \lambda_j(t)\delta_{\mathbf{S}_j} \tag{4.3}$$

where $\delta_{\mathbf{S}}$ stands for the Dirac distribution at point $\mathbf{S}$ and m is an integer. The points $\mathbf{S}_j = (S_{j,a}, S_{j,b}, S_{j,c}) \in \Omega$ are assumed to be mutually distinct and the coefficients $\lambda_j(t)$ are supposed to be non-zero functions that belong to $L^2(\Omega)$. Then, the inverse problem becomes the problem of determining the number of sources m, their locations $\mathbf{S}_j$ and the coefficients $\lambda_j(t)$ using boundary measurements.

A novelty, in here, with respect to former works, is the nonnecessity of neither the inactivity of the intensities after a certain time T^* nor their positivity.

4.2. Forward problem regularity

In order to study the inverse problem, one must attain the boundary measurement in its convenient space and hence the need to study the forward problem regularity.

Before stating the regularity of the direct problem, the following functional spaces are needed:

The Lebesgue space of functions square integrable over Ω is denoted by $L^2(\Omega)$. The set of all functions $u \in L^2(\Omega)$, such that for every multi-index α with $|\alpha| \leq 2$, the weak derivative $D^\alpha u \in L^2(\Omega)$, is denoted by $H^2(\Omega)$. We use also the vector valued Sobolev space

$$H^{2,1}(Q_T) = \{u \in L^2\big(0, T; H^2(\Omega)\big) \cap H^1\big(0, T; L^2(\Omega)\big)\}$$

and for the positive reals r and s:

$$H^{r,s}(\Sigma_T) = L^2\big(0,T;H^r(\Sigma_T)\big) \cap H^s\big(0,T;L^2(\Sigma_T)\big).$$

For more details concerning these spaces, see [LMK72].

Forward Problem. Given the source term F (which means given m, $\lambda_j(t)$ and $\mathbf{S}_j$), the forward problem consists in determining the trace $u|_{\Sigma_T}$ of the solution of the problem (4.2).

In fact, let us consider, for $m = 1$, the Cauchy problem

$$\begin{array}{lcll} \frac{1}{c}\frac{\partial \omega}{\partial t} - \sigma\Delta\omega & = & \lambda(t)\delta_{\mathbf{S}} & \text{in} \quad \mathbb{R}^3 \times (0,T) \\ \omega(\mathbf{X},0) & = & 0 & \text{in} \quad \mathbb{R}^3. \end{array}$$

Its solution is given explicitly by

$$\omega(\mathbf{X},t) = \frac{Y(t)}{(4\pi c\sigma)^{3/2}} \int_0^t \frac{c\lambda(\tau)}{(t-\tau)^{3/2}} e^{-\frac{|\mathbf{X}-S|^2}{4c\sigma(t-\tau)}}\, d\tau,$$

where Y is the Heaviside function. Let φ be the difference $\omega - u$, solution to the non-homogeneous initial-boundary value problem

$$\begin{array}{lcll} \frac{1}{c}\frac{\partial \varphi}{\partial t} - \sigma\Delta\varphi & = & 0 & \text{in} \quad Q_T \\ \varphi + 2\sigma\frac{\partial \varphi}{\partial n} & = & q & \text{on} \quad \Sigma_T \\ \varphi(\mathbf{X},0) & = & 0 & \text{in} \quad \Omega \end{array}$$

where $q = \omega + 2\sigma\frac{\partial \omega}{\partial \nu}$.

We see that ω is a C^∞ function of $(\mathbf{X},t)$ in $\mathbb{R}^3 \backslash \{\mathbf{S}\} \times (0,T)$. Consequently q is smooth near the boundary Σ_T, in particular, one has that $q \in H^{\frac{1}{2},\frac{1}{4}}(\Sigma_T)$. Thus, according to [[LMK72],Theorem 4.3,Theorem 2.1], one has $\varphi \in H^{2,1}(Q_T)$ and consequently $\varphi_{|\Sigma_T} \in H^{\frac{3}{2},\frac{3}{4}}(\Sigma_T)$.

Because of the regularity of both φ and w on Σ_T, one has that $u_{|\Sigma_T} \in H^{\frac{3}{2},\frac{3}{4}}(\Sigma_T)$ and therefore

$$u_{|\Sigma_T} \in L^2(\Sigma_T).$$

We note that the same conclusion is drawn for $m > 1$. Then, one can define the application

$$\Lambda(F) = u_{|\Sigma_T}, \tag{4.4}$$

which defines the forward problem.

The inverse problem we are concerned with can then be stated as follows.

Inverse Problem. Given a function $f \in \mathrm{L}^2(\Sigma_T)$, the goal is to determine m, $\mathbf{S}_j$ and $\lambda_j(t)$, such that

$$\Lambda(F) = f. \tag{4.5}$$

Definition 4.1. *We say that f is a compatible data if the inverse problem (4.5) admits a solution F.*

* * *

4.3. Identifiability issue

Uniqueness of the number m, the locations $\mathbf{S}_j$ and the intensities λ_j is shown in [AEB12]. Therefore, in this work, we focus on, the identification issue which is the objective of the following section and we simply give a brief reminder of the uniqueness issue in this section.

Theorem 16. *Let F^ℓ, $\ell = 1, 2$, be two sources of the form (4.3) and let u_ℓ be the corresponding solutions of (4.2) such that $f^1 = f^2$. Then,*

$$m^1 = m^2 = m$$

and there exists a permutation π of the integers $1, ..., m$ such that

$$\boldsymbol{S}_j^1 = \boldsymbol{S}_{\pi(j)}^2, \qquad j = 1, \cdots, m$$

$$\lambda_j^1(t) = \lambda_{\pi(j)}^2(t), \qquad \forall t \in (0, T), \qquad j = 1, \cdots, m.$$

* * *

Proof: The same logic as that done in order to prove the uniqueness in the stationary case is employed here (see Proof in Subsection 2.2.1). Indeed, using the unique continuation of Mizohata's theorem [Miz58; SS87] and the regularity of the Dirichlet problem, one gets

$$F^1 = F^2.$$

Moreover, due to the linear independence of Dirac deltas, we obtain the uniqueness of the number and the locations of the sources. Therefore, we have

$$\sum_{j=1}^{m}(\lambda_j^2 - \lambda_j^1)(t)\delta_{\mathbf{S}_j} = 0. \tag{4.6}$$

We define, as done in [AEB12], for $k = 1, ..., m$,

$$w_k(\mathbf{X}, t) = \begin{cases} 1 & \text{in} \quad \mathcal{V}(\mathbf{S}_k) \times (0, T) \\ \\ 0 & \text{Otherwise} \end{cases}$$

where $\mathcal{V}(\mathbf{S}_k)$ is a neighborhood of the point $\mathbf{S}_k$ that doesn't contain any $S_j, j \neq k, j = 1, ..., m$. Now, let (φ_i) be an orthonormal basis of $L^2(0, T)$. Multiplying (4.6) by $w_k(\mathbf{X}, t)\varphi_i(t)$ and integrating over Q_T, we get

$$\int_0^T (\lambda_k^2 - \lambda_k^1)\varphi_i(t)\, dt = 0,$$

and thus we obtain

$$\lambda_k^2 = \lambda_k^1 \qquad \forall k = 1, \cdots, m$$

i.e. one proves that the source number, positions and intensities are uniquely determined using the boundary measurement f. $\square$

4.4. The principle of the reconstruction method

As in the stationary case and since the two-dimensional space is harder to manipulate with our approach than that of three-dimensional space, we will consider the domain Ω in $\mathbb{R}^3$. Our identification method is a quasi-algebraic method composed of two parts. The first one consists in determining the sources number and positions using the algebraic method developed in Chapter 2 and the second part deals with the identification of the source intensities by means of an optimization method over a Kohn-Vogelius type functional.

First, since the source F is a finite linear combination of Dirac distributions, one has to consider the solution of (4.2) in a weak sense, that is

$$\sum_{j=1}^{m}\int_0^T \lambda_j(t)v(\mathbf{S}_j,t)dt = \int_{\Sigma_T}\sigma(\frac{\partial v}{\partial\nu}+\frac{v}{2\sigma})\,u\,dsdt + \frac{1}{c}\int_\Omega u(\mathbf{X},T)v(\mathbf{X},T)\,d\mathbf{X}, \quad (4.7)$$

for every function v solution of the adjoint equation

$$\tfrac{1}{c}\tfrac{\partial v}{\partial t}(\mathbf{X},t)+\sigma\Delta v \;=\; 0 \;\text{ in }\; Q_T. \quad (4.8)$$

To solve this inverse problem, we need the knowledge of the value of $u(\mathbf{X},T)$, unless if we impose that the solution v of (4.8) satisfies

$$v(\mathbf{X},T)=0 \quad \text{in}\,\Omega. \quad (4.9)$$

To overcome this difficulty, in [EBHD02; EBHDH05; AEB12], the authors opted for the determination of the value of the unknown $u(\mathbf{X},T)$ using the fact that the intensities $\lambda_j(t)$ become inactive after a certain time $T^* < T$ and applying the null contrability approach.

In here, this approach isn't employed where we opt for the choice of the condition (4.9). Indeed, we introduce what one calls test functions, the solutions of (4.8) verifying the condition (4.9) and we denote by $\mathcal{T}$ the set of the test functions satisfying (4.8-4.9). Defining the operator

$$\mathcal{R}(v)=\int_{\Sigma_T}\sigma(\frac{\partial v}{\partial\nu}+\frac{v}{2\sigma})\,u\,dsdt \;\text{ for all }\; v\in\mathcal{T},$$

and thanks to the identifiability issue, we know that there is a unique set of point sources $(m,\mathbf{S}_j,\lambda_j)$ that satisfy the algebraic equations

$$\mathcal{R}(v)=\sum_{j=1}^{m}\int_0^T \lambda_j(t)v(\mathbf{S}_j,t)\,dt \quad \text{for all }\; v\in\mathcal{T}. \quad (4.10)$$

In the following, we will show how an appropriate choice of test functions unveils the desired information.

4.5. Recovering of point sources

The general idea behind our identification method is the projection of the problem onto chosen test functions. This idea is not new, however our approach employs a specific family of functions that allow a practical solution.

Assume that the domain Ω can be defined by:

$$\Omega = \{(x, y, z) \in \mathbb{R}^3,\ a \ \leq\ z\ \leq\ b,\ (x, y) \in D_z\},$$

where D_z is the intersection of the domain Ω and the plane of level z parallel to xOy. Consider, now, the one-dimensional parabolic equation

$$\begin{array}{lcl} \frac{1}{c}\frac{\partial \rho}{\partial t}(z,t) + \sigma \rho_{zz}(z,t) & = & 0 \ \text{ in } \ (a,b)\times(0,T) \\ \rho(z,T) & = & 0 \ \text{ in } \ (a,b). \end{array} \tag{4.11}$$

Remark 29. *Note that without the use of the change of variables (4.1), the parabolic equation (4.11) would have been*

$$\frac{1}{c}\frac{\partial \rho}{\partial t}(z,t) + \sigma \rho_{zz}(z,t) + \mu\rho(z,t) = 0 \qquad in\,(a,b)\times(0,T).$$

So, employing the test functions

$$v_n^a(x, y, z, t) = \rho(z, t)(x + iy)^n,\ n \in \mathbb{N}, \tag{4.12}$$

the relation (4.10) becomes

$$\alpha_n^a = \sum_{j=1}^{m} \mu_j^a (P_j^a)^n \quad \text{for all } \ n \in \mathbb{N}, \tag{4.13}$$

where

$$\alpha_n^a = \mathcal{R}(v_n^a), \quad \mu_j^a = \int_0^T \lambda_j(t)\rho(t, S_{j,c})dt,$$

and P_j^a is the 2D projection of $\mathbf{S}_j$ on the $xy-$ complex plane defined as

$$P_j^a = S_{j,a} + iS_{j,b}.$$

Before solving the equations (4.13), we need to assure that the projections P_j^a are mutually distinct, which is necessary in order to use the algebraic method proposed below. Indeed, as mentioned before and without loss of generality, we can assume that:

(H3) The projections onto the xy, yz and xz-planes, of points $\mathbf{S}_j$ are mutually distinct.

Moreover, denote by P_j^b and P_j^c, the projections of $\mathbf{S}_j$ onto the yz and xz-complex planes respectively. Then, using, in (4.10), the test functions

$$v_n^b = \rho(x,t)(y+iz)^n \quad \text{and} \quad v_n^c = \rho(y,t)(x+iz)^n \tag{4.14}$$

with $v_n^b, v_n^c \in \mathcal{T}$, one has, as in (4.13), the following algebraic equations

$$\alpha_n^b = \sum_{j=1}^m \mu_j^b (P_j^b)^n \quad \text{for all} \;\; n \in \mathbb{N} \tag{4.15}$$

and

$$\alpha_n^c = \sum_{j=1}^m \mu_j^c (P_j^c)^n \quad \text{for all} \;\; n \in \mathbb{N} \tag{4.16}$$

where we note

$$\alpha_n^b = \mathcal{R}(v_n^b), \quad \mu_j^b = \int_0^T \lambda_j(t)\rho(S_{j,a},t)dt,$$

and

$$\alpha_n^c = \mathcal{R}(v_n^c), \quad \mu_j^c = \int_0^T \lambda_j(t)\rho(S_{j,b},t)dt.$$

Finally, bringing together the three equations (4.13), (4.15) and (4.16), we can write

$$\alpha_n^r = \sum_{j=1}^m \mu_j^r (P_j^r)^n, \qquad r = a,b,c. \tag{4.17}$$

Therefore, the problem is reduced to that of determining the parameters $(m, \mathbf{S}_j, \mu_j^r)$ from the knowledge of α_n^r for all $n \in \mathbb{N}$. These parameters are reconstructed using the algebraic method given in [EBHD00a] and revisited in Chapter 2 and presented briefly below.

First, assume that we know an upper bound of the number of monopoles denoted by

$\bar{m}$ and define the $\bar{m} \times \bar{m}$ Hankel matrix

$$H^r_{\bar{m}} = \begin{pmatrix} \alpha^r_0 & \alpha^r_1 & \cdots & \alpha^r_{\bar{m}-1} \\ \alpha^r_1 & \alpha^r_2 & \cdots & \alpha^r_{\bar{m}} \\ \vdots & \vdots & \vdots & \vdots \\ \alpha^r_{\bar{m}-1} & \alpha^r_{\bar{m}} & \cdots & \alpha^r_{2\bar{m}-2} \end{pmatrix}. \tag{4.18}$$

Then, the number of sources can be determined as stated in the theorem below.

Theorem 17. *Let $H^r_{\bar{m}}$ be the Hankel matrix defined in (4.18) where $\bar{m}$ is a known upper bound of m. Under hypothesis **(H3)**, we have*

$$rank\,(H^r_{\bar{m}}) = m \qquad \textit{if and only if} \qquad \mu^r_j \neq 0 \quad \textit{for} \quad r = a, b, c.$$

* * *

Proof: The proof is the similar to that proof of [Theorem 4, Chapter 2]. □

Remark 30. *Observe that thanks to the maximum principle and an appropriate choice of boundary conditions in (4.11), the corresponding functions ρ are positive. Therefore, if the intensities λ_j are assumed to be positive, one assures the non-nullity of the coefficients μ^a_j.*

To reconstruct the location of the sources, introduce the companion matrix

$$B^r = \begin{pmatrix} 0 & 1 & \cdots & 0 & 0 \\ 0 & 0 & 1 & \cdots & 0 \\ \vdots & \vdots & \ddots & \ddots & 0 \\ \vdots & \vdots & \ddots & \ddots & 1 \\ d^r_0 & d^r_1 & \cdots & \cdots & d^r_{m-1} \end{pmatrix} \tag{4.19}$$

where the vector $D^r = (d^r_0, ..., d^r_{m-1})^t$ is solution of the linear system

$$H^r_{\bar{m}} D^r = \xi^r_m$$

with $\xi^r_m = (\alpha_m, \cdots, \alpha_{2m-1})^t$. Then, we obtain the source locations via the following theorem:

Theorem 18. *Let m be a non-negative integer. Then, the companion matrix B^r, defined in (4.19), admits m simple eigenvalues. These eigenvalues are the projections P^r_j of the points $\boldsymbol{S}_j$.*

* * *

4.6. Recovering the intensity functions

This subsection deals with the identification of the intensities. At this step, the number m of the sources and the locations $\mathbf{S}_j$ are already obtained. Therefore, several approaches for determining the intensities λ_j could be considered. Our choice, in here, is to focus on the classical minimization problem using a Kohn-Vogelius objective functional.

4.6.1. Kohn-Vogelius's fonctional

Let us denote by $F(\mathbf{S}_j, \phi)$ the source of form (4.3) where $\phi = (\lambda_j(t))_{j=1}^m$. Consider a variant of the Kohn-Vogelius type objective function.

Indeed, introduce the objective functional

$$J_{KV}(\phi) = \int_{Q_T} \sigma |\nabla w|^2 d\mathbf{X}dt + \frac{1}{2c}\int_\Omega w^2(\mathbf{X}, T)\, d\mathbf{X}$$

with $w = u_r - u_d$ where $u_r = u_r(\phi)$ satisfies the system

$$\left\{\begin{array}{rclll} \frac{1}{c}\frac{\partial u_r}{\partial t} - \sigma\Delta u_r &=& F(\mathbf{S}_j, \phi) & \text{in} & Q_T \\ f + 2\sigma\frac{\partial u_r}{\partial \nu} &=& 0 & \text{on} & \Sigma_T \\ u_r(\mathbf{X}, 0) &=& 0 & \text{in} & \Omega \end{array}\right. \tag{4.20}$$

and u_d is the solution of

$$\left\{\begin{array}{rclll} \frac{1}{c}\frac{\partial u_d}{\partial t} - \sigma\Delta u_d &=& F(\mathbf{S}_j, \phi) & \text{in} & Q_T \\ u_d &=& f & \text{on} & \Sigma_T \\ u_d(\mathbf{X}, 0) &=& 0 & \text{in} & \Omega \end{array}\right. \tag{4.21}$$

Thus, w satisfies the homogenous parabolic equation

$$\frac{1}{c}\frac{\partial w}{\partial t} - \sigma \Delta w = 0 \tag{4.22}$$

with the initial condition $w(\mathbf{X}, 0) = 0$ and the boundary condition

$$w = u_r - f \qquad \text{on} \quad \Sigma_T.$$

Multiplying (4.22) by w and then integrating over Q_T, we obtain that

$$J_{KV}(\phi) = \int_{\Sigma_T} (f - u_r)(\sigma \frac{\partial u_d}{\partial \nu} + \frac{f}{2})\, dsdt. \tag{4.23}$$

Our goal is to solve the optimization problem whose aim is to recover the optimal intensities $\tilde{\phi}$ in

$$J_{KV}(\tilde{\phi}) = \min_{\phi \in [L^2(0,T)]^m} J_{KV}(\phi) \tag{4.24}$$

Proposition 1. *Let $f \in L^2(\Sigma_T)$ be a compatible data for the inverse problem (4.5). Then, the minimization problem (4.24) is equivalent to the inverse problem (4.5).*

Proof: Indeed, let $\bar{\phi}$ be the solution of the inverse problem (4.5) related to f. Then, we have $\Lambda(u_r) = f$ i.e. $u_{r|_{\Sigma_T}} = f = u_{d|_{\Sigma_T}}$. Thus, we obtain $w = 0$ over Σ_T and consequently w is identically null over Q_T (since it verifies (4.22) with $w(\mathbf{X}, 0) = 0$ over Ω). Therefore, one has

$$J_{KV}(\bar{\phi}) = 0 = \min_{\phi \in \Phi} J_{KV}(\phi),$$

and consequently $\bar{\phi}$ is also the solution of the optimization problem (4.24).

On the other hand, let $\tilde{\phi}$ be the global minimum of the optimization problem (4.24), then

$$J_{KV}(\tilde{\phi}) \leq J_{KV}(\phi) \qquad \forall\ \phi \in [L^2(0,T)]^m.$$

This leads us to have $J_{KV}(\tilde{\phi}) = 0$. Therefore, $w(\mathbf{X}, t) = c(t)$ in Q_T. Since $w(\mathbf{X}, 0) = 0$, one has $w \equiv 0$ over Q_T leading to

$$u_{r|_{\Sigma_T}} = f = u_{d|_{\Sigma_T}}.$$

Then, we have

$$\Lambda(F(\mathbf{S}_j, \tilde{\phi})) = \Lambda(F(\mathbf{S}_j, \bar{\phi})).$$

Therefore, due the injectivity of the application $F \to \Lambda(F)$ (the uniqueness property), one obtains $\tilde{\phi} = \bar{\phi}$. □

4.6.2. Calculation of the gradient ∇J_{KV}

To solve the optimization problem (4.24) using the gradient or quasi-Newton methods, we need to calculate the gradient of the functional J_{KV} with respect to ϕ. To do so, we opt for the classical adjoint state method as follows.

Indeed, by means of the classical Lagrangian method, one can define λ_r and λ_d, the adjoint states of u_r and u_d solutions of (4.20) and (4.21), as the respective solutions of:

$$\left\{ \begin{array}{rclcc} -\frac{1}{c}\frac{\partial \lambda_r}{\partial t} - \sigma\Delta\lambda_r & = & 0 & \text{in} & Q_T \\ \sigma\frac{\partial \lambda_r}{\partial \nu} & = & \frac{f}{2} + \sigma\frac{\partial u_d}{\partial \nu} & \text{on} & \Sigma_T \\ \lambda_r(\mathbf{X}, T) & = & 0 & \text{in} & \Omega \end{array} \right. \tag{4.25}$$

and

$$\left\{ \begin{array}{rclcc} -\frac{1}{c}\frac{\partial \lambda_d}{\partial t} - \sigma\Delta\lambda_d & = & 0 & \text{in} & Q_T \\ \lambda_d & = & f - u_r & \text{on} & \Sigma_T \\ \lambda_d(\mathbf{X}, T) & = & 0 & \text{in} & \Omega \end{array} \right. \tag{4.26}$$

Moreover, recall that the gradient ∇J_{KV} of the functional J_{KV} is such that

$$J_{kv}(\phi + \phi_1) - J_{kv}(\phi) = (\nabla J_{kv}, \phi_1)_{L^2} + O(|\phi_1|^2_{L^2})$$

with

$$\phi_1 = (h_j)_{j=1}^m.$$

Taking the linear part of $J_{kv}(\phi + \phi_1) - J_{kv}(\phi)$ leads to

$$(\nabla J_{kv}, \phi_1)_{L^2} = \int_\Sigma \sigma(f - u_r)\frac{\partial u_d^1}{\partial \nu}\, d\sigma - \int_\Sigma \sigma u_r^1 (\frac{\partial u_d + f)}{\partial \nu}\, d\sigma \tag{4.27}$$

where the sensitivity functions u_r^1 and u_d^1 satisfy respectively the systems

$$\begin{cases} \frac{1}{c}\frac{\partial u_r^1}{\partial t} - \sigma \Delta u_r^1 & = & F(\mathbf{S}_j, \phi_1) & \text{in} & Q_T \\ \sigma \frac{\partial u_r^1}{\partial \nu} & = & 0 & \text{on} & \Sigma_T \\ u_r^1(\mathbf{X}, 0) & = & 0 & \text{in} & \Omega \end{cases}$$

and

$$\begin{cases} \frac{1}{c}\frac{\partial u_d^1}{\partial t} - \sigma \Delta u_d^1 & = & F(\mathbf{S}_j, \phi_1) & \text{in} & Q_T \\ u_d^1 & = & 0 & \text{on} & \Sigma_T \\ u_d^1(\mathbf{X}, 0) & = & 0 & \text{in} & \Omega. \end{cases}$$

According to the regularity of the compatible data f and the traces of u_r and u_d on the boundary Σ_T, the adjoint states $\lambda_r, \lambda_d \in H^{2,1}(Q_T)$.

Finally, by integrating by parts the expression

$$\int_{Q_T} \left[\lambda_r (\frac{\partial u_r^1}{\partial t} - \sigma \Delta u_r^1) + \lambda_d (\frac{\partial u_d^1}{\partial t} - \sigma \Delta u_d^1) \right] dx\, dt,$$

equation (4.27) can be rewritten as

$$(\nabla J_{kv}, \phi_1)_{L^2} = - \sum_{j=1}^{m} \int_0^{T^*} \big(\lambda_n(\mathbf{S}_j, t) + \lambda_d(\mathbf{S}_j, t)\big) h_j^1 \, dt$$

Therefore, the gradient of the Kohn-Vogeluis functional is given by:

$$\nabla J_{KV} = - \left(\lambda_r(\mathbf{S}_j, t) + \lambda_d(\mathbf{S}_j, t)\right)_{j=1}^{m}$$

4.7. The quasi-algebraic algorithm

Step 1: *Calculation of the test functions*

Since the test functions (4.12) used in the reconstruction method depends on $\rho(z,t)$ then one needs the resolution of the forward 1-D parabolic system (4.11). To assure the positivity of ρ, see Remark 30, numerically the boundary conditions are taken as:

$$\begin{array}{rcll} \rho(a,t) & = & 0 & \text{on} \quad (0,T) \\ \rho(b,t) & = & h & \text{on} \quad (0,T), \end{array} \tag{4.28}$$

where h is a positive constant over $(0,T)$.

We note $\psi(z,t) = p(z,t) - \rho(z,T-t)$, where p is defined as

$$p(z,t) = \frac{z-a}{b-a}h,$$

then, ψ satisfies

$$\begin{array}{lcll} \frac{1}{c}\frac{\partial\psi}{\partial t}(z,t) - \sigma\psi_{zz}(z,t) & = & 0 & \text{in} \quad (a,b)\times(0,T) \\ \psi(z,0) & = & p(z,0) & \text{in} \quad (a,b) \end{array} \tag{4.29}$$

with homogenous boundary conditions, with $\psi(a,t) = \psi(b,t) = 0$ over $(0,T)$.

Let V be the Hilbert space $V = H_0^1((a,b))$, then, using integration by parts, we get, for all $v \in V$,

$$\frac{1}{c}\frac{d}{dt}\int_a^b (\psi(t),v)\,dz + \sigma\int_a^b \frac{d\psi(t)}{dz}\frac{dv(t)}{dz}\,dz = 0$$

The variational formulation is then defined as finding ψ that satisfies

$$\left\{ \begin{array}{lcl} \frac{1}{c}\frac{d}{dt}(\psi(t),v) + a(\psi(t),v) & = & 0 \\ \\ \psi(0) & = & \psi_0 \end{array} \right. \tag{4.30}$$

in the distribution sense of for all $v \in V$. The bilinear form $a : V \times V \to \mathbb{R}$ is defined as

$$a(\psi(t),v) = \sigma\int_a^b \frac{d\psi(t)}{dz}\frac{dv(t)}{dz}\,dz.$$

Since the bilinear form a is continuous over $V \times V$ and coercive with respect to V and the initial condition belongs to $L^2(0,T)$, then, there exists a unique solution $\psi \in L^2(0,T;H_0^1) \cap \mathcal{C}^0(0,T,L^2)$ satisfying (4.30).

To solve numerically this one-dimensional parabolic problem, we discretize the problem where we consider finite dimensional approximations that approach the solution in the limit. This is done using the finite element Galerkin approximation in space V and using finite difference method for time discretization.

We use the one-ordered lagrange triangular finite elements over (a,b), that is, approximating the Hilbert space V by the subspaces V_h defined as

$$V_h = \{v \in C((a,b)); v|_{K_i} \in \mathbf{P}_1\}$$

where $K_i = [z_i, zi+1] \in T_h, \qquad 0 \le i \le n,$

$$\begin{aligned}\mathbf{P}_k &= \{P \in \mathbf{R}[X]; \text{degree}(P) \le 1\}\\ &= \text{polynomials of real coefficients of degree} \le 1\end{aligned}$$

and

$$T_h \quad = \quad \text{a uniform discretization of the interval [a,b] into } n+1 \text{ sub-intervals}$$

and V_{0h} are subspaces of V_h with $v(a) = v(b) = 0$.

The objective is, thus, to replace the continuous problem by an other that searches to find the approximated values $\psi_h(t)$ of the exact solution $\psi(t)$ over the mesh points. First, we decompose $\psi_h(t)$ in the basis of $(\varphi_i)_{i=1}^n$ of V_h where $\psi_h(t) = \sum_{i=1}^n \psi_i(t)\varphi_i$. Thus, we obtain, for $v_h = \varphi_j$,

$$\frac{1}{c}\frac{d}{dt}\psi_i(t)\sum_{i=1}^n \int_a^b \varphi_i(z)\varphi_j(z)\,dz + \sigma\psi_i(t)\sum_{i=1}^n \int_a^b \varphi'_i(z)\varphi'_j(z)\,dz = 0 \qquad 1 \le j \le n.$$

Hence, the approximated problem becomes of the form:

$$\left\{\begin{array}{rcl} M\frac{\partial \Psi}{\partial t}(t) + R\Psi(t) &=& 0 \quad 0 \le t \le T \\ \\ \Psi(0) &=& \psi_0 \end{array}\right. \tag{4.31}$$

with

$$\Psi(t) = (\psi_1(t), \psi_2(t), \cdots, \psi_n(t))^t \qquad M = \frac{1}{c}\left(\int_a^b \varphi_i\varphi_j\,dz\right)_{1\le i,j\le n}$$

$$R = \sigma\left(\int_a^b \varphi'_i\varphi'_j\,dz\right)_{1\le i,j\le n},$$

where the rigid and mass matrices are constructed classically [RT83].

To complete the numerical solution of (4.29), we discretize the time variable. The method used for the time discretization is the finite difference method where a simple finite difference approximation is given by

$$\frac{d\Psi^i}{dt} \approx \frac{1}{\triangle t}(\Psi^i - \Psi^{i-1}) \tag{4.32}$$

where Ψ^i is used to denote the value of Ψ at the i^{th} time-step. The time interval $(0, T)$ is discretized into N sub-intervals with equally spaced points $t = \{t_0, t_1, \cdots, t_N\}$ and therefore $\triangle t = \frac{T}{N}$. We use the interpolated state $\Psi^{i+\theta}$ given by

$$\Psi^{i+\theta} = \theta\Psi^{i+1} + (1-\theta)\Psi^i$$

where $0 \le \theta \le 1$. Thus, (4.31) becomes

$$\begin{cases} (M + \theta\triangle tR)\Psi^{i+1} & = & (M - (1-\theta)\triangle tR)\Psi^i \\ \\ \Psi(0) & = & \psi_0 \end{cases} \tag{4.33}$$

which can be written as

$$\begin{cases} P\Psi^{i+1} & = & Q\Psi^i \\ \\ \Psi(0) & = & \psi_0 \end{cases} \tag{4.34}$$

where

$$\begin{aligned} P &= M + \theta\triangle tR \\ \\ Q &= M - (1-\theta)\triangle tR \end{aligned} \tag{4.35}$$

Varying $0 \le \theta \le 1$ allows us to construct different time discretization schemes. For particular values of θ, we recover the finite difference schemes tabulated in Table 4.1. As shown in [RT83], the Crank-Nicolson method is proven to be the more stable method than the other two schemes. Therefore, we use this method for the reconstruction of ρ.

θ	Scheme	Description
0	Fully or Euler explicit	Forward difference method.
$\frac{1}{2}$	Semi-implicit	Crank-Nicolson method.
1	Fully or Euler implicit	Backward difference method.

Table 4.1.: *Different values of θ.*

Step 2: *Determination of the number of sources*

Using the measured data f on the boundary Σ_T and the test functions (4.12) and (4.14) with the function ρ calculated above in Step 1, our goal, first, is to compute $\alpha_0^r, \alpha_1^r, \cdots, \alpha_{2\bar{m}-1}^r$. Then, the number m can be determined by the rank of one of the three Hankel matrices $H_{\bar{m}}^r$, defined in (4.18), corresponding to the three projections, estimated using the Singular Value Decomposition method with an appropriate threshold, following [Han98].

Step 3: *Determination of the source locations*

As done before, we start by solving the linear system

$$H_m^r D = \xi_m^r,$$

in order to obtain the companion matrix defined in (4.19). Then, the projection points P_j^r of the monopolar sources are obtained as the m simple eigenvalues of the companion matrix B^r and consequently obtaining the locations S_j of the sources.

Step 4. *Determination of the moment*

The three vectors $\mu^r = (\mu_1^r, \cdots, \mu_m^r)$, $r = a, b, c$, are obtained by solving the systems

$$A_0^r \mu^r = \xi_0^r$$

where A_0 is the Vandremonde matrix defined by

$$A_0^r = \begin{pmatrix} 1 & 1 & \ldots & 1 \\ P_1^r & P_2^r & \ldots & P_m^r \\ \vdots & \vdots & \vdots & \vdots \\ (P_1^r)^{m-1} & (P_2^r)^{m-1} & \ldots & (P_m^r)^{m-1} \end{pmatrix}.$$

Step 5: Recovering the intensities λ_j:

To reconstruct the optimal intensities $\tilde{\phi}$, we seek to minimize the Kohn-Vogelius functional (4.23) by solving sequentially the direct problems (4.20, 4.21) and the corresponding adjoint problems (4.25, 4.26) using the finite element method. The algorithm used to determine the optimal intensities for the functional is based on the BFGS gradient conjugate method. In fact, we prescribe an initial guess for the intensities ϕ_0, then at the iteration k, the updated intensities ϕ_k is given by

$$\phi_k = \phi_{k-1} - \gamma_{k-1} {H_{k-1}}^{-1} \nabla J_{KV}(\phi_{k-1})$$

where the BFGS method is used to estimate and update H_k and the Wolfe's stepsize linear search is used to determine the optimal step γ_{k-1}.

Although the iteration process is regularizing, the problem remains unstable thus the need to use a stopping criterion. To fulfill this purpose, we use a stopping criterion based on the discrepancy principal of Morozov [Kir96]. In fact, we stop the iteration when

$$|u_k - f^{\varepsilon}|_{L^2(\Sigma_T)} \leq a\varepsilon \qquad a > 1 \tag{4.36}$$

where f^{ε} is a perturbed measurement relative to the noise level ε and u_k is the recovered solution trace of the direct problem at the k^{th} iteration.

4.8. Numerical Results

The proposed algebraic algorithm is verified numerically in this section over the heat equation for pollution applications where c is taken equal to 1. Here, Γ is assumed to be a unit sphere whose center is the origin O and the Cauchy data (f, g) on the boundary Σ_T are computed using the fundamental solution of the parabolic equation (4.2) in $\mathbb{R}^3$ over a uniform meshing of distributed points on the unit sphere. In fact, f and g are respectively the trace and the normal trace of w on Σ_T, where w is the fundamental solution corresponding to F, defined in the free space as:

$$w(\mathbf{X}, t) = Y(t) \sum_{j=1}^{m} \int_0^t \lambda(\tau) w_0(\mathbf{X} - \mathbf{S}_j, t - \tau)\, d\tau$$

where Y is the Heaviside function, $\mathbf{X} = (x, y, z)$ a point on Γ and w_0 is defined as

$$w_0(\mathbf{X}, t) = \frac{1}{(4\pi\sigma t)^{\frac{3}{2}}} e^{-\frac{\mathbf{x}^2}{4\sigma t}}.$$

Although a related stability estimate isn't yet performed to determine the factors that have an impact on the reconstruction process, we are based on the stationary case factors. Therefore, in the following subsections, we study the effect of the number of sensors, the supposed number upper bound, the separability coefficient between the sources and that of the noise.

As mentioned and proven in the stationary case, the identification of the number of sources forms the most important step in the reconstruction method. As before, theoretically their number is the rank of the Hankel matrices $H_{\bar{m}}^{r}$ which is numerically determined using SVD method with an appropriate threshold. Therefore, in our study, due to the classical estimate,[Han98],

$$|\sigma_{m+1}| \leq \|\delta H_{\bar{m}}\|_F, \tag{4.37}$$

we truncate beyond a threshold inferior to $\|\delta H_{\bar{m}}\|_F$. Here, $\|\cdot\|_F$ is the corresponding Frobenius norm and $\delta H_{\bar{m}}$ is the perturbation of $H_{\bar{m}}$ that originates from the noise in data as well as from the numerical quadrature error using a finite number of sensors on Γ and a specific time discretization level over $(0, T)$.

Remark 31. *The construction of the matrix $H^r_{\bar{m}}$ necessitates the calculation of the function ρ which can be obtained using the basis family*

$$\varphi_i(z_j) = \delta_{i,j}, \qquad 1 \leq j \leq n,$$

where $\delta_{i,j}$ is the Kronecker function defined as

$$\delta_{i,j} = \begin{cases} 1 & \text{if } i = j \\ 0 & \text{otherwise.} \end{cases}$$

4.8.1. Determining the number and the position of monopole sources

In the following subsubsections, unless mentioned otherwise, we fix the number of monopoles at 3 whose positions are taken as in Table 4.2 and we consider the projection onto the xy plane. The intensities are considered for $j = 1, 2, 3$ as, see Figure 4.1,

$$\lambda_j(t) = 0.1 - tanh(t - 0.9 * 1.84)./(2.8 * 0.45).$$

j (location $\sharp$)	1	2	3
$\mathbf{S}_j$	(0.6,-0.3,0.1)	(-0.7,0.3,-0.2)	(0.5,0.5,0.2)

Table 4.2.: *The source positions.*

a. The impact of the number of sensors

The choice of the number of sensors is an important issue in the recovery of the number and the position of the sources. Refining more the mesh (here 10^2 to 50^2 sensors), as seen in Figure 4.2 and using the truncation level $\|\delta H^a_6\|_F$ computed in Table 4.3, permits us to approach better the true number of sources. Indeed, the gap

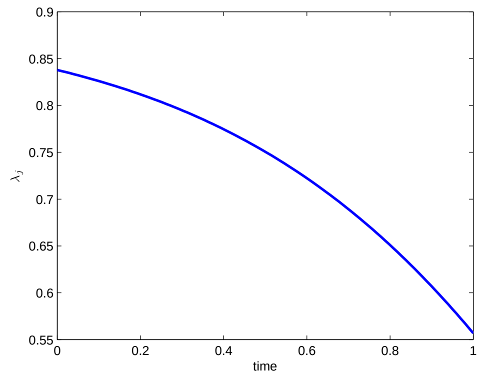

Figure 4.1.: The source intensities.

between the 3^{rd} and the 4^{th} singular value increases with respect to the number of sensors. However, one can see that starting from 25^2 sensors, where the number of sources is well-approximated, the reconstruction process improves minorly even with a higher number of sensors. This is validated also in the location approximation of these sources in Figure 4.2 (left).

Number of sensors	10^2	25^2	35^2	50^2
$\|\delta H_6^a\|_F \simeq$	0.48	0.30	0.25	0.21

Table 4.3.: The Frobenius norm of δH_6^a with respect to the sensors.

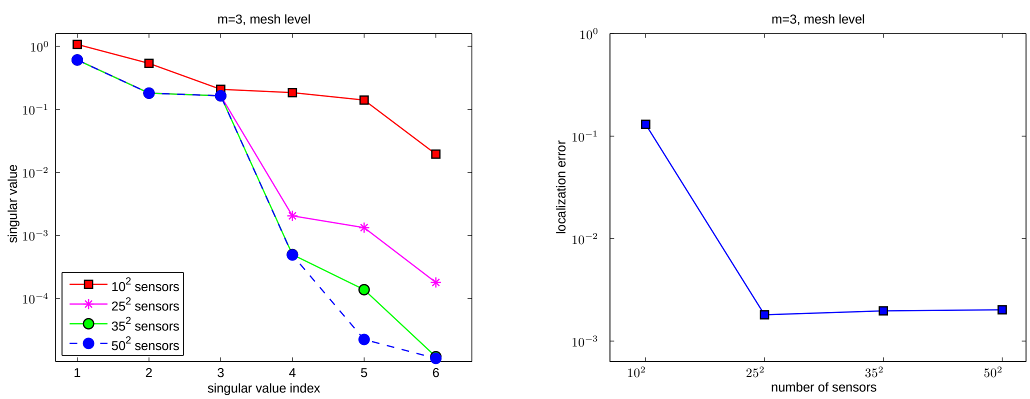

Figure 4.2.: Singular value of H_6^a (left) and the localization error (right) projected on the xy plane for $m = 3$ with respect to the number of sensors.

For a better clarification, we present the numerical results explicitly in Table 4.4.

Number of sensors	Estimated 2D Positions	Localization Error level
10^2	0.6579 - 0.4283i 0.5446 + 0.4103i -0.5990 + 0.3195i	0.115
25^2	0.5988 - 0.3023i 0.5003 + 0.5018i -0.7027 + 0.2982i	0.003
35^2	0.5975 - 0.3025i 0.4994 + 0.5035i -0.7006 + 0.2984i	0.003
50^2	0.5975 - 0.3026i 0.4995 + 0.5037i -0.7007 + 0.2983i	0.003

Table 4.4.: *The calculated $xy-$ source positions and their error for $m = 3$ varying the number of sensors.*

From now on, we fix our study to 25^2 sensors that enable us to recover precisely the number and the location of up to 3 monopoles.

b. The impact of the time discretization level

In the previous subsubsection, the time discretization step was fixed at 25 points over$(0, 1)$. However, this level could have an impact on the reconstruction process. To study its effect, we vary this discretization step from 10 to 50 points. As seen in Figure 4.3, this level has a very minor effect on both the number and the localization estimation whose error stays of the order 10^{-3}. Therefore, for computation-time minimization and better position approximation, we continue the tests with 25 time-discretization points.

c. The impact of the supposed number upper bound

To study the effect of the supposed upper bound $\bar{m}$ of the number of sources, we vary its value gradually. As seen in Figure 4.4 and applying the truncation threshold (4.37), with $\|\delta H^a_{\bar{m}}\|_F$ computed in Table 4.5, we observe that the gap between the 3^{rd} and the 4^{th} singular value decreases as we go farther than the desired number. Thus, the need of a good *a priori* information on the number of sources.

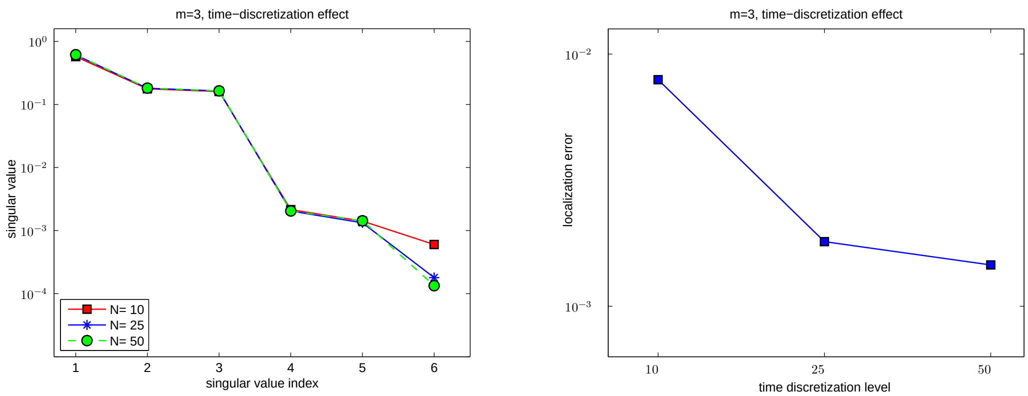

Figure 4.3.: *Singular value of H^a_6 (left) and the localization error (right) projected on the xy plane for $m = 3$ with respect to the time discretization level.*

$\bar{m}$	4	5	6	7
$\lVert \delta H^a_{\bar{m}} \rVert_F \simeq$	0.20	0.25	0.30	0.35

Table 4.5.: *The Frobenius norm of $\delta H^r_{\bar{m}}$ with respect to $\bar{m}$.*

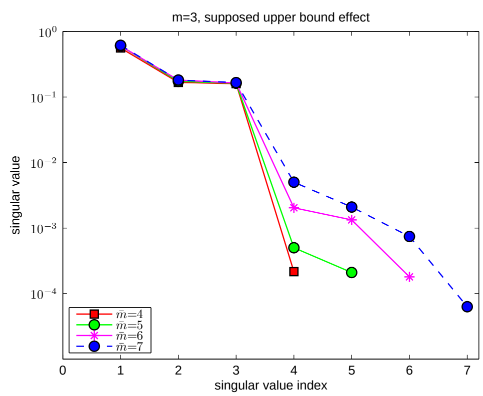

Figure 4.4.: *The localization error projected on the xy plane for $m = 3$ with respect to the number upper bound.*

d. Obtaining the 3D coordinates and the effect of the separability coefficient

To obtain the 3D coordinates of the sources, we use consequently the projections on the xy, yz and xz planes in the case of 3 monopoles as shown in Figure 4.5 and Figure 4.6. Note that, theoretically, according to hypothesis **(H3)**, the number of sources must be the same whatever the complex plane onto which the projections are performed. However, numerically the situation may be different since the number depends also on the separability of these projections. In fact, to recover their number we consider the numerical rank of the three Hankel matrices $H^r_{\bar{m}}$, $r = a, b, c$, obtained respecting the truncation threshold (4.37) and then we take the maximum between them as shown in Figure 4.5. Note that Figure 4.5 reflects the largest gap between the 3^{rd} and the 4^{th} singular value of H^r_6 in the xy plane which has the highest separability coefficients. Therefore, an exact number estimation is obtained better on the xy plane than the other planes since $\|\delta H^r_6\|_F \simeq 0.30$. Hence, a better localization accuracy is obtained as seen in Figure 4.6.

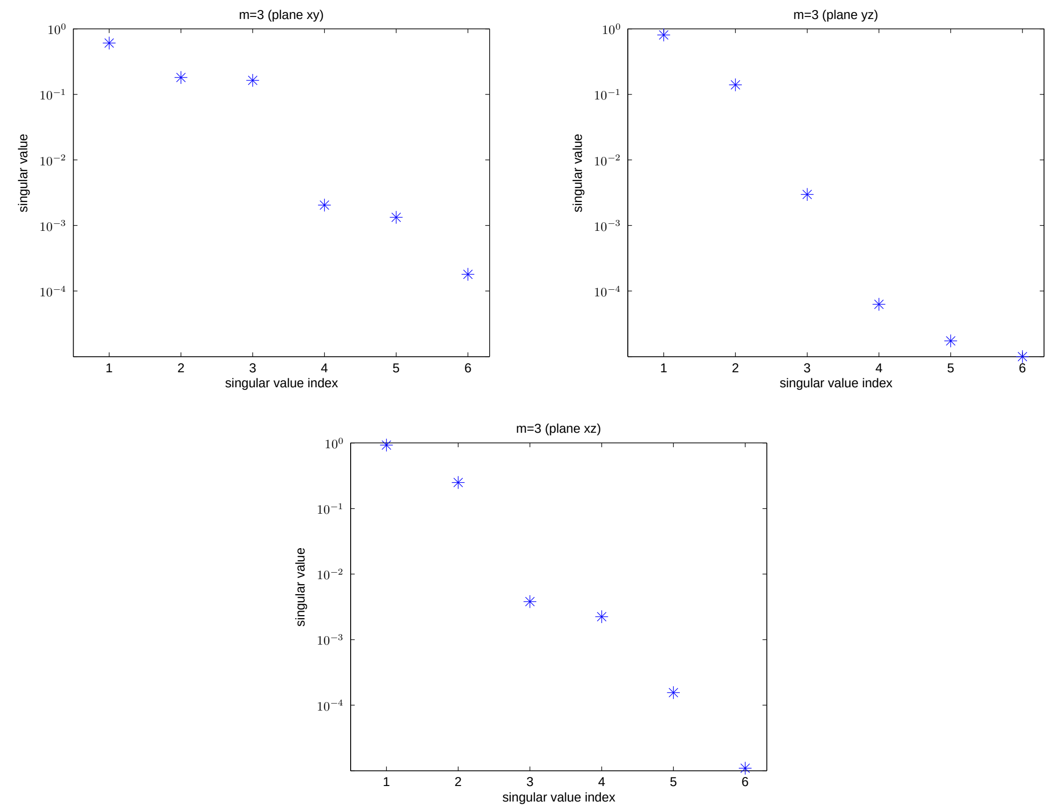

Figure 4.5.: *Singular values of H^r_6 for $m = 3$ where $r = a, b, c$.*

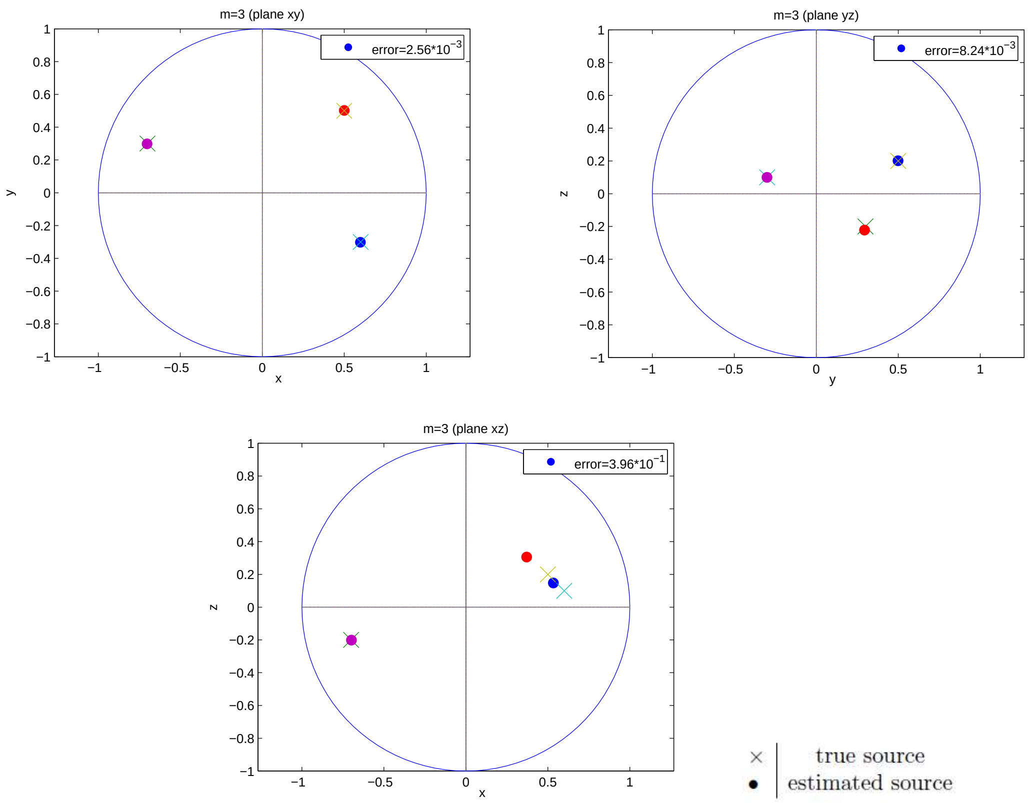

Figure 4.6.: Estimation results projected on the xy,yz and xz− planes when $m = 3$.

Note that the precision quality of the number and the location of the sources depend on the separability coefficient between the projected points as we have just seen numerically. Consequently, their reconstruction depends strongly on the plane of projection. Therefore, a good strategy is to choose the best projection plane that leads to the highest separability coefficient for a better number estimation as mentioned in the stationary case.

e. Impact of the noise

Reconstruction stability on the xy projections with respect to the noise level is examined in this subsubsection. In fact, Gaussian noise is added to f (and g) where the noise standard deviation added varies from 10^{-2} to 10^{1} % (see Figure 4.7). We have noted studying the singular values of the Hankel matrix H_6^a and using Table 4.6

that the number of monopoles is well estimated when the percentage of noise doesn't exceed $10^0\%$. Beyond that, their number is not well determined anymore. Moreover, we note that the localization error increases linearly as the percentage of the noise added increases.

Noise percentage	$10^{-2}\%$	$10^{-1}\%$	$10^{0}\%$	$10^{1}\%$
$\|\delta H_6^a\|_F \simeq$	0.30	0.30	0.31	0.41

Table 4.6.: *The Frobenius norm of δH_6^a with respect to the sensors.*

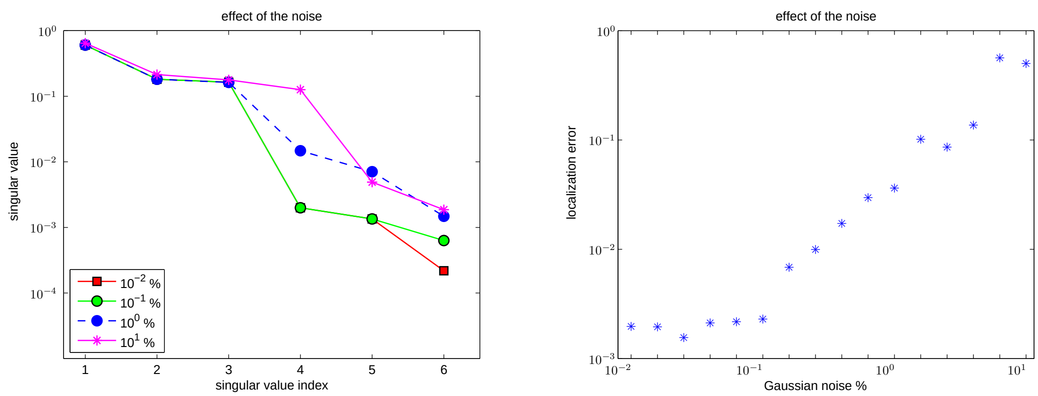

Figure 4.7.: *Singular values of H_6^a (left) and the localization errors (right) projected on the xy plane with 25^2 sensors and $\bar{J} = 6$ with respect to noise.*

f. Comparison with the stationary case

In here, we aim to compare both the stationary and the non-stationary cases representing the equations (2.1) and (4.2) respectively with monopole sources F of form (4.3). We consider the case of 3 monopoles with constant intensities $\lambda_j = 1, j = 1, 2, 3$ whose positions are defined as in Table 4.2. When studying the singular values of the corresponding Hankel matrices H_6^a and the localization accuracy on the $xy-$ projections of these monopoles with respect to the number of sensors, we observe in the following example the following issues. Although, as seen in Figure 4.8 and Figure 4.9 and using Table 4.3 and Table 4.7, the needed gap between the 4^{th} and the 3^{rd} singular is obtained with 25^2 sensors in both cases and although both show similar localization error, adding more than 25^2 sensors in the parabolic case doesn't improve the identification process. Whereas, in the static problem, more sensors lead to better results. Moreover, it is important to mention that the computation time is much less in the stationary problem. However, one can't give a conclusive idea with respect to these 2 cases.

Number of sensors	10^2	25^2	35^2	50^2
$\|\delta H_6^a\|_F \simeq$	2.67	1.07	0.76	0.53

Table 4.7.: The Frobenius norm of δH_6^a with respect to the sensors in the stationary case.

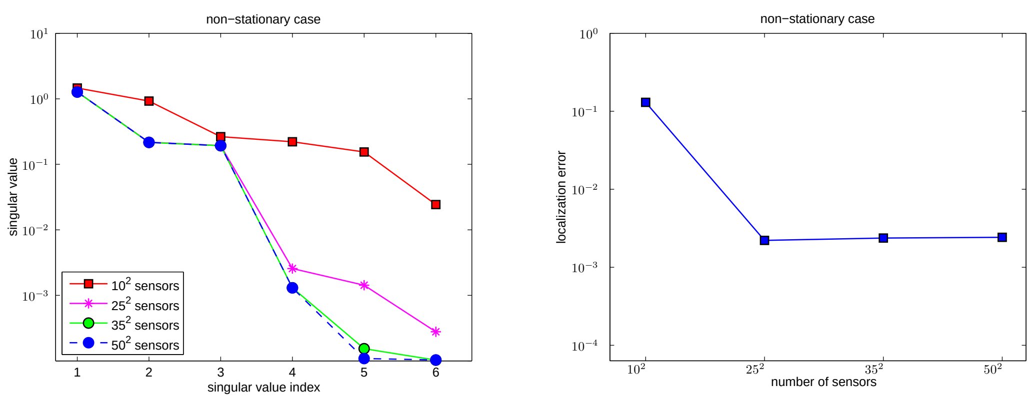

Figure 4.8.: Singular value of H_6^a (left) and the localization error (right) projected on the xy plane for $m = 3$ with constant intensities with respect to the number of sensors (non-stationary case).

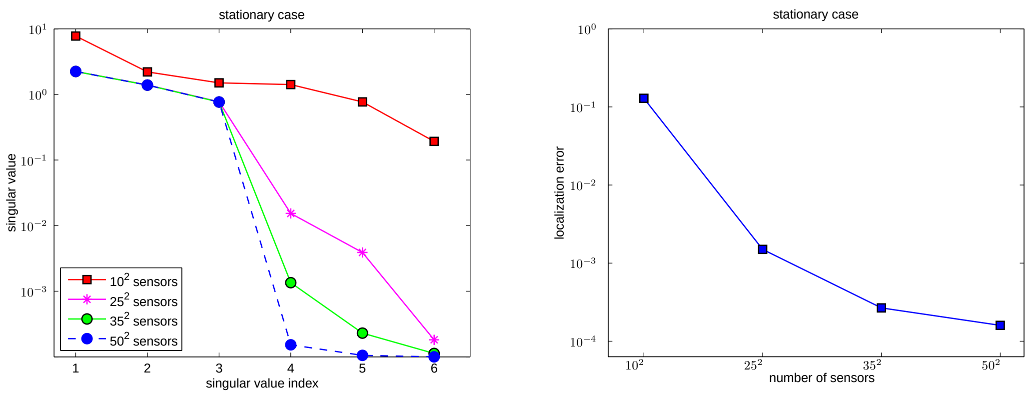

Figure 4.9.: *Singular value of H_6^a (left) and the localization error (right) projected on the xy plane for $m = 3$ with constant intensities with respect to the number of sensors (stationary case).*

Conclusions and perspectives

Everything is possible. The impossible just takes longer.

(Dan Brown)

Conclusions

This thesis deals with inverse source problems in 2 cases: stationary source in 2D and 3D elliptic equations and a non stationary source in a diffusion equation. The main form of sources considered are pointwise sources (monopoles, dipoles and multipolar sources) and sources having compact support within a finite number of small subdomains modelling EEG/MEG and BLT problems. The purpose of this thesis is mainly to propose robust identification methods that enable us to reconstruct the number, the intensity and the location of the sources. Direct algebraic methods are used to identify the stationary sources and a quasi-algebraic method mixed with an optimization method is employed to recover sources with time-variable intensities.

The algebraic method [EBHD00a] is a direct non-iterative resolution process. It consists in finding the relation between the source parameters and the corresponding Cauchy data pair by means of Green's formula and the use of suitable test functions. This approach is the main identification process used throughout this thesis to identify pointwise sources generalizing former related works [EBN11a].

Numerical results are shown using this approach on different frameworks over spherical and circular geometries and using the fundamental solution of the equation under study.

The optimization method proposed in Chapter 4, that aims to recover the time-variable intensities, is based on the minimization of a functional of a Kohn-Vogelius type. The method is proposed in here theoretically having as a perspective the needed numerical development behind this process. The gradient is calculated using the adjoint state method and the optimization process is based on the use of a BFGS-gradient conjugate algorithm with Morozov's stop criterion.

In the 3D stationary case, we have considered an inverse source problem, via boundary measurements, for the elliptic equation $\Delta u + \mu u = F$ from a single coefficient μ. This problem is applied, based on the sign of μ, along with Helmholtz equation ($\mu > 0$), on EEG/MEG problems ($\mu = 0$) and the BLT problem ($\mu < 0$). After proving the uniqueness for a combination of monopoles and dipoles and presenting the related stability estimates proven in [EBEH13], we arrive to establish a direct algebraic algorithm that enables us to recover the number, the moments and the positions (based on their 2D projections) of multipolar pointwise sources. The algorithm is then applied on sources having compact supports over discs and over general linear combination of subdomains that are well-recovered modulo (ϵ). This proposed method generalizes former works, [CKC12; EBHD00a; EBN11a; Nar12], by extending existing algorithms to the case $\mu \neq 0$ with more general source types. Moreover, it is presented with a simple and elegant proof. However, this direct method is not applied on the $2-$dimensional spaces unless $\mu = 0$ (see [EBHD00b]).

It is important to mention that the number determination is the most essential step in the source reconstruction since its wrong estimation causes consequently a bad identification of the source positions. However, the Hankel matrix, constructed from the boundary observations and responsible for the number recovery, is ill-conditioned. Therefore, a Singular Value Decomposition method with a specific truncation threshold, (2.53), is utilized. Numerically, several factors have an impact on the identification process and they are studied and analyzed mainly in the case of dipoles and a combination of monopoles and dipoles. In fact, the mesh level has a great impact on the reconstruction of these sources. Indeed, refining the mesh allows more accessibility to the boundary measurements with less noise. Therefore, as seen numerically, adding more sensors increases the number and localization accuracy and allows to determine more and more sources. Moreover, the number upper bound has an effect on the identification process since the farther it is than the real number, the worse is its reconstructions. However, the separability between these sources also plays a role on their identification. Therefore, to well-estimate the source parameters, one should choose the best projection planes having the highest separability coefficients in order to recuperate the right number and consequently the right $3D$ position of the sources. However, this direct algorithm is sensible against noise, where the number is well-determined when the noise doesn't exceed a certain limit (about 1% Guassian noise).

Several comparisons are performed in this 3D case mainly related to the source type and the coefficient μ. Indeed, comparing monopoles identification with that of dipoles, we observe that the proposed algebraic method shows even better results with much less errors and with more robustness with respect to noise. With respect to the coefficient μ, the only remark is that although changing the sign of μ has a minor effect on the reconstruction process, one sees that diffusion phenomenon for BLT problem causes more errors than the propagation one (Helmholtz equation).

In the 2D stationary case, we have considered an inverse source problem, via boundary measurements, for the Helmholtz equation $\Delta u + \kappa^2 u = F$ where F are monopolar sources. The number, the location and the intensities of these sources, along with sources having compact supports are well-reconstructed (modulo ϵ) using a single wave number with a suitable transformation to a 3-dimensional space and employing the algebraic method proposed previously. However, using multiple frequencies can restore algebraically these sources directly on the $2-$dimensional space without any constraints. Numerical experiments is this framework were performed to study the impact of the several factors on the proposed identification process. In fact, as observed in the 3D problem, the increase in the mesh level and the separability coefficients enhance the reconstruction of the number and the position of the sources. Moreover, the process is somewhat robust with respect to the noise. On the other hand, in here, the choice of the wavenumbers and the supposed number upper bound play an important role on the parameters recovery. Indeed, employing higher wavenumbers cause a wrong number and consequently location determination. The latter observation is physically due to the fact that higher wavenumbers causes less points in the domain to be touched by the photon wavelength. Moreover, numerically, it increases the ill-conditionality of the related Hankel matrix whose rank corresponds to the number reconstruction.

In the non-stationary case, we have considered an inverse source problem, via boundary measurements, for the parabolic equation $\frac{1}{c}\frac{\partial u}{\partial t} - \Delta u + \mu u = F$ where F are monopolar sources. Along with non-stationary BLT study, a main motivation behind this inverse problem is the problem of the identification of pollutants in a contaminant. A direct algebraic method, using specific test functions, mixed with a proper optimization method are employed for the reconstruction of stationary monopoles with time-variant intensities. The numerical results performed reflect the same observations as in the stationary case. Comparing these two cases, one notes that less error is caused in the stationary case than that in the non-stationary one. This is normal since the noise caused by the numerical quadrature error is less in the static case.

General conclusion

Direct algebraic algorithms are proposed in order to recover, from a single boundary measurement and using a single coefficient μ, pointwise sources in certain $2-$ and $3-$dimensional elliptic and parabolic equations. Knowing that the number determination of these sources are the most crucial step, it is very important to employ a good truncation level that enables us to reconstruct the number, based on the rank of a Hankel matrix. To improve the reconstruction process, one should have

1. A sufficient number of sensors, whose increase augments the identification accuracy and thus one could obtain more and more number of sensors.
2. A good *a priori* knowledge on the upper bound of the number of sources where going farther causes more errors.
3. A good separability coefficient between the projection of the sources. This condition depends on both the number of sources and on the choice of the projection plane. Indeed, as we add more sources, the separability diminishes especially using a fixed-sized domains. Moreover, to choose the projection plane that establishes the highest separability coefficient as mentioned in Remark 8.

Between these sources, monopoles behave better than dipoles.

Perspectives

Several perspectives can be considered and are to be done in future works mainly for the non-stationary inverse problem.

- Concerning the reconstruction of the time-variable intensities, a numerical development of the proposed Kohn-Vogelius optimization problem is to be performed. Moreover, due to the calculation of the moments through the algebraic algorithm, a moment problem can be considered in order to reconstruct the needed intensity functions.

- The generalization of the type of sources to multipolar sources is interesting to study for their moments reconstruction since the number, positions and quantities related to their moments are reconstructed by the method proposed in Chapter 2.
- The stability of the diffusion equation including the time-variable intensities.
- Reconstruction of inhomogeneous conductivities using multipolar sources methodology.

Appendices

APPENDIX A

Explicit Calculation of $I_{\alpha,j}$

Knowing that,

$$I_{\alpha,j} = \int_{\mathbb{R}} e^{-i\varepsilon_1 a_j \sqrt{\omega^2 + (\frac{\kappa}{\varepsilon_1})^2}} \delta^{(\alpha)}(\omega)\, d\omega,$$

these functions can be calculated explicitly recursively.

Indeed, in the distribution sense,

$$\begin{array}{rcl} I_{\alpha,j} & = & < e^{-i\varepsilon_1 a_j \sqrt{\omega^2 + (\frac{\kappa}{\varepsilon_1})^2}}, \delta^{(\alpha)}(\omega) > \\ & = & (-1)^{\alpha} < \frac{d^{(\alpha)}}{d\omega} e^{-i\varepsilon_1 a_j \sqrt{\omega^2 + (\frac{\kappa}{\varepsilon_1})^2}}, \delta_0(\omega) > \\ & = & (-1)^{\alpha} \left(\frac{d^{(\alpha)}}{d\omega} e^{-i\varepsilon_1 a_j \sqrt{\omega^2 + (\frac{\kappa}{\varepsilon_1})^2}} \right) |_{\omega=0}\ . \end{array}$$

We can directly see that

$$I_{0,j} = e^{-i a_j \kappa}.$$

Now, for $\alpha \geq 1$, using "MUPAD" toolbox in Matlab as seen just afterwards, we obtain the needed result.

```
I1:=subs(diff(exp(-I*aj*sqrt(w^2+k^2)), w),w=0)
```

$$0$$

```
I2:=simplify(subs(diff(exp(-I*aj*sqrt(w^2+k^2)), w$2),w=0))
```

$$-\frac{\mathrm{aj}\,\frac{1}{e^{\mathrm{aj}\,k\,\mathrm{i}}}\,\mathrm{i}}{k}$$

```
I4:=simplify(subs(diff(exp(-I*aj*sqrt(w^2+k^2)), w$4),w=0))
```

$$-\frac{3\,\mathrm{aj}\,\frac{1}{e^{\mathrm{aj}\,k\,\mathrm{i}}}\,(\mathrm{aj}\,k-\mathrm{i})}{k^3}$$

```
I5:=simplify(subs(diff(exp(-I*aj*sqrt(w^2+k^2)), w$5),w=0))
```

$$0$$

```
I6:=simplify(subs(diff(exp(-I*aj*sqrt(w^2+k^2)), w$6),w=0))
```

$$\frac{15\,\mathrm{aj}\,\frac{1}{e^{\mathrm{aj}\,k\,\mathrm{i}}}\,(\mathrm{aj}^2\,k^2\,\mathrm{i}+3\,\mathrm{aj}\,k-3\,\mathrm{i})}{k^5}$$

```
I7:=simplify(subs(diff(exp(-I*aj*sqrt(w^2+k^2)), w$7),w=0))
```

$$0$$

```
I8:=simplify(subs(diff(exp(-I*aj*sqrt(w^2+k^2)), w$8),w=0))
```

$$-\frac{105\,\mathrm{aj}\,\frac{1}{e^{\mathrm{aj}\,k\,\mathrm{i}}}\,(-\mathrm{aj}^3\,k^3+6\,\mathrm{aj}^2\,k^2\,\mathrm{i}+15\,\mathrm{aj}\,k-15\,\mathrm{i})}{k^7}$$

```
I9:=simplify(subs(diff(exp(-I*aj*sqrt(w^2+k^2)), w$9),w=0))
```

$$0$$

```
I10:=simplify(subs(diff(exp(-I*aj*sqrt(w^2+k^2)), w$10),w=0))
```

$$-\frac{945\,\mathrm{aj}\,\frac{1}{e^{\mathrm{aj}\,k\,\mathrm{i}}}\,(\mathrm{aj}^4\,k^4\,\mathrm{i}+10\,\mathrm{aj}^3\,k^3-45\,\mathrm{aj}^2\,k^2\,\mathrm{i}-105\,\mathrm{aj}\,k+105\,\mathrm{i})}{k^9}$$

Figure A.1.: *The calculation of the derivatives using MUPAD.*

Coefficients of Bessel polynomials:

```
calpha:=proc(n,kk)
begin;
c:=(1/(2^kk))*(fact(n+kk)/(fact(kk)*fact(n-kk)));
return(c);
end_proc;
```

proc calpha(n, kk) ... end

```
c2:=matrix([[calpha(0,0)]])
```

(1)

```
c4:=matrix([[calpha(1,0),calpha(1,1)]])
```

(1 1)

```
c6:=matrix([[calpha(2,0),calpha(2,1),calpha(2,2)]])
```

(1 3 3)

```
c8:=matrix([[calpha(3,0),calpha(3,1),calpha(3,2),calpha(3,3)]])
```

(1 6 15 15)

```
c10:=matrix([[calpha(4,0),calpha(4,1),calpha(4,2),calpha(4,3),calpha(4,
```

(1 10 45 105 105)

Figure A.2.: *The verification of the Bessel coefficients using MUPAD.*

Bibliography

[ABEB11] Michael Andrle, F Ben Belgacem, and A El Badia. "Identification of moving pointwise sources in an advection–dispersion–reaction equation". In: *Inverse Problems* 27.2 (2011), p. 025007 (cit. on p. 118).

[Ada+02] Jason Y Adams, Mai Johnson, Makoto Sato, Frank Berger, Sanjiv S Gambhir, Michael Carey, M Luisa Iruela-Arispe, and Lily Wu. "Visualization of advanced human prostate cancer lesions in living mice by a targeted gene transfer vector and optical imaging". In: *Nature medicine* 8.8 (2002), pp. 891–896 (cit. on p. 8).

[AEB12] M. Andrle and A. El Badia. "Identification of multiple moving pollution sources in surface waters or atmospheric media with boundary observations". In: *Inverse Problems* 28.7 (2012), pp. 075009, 22. DOI: 10.1088/0266-5611/28/7/075009 (cit. on pp. 121–123).

[AEBEH13] Batoul Abdelaziz, Abdellatif El Badia, and Ahmad El Hajj. "Reconstruction of extended sources with small supports in the elliptic equation Δu+ μu= F from a single Cauchy data," in: *Comptes Rendus Mathematique* 351.21 (2013), pp. 797–801 (cit. on p. xv).

[AEBEH14a] Batoul Abdelaziz, Abdellatif El Badia, and Ahmad El Hajj. "Algebraic method to identify impulse sources in 2D Helmholtz equtaion". In: *submitted* (2014) (cit. on p. xv).

[AEBEH14b] Batoul Abdelaziz, Abdellatif El Badia, and Ahmad El Hajj. "Direct algorithm for multipolar sources reconstruction". In: *to appear in Journal of Mathematical Analysis and Applications* (2014) (cit. on p. xv).

[AEBEH14c] Batoul Abdelaziz, Abdellatif El Badia, and Ahmad El Hajj. "Identification of monopolar sources in a bioluminescent tomography problem". In: *ESAIM: PROCEEDINGS AND SURVEYS*. Vol. 45. EDP Sciences, SMAI. 2014, pp. 390–399 (cit. on pp. xv, 55).

[AK04] Habib Ammari and Hyeonbae Kang. *Reconstruction of small inhomogeneities from boundary measurements*. 1846. Springer, 2004 (cit. on p. 20).

[AKS09] Carlos Alves, Rainer Kress, and Pedro Serranho. “Iterative and range test methods for an inverse source problem for acoustic waves”. In: *Inverse Problems* 25.5 (2009), pp. 055005, 17 (cit. on p. 20).

[AMR09] Carlos J. S. Alves, Nuno F. M. Martins, and Nilson C. Roberty. “Full identification of acoustic sources with multiple frequencies and boundary measurements”. In: *Inverse Probl. Imaging* 3.2 (2009), pp. 275–294. DOI: 10.3934/ipi.2009.3.275 (cit. on p. 22).

[Ana+07] Mark A. Anastasio, Jin Zhang, Dimple Modgil, and Patrick J. La Rivière. “Application of inverse source concepts to photoacoustic tomography”. In: *Inverse Problems* 23.6 (2007), S21–S35 (cit. on p. 6).

[Arr99] Simon R Arridge. “Optical tomography in medical imaging”. In: *Inverse problems* 15.2 (1999), R41 (cit. on pp. 6, 12, 13).

[Bar+05] L Baratchart, A Ben Abda, F Ben Hassen, and J Leblond. “Recovery of pointwise sources or small inclusions in 2D domains and rational approximation”. In: *Inverse problems* 21.1 (2005), p. 51 (cit. on p. 20).

[Bar+99] L Baratchart, J Leblond, F Mandréa, and EB Saff. “How can the meromorphic approximation help to solve some 2D inverse problems for the Laplacian?” In: *Inverse problems* 15.1 (1999), pp. 79–90 (cit. on p. 20).

[BC77] Norman Bleistein and Jack K. Cohen. “Nonuniqueness in the inverse source problem in acoustics and electromagnetics”. In: *J. Mathematical Phys.* 18.2 (1977), pp. 194–201 (cit. on p. 22).

[BLM+06] Laurent Baratchart, Juliette Leblond, Jean-Paul Marmorat, et al. “Inverse source problem in a 3D ball from best meromorphic approximation on 2D slices”. In: *Electronic Transactions on Numerical Analysis* 25 (2006), pp. 41–53 (cit. on p. 21).

[BLT11] Gang Bao, Junshan Lin, and Faouzi Triki. “An inverse source problem with multiple frequency data”. In: *C. R. Math.* 349.15–16 (2011), pp. 855–859 (cit. on p. 26).

[Can68] JR Cannon. “Determination of an unknown heat source from overspecified boundary data”. In: *SIAM Journal on Numerical Analysis* 5.2 (1968), pp. 275–286 (cit. on p. 118).

[Cao+06] Feng Cao, Shuan Lin, Xiaoyan Xie, Pritha Ray, Manishkumar Patel, Xianzhong Zhang, Micha Drukker, Scott J Dylla, Andrew J Connolly, Xiaoyuan Chen, et al. “In vivo visualization of embryonic stem cell survival, proliferation, and migration after cardiac delivery”. In: *Circulation* 113.7 (2006), pp. 1005–1014 (cit. on p. 8).

[CC09] Yun-Sung Chung and Soon-Yeong Chung. “Identification of the combination of monopolar and dipolar sources for elliptic equations”. In: *Inverse Problems* 25.8 (2009), pp. 085006, 16 (cit. on pp. 20, 22, 23).

[CH89] R. Courant and D. Hilbert. *Methods of mathematical physics. Vol. II.* Partial differential equations, Reprint of the 1962 original, A Wiley-Interscience Publication. John Wiley & Sons Inc., 1989, pp. xxii+830 (cit. on pp. 48, 108).

[Che+10] Xiaojuan Chen, Courtney S Larson, Jason West, Xiaomin Zhang, and Dixon B Kaufman. “In vivo detection of extrapancreatic insulin gene expression in diabetic mice by bioluminescence imaging”. In: *PloS one* 5.2 (2010), e9397 (cit. on p. 8).

[CKC12] Y.-S. Chung, J. E. Kim, and S.-Y. Chung. “Identification of multipoles via boundary measurements”. In: *European J. Appl. Math.* 23.2 (2012), pp. 289–313. DOI: 10.1017/S0956792511000386 (cit. on pp. 20, 22, 23, 54, 146).

[Con+05] Wenxiang Cong, Ge Wang, Durairaj Kumar, Yi Liu, Ming Jiang, Lihong V Wang, Eric A Hoffman, Geoffrey McLennan, Paul B McCray, Joseph Zabner, et al. “Practical reconstruction method for bioluminescence tomography”. In: *Opt. Express* 13.18 (2005), pp. 6756–6771 (cit. on pp. 7, 20, 21).

[Das09] George Dassios. “Electric and magnetic activity of the brain in spherical and ellipsoidal geometry”. In: *Mathematical modeling in biomedical imaging. I.* Vol. 1983. 2009, pp. 133–202 (cit. on p. 6).

[DW73] A. J. Devaney and E. Wolf. “Radiating and Nonradiating Classical Current Distributions and the Fields They Generate”. In: *Phys. Rev. D* 8 (4 1973), pp. 1044–1047. DOI: 10.1103/PhysRevD.8.1044 (cit. on p. 22).

[EB05] Abdellatif El Badia. “Inverse source problem in an anisotropic medium by boundary measurements”. In: *Inverse Problems* 21.5 (2005), pp. 1487–1506. DOI: 10.1088/0266-5611/21/5/001 (cit. on pp. 20, 22, 23, 38).

[EBD98] Abdellatif El Badia and T Ha Duong. “Some remarks on the problem of source identification from boundary measurements”. In: *Inverse Problems* 14.4 (1998), p. 883 (cit. on p. 22).

[EBEH12] Abdellatif El Badia and Ahmad El Hajj. “Hölder stability estimates for some inverse pointwise source problems”. In: *Comptes Rendus Mathematique* (2012) (cit. on pp. 17, 26–28).

[EBEH13] Abdellatif El Badia and Ahmad El Hajj. “Identification of Dislocations in Materials from Boundary Measurements”. In: *SIAM J. Appl. Math.* 73.1 (2013), pp. 84–103 (cit. on pp. 6, 55, 146).

[EBF10] A El-Badia and M Farah. “A stable recovering of dipole sources from partial boundary measurements”. In: *Inverse Problems* 26.11 (2010), p. 115006 (cit. on pp. 20, 21).

[EBHD00a] Abdellatif El Badia and Tuong Ha-Duong. "An inverse source problem in potential analysis". In: *Inverse Problems* 16 (2000), pp. 651–663. DOI: 10.1088/0266-5611/21/5/001 (cit. on pp. 20–23, 125, 145, 146).

[EBHD00b] Abdellatif El Badia and Tuong Ha-Duong. "An inverse source problem in potential analysis". In: *Inverse Problems* 16 (2000), pp. 651–663. DOI: 10.1088/0266-5611/21/5/001 (cit. on p. 146).

[EBHD02] A El Badia and T Ha-Duong. "On an inverse source problem for the heat equation. Application to a pollution detection problem". In: *JOURNAL OF INVERSE AND ILL POSED PROBLEMS* 10.6 (2002), pp. 585–600 (cit. on pp. 6, 117, 119, 123).

[EBHDH05] A El Badia, T Ha-Duong, and A Hamdi. "Identification of a point source in a linear advection–dispersion–reaction equation: application to a pollution source problem". In: *Inverse Problems* 21.3 (2005), p. 1121 (cit. on pp. 118, 123).

[EBN11a] Abdellatif El Badia and Takaaki Nara. "An inverse source problem for Helmholtz's equation from the Cauchy data with a single wave number". In: *Inverse Problems* 27.10 (2011), pp. 105001, 15 (cit. on pp. 19, 20, 22, 23, 48, 55, 81, 145, 146).

[EBN11b] Abdellatif El Badia and Takaaki Nara. "An inverse source problem for Helmholtz's equation from the Cauchy data with a single wave number". In: *Inverse Problems* 27.10 (2011), pp. 105001, 15 (cit. on pp. 96, 108).

[ESY94] Heinz W Engl, Otmar Scherzer, and Masahiro Yamamoto. "Uniqueness and stable determination of forcing terms in linear partial differential equations with overspecified boundary data". In: *Inverse Problems* 10.6 (1994), p. 1253 (cit. on p. 118).

[FL06] Adrian Farcas and Daniel Lesnic. "The boundary-element method for the determination of a heat source dependent on one variable". In: *Journal of Engineering Mathematics* 54.4 (2006), pp. 375–388 (cit. on p. 118).

[Han08] Martin Hanke. "On real-time algorithms for the location search of discontinuous conductivities with one measurement". In: *Inverse Problems* 24.4 (2008), p. 045005 (cit. on p. 20).

[Han98] Per Christian Hansen. *Rank-deficient and discrete ill-posed problems*. Numerical aspects of linear inversion. Society for Industrial and Applied Mathematics (SIAM), 1998, pp. xvi+247 (cit. on pp. 38, 56, 100, 109, 134, 136).

[HCW06] Weimin Han, Wenxiang Cong, and Ge Wang. "Mathematical theory and numerical analysis of bioluminescence tomography". In: *Inverse Problems* 22.5 (2006), p. 1659 (cit. on pp. 20, 21).

[HR01] Frank Hettlich and William Rundell. "Identification of a discontinuous source in the heat equation". In: *Inverse Problems* 17.5 (2001), p. 1465 (cit. on p. 118).

[HR11] Martin Hanke and William Rundell. "On rational approximation methods for inverse source problems". In: *Inverse Probl. Imaging* 5.1 (2011), pp. 185–202. DOI: 10.3934/ipi.2011.5.185 (cit. on pp. 20, 54).

[HYC11] Hao Hong, Yunan Yang, and Weibo Cai. "Imaging gene expression in live cells and tissues". In: *Cold Spring Harbor Protocols* 2011.4 (2011), pdb–top103 (cit. on p. 8).

[Ike99] Masaru Ikehata. "Reconstruction of a source domain from the Cauchy data". In: *Inverse Problems* 15.2 (1999), p. 637 (cit. on p. 20).

[Isa98] Victor Isakov. *Inverse problems for partial differential equations*. Vol. 127. Springer-Verlag, 1998, pp. xii+284 (cit. on p. 6).

[Jeo+06] Yong Hyun Jeon, Yun Choi, Joo Hyun Kang, June-Key Chung, Yong Jin Lee, Chul Woo Kim, Jae Min Jeong, Dong Soo Lee, and Myung Chul Lee. "In vivo monitoring of DNA vaccine gene expression using firefly luciferase as a naked DNA". In: *Vaccine* 24.16 (2006), pp. 3057–3062 (cit. on p. 8).

[Jer+02] K. Jerbi, J. C. Mosher, S. Baillet, and R. M. Leahy. "On MEG forward modeling using multipolar expansions". In: *Phys. Med. Bio.* 47.2 (2002), pp. 523–555 (cit. on pp. 6, 19).

[Jer+04] K. Jerbi, S. Baillet, J. C. Mosher, G Nolte, L Garnero, and R. M. Leahy. "Localization of realistic cortical cavity in MEG using current multipoles". In: *NeuroImage* 22.2 (2004), pp. 779–793 (cit. on pp. 6, 19).

[Kir96] Andreas Kirsch. *An Introduction to the Mathematical Theory of Inverse Problems*. Springer-Verlag New York, Inc., 1996 (cit. on p. 135).

[KR13] Rainer Kress and William Rundell. "Reconstruction of extended sources for the Helmholtz equation". In: *Inverse Problems* 29 (2013), p. 035005 (cit. on p. 20).

[KV85] Robert V Kohn and Michael Vogelius. "Determining conductivity by boundary measurements II. Interior results". In: *Communications on Pure and Applied Mathematics* 38.5 (1985), pp. 643–667 (cit. on p. 21).

[KW08] Steven Kusiak and John Weatherwax. "Identification and characterization of a mobile source in a general parabolic differential equation with constant coefficients". In: *SIAM Journal on Applied Mathematics* 68.3 (2008), pp. 784–805 (cit. on p. 118).

[Lin+06] Leevan Ling, Masahiro Yamamoto, YC Hon, and Tomoya Takeuchi. "Identification of source locations in two-dimensional heat equations". In: *Inverse Problems* 22.4 (2006), p. 1289 (cit. on p. 118).

[LM10] Byeong Il Lee and Jung-Joon Min. "Molecular imaging using bioluminescence". In: *Open Nucl Med J* 2 (2010), pp. 157–165 (cit. on p. 8).

[LMK72] Jacques Louis Lions, Enrico Magenes, and P Kenneth. *Non-homogeneous boundary value problems and applications*. Vol. 1. Springer Berlin, 1972 (cit. on p. 120).

[Miz58] Sigeru Mizohata. "Unicité du prolongement des solutions pour quelques opérateurs différentiels paraboliques". In: *Kyoto Journal of Mathematics* 31.3 (1958), pp. 219–239 (cit. on p. 121).

[MLL92] J. C. Mosher, P. S. Lewis, and R. M. Leahy. "Multiple dipole modeling and localization from spatio-temporal MEG data". In: *Biomedical Engineering, IEEE Transactions on* 39.6 (1992), pp. 541–557. DOI: 10.1109/10.141192 (cit. on pp. 6, 20).

[MV+12] Rafael A Madero-Visbal, Jimmie F Colon, Ingrid C Hernandez, Arati Limaye, Joshua Smith, Christopher M Lee, Philip A Arlen, Luis Herrera, and Cheryl H Baker. "Bioluminescence imaging correlates with tumor progression in an orthotopic mouse model of lung cancer". In: *Surgical oncology* 21.1 (2012), pp. 23–29 (cit. on pp. 7, 117).

[Nar08] Takaaki Nara. "An algebraic method for identification of dipoles and quadrupoles". In: *Inverse Problems* 24.2 (2008), pp. 025010, 19. DOI: 10.1088/0266-5611/24/2/025010 (cit. on pp. 20, 22, 23).

[Nar12] Takaaki Nara. "Algebraic reconstruction of the general-order poles of a meromorphic function". In: *Inverse Problems* 28.2 (2012), pp. 025008, 19. DOI: 10.1088/0266-5611/28/2/025008 (cit. on pp. 20, 22, 23, 54, 146).

[NW01] Frank Natterer and Frank Wubbeling. *Mathematical methods in image reconstruction*. Society for Industrial and Applied Mathematics, 2001 (cit. on p. 12).

[OL01] Akira Okubo and Smon A Levin. *Diffusion and ecological problems: modern perspectives*. Vol. 14. Springer, 2001 (cit. on p. 117).

[RT83] Pierre-Arnaud Raviart and Jean-Marie Thomas. *Introduction à l'analyse numérique des équations aux dérivées partielles*. Vol. 6. Masson, 1983 (cit. on pp. 132, 133).

[Sch+95] M Schweiger, SR Arridge, M Hiraoka, and DT Delpy. "The finite element method for the propagation of light in scattering media: boundary and source conditions". In: *Medical Physics* 22 (1995), p. 1779 (cit. on p. 14).

[Sch43] Laurent Schwartz. *Étude des sommes d'exponentielles réelles*. fre. 1943 (cit. on p. 25).

[SS87] Jean-Claude Saut and Bruno Scheurer. “Unique continuation for some evolution equations”. In: *Journal of differential equations* 66.1 (1987), pp. 118–139 (cit. on p. 121).

[Ste73a] G. W. Stewart. *Introduction to matrix computations*. Computer Science and Applied Mathematics. Academic Press [A subsidiary of Harcourt Brace Jovanovich, Publishers], New York-London, 1973, pp. xiii+441 (cit. on p. 54).

[Ste73b] G. W. Stewart. *Introduction to matrix computations*. Computer Science and Applied Mathematics. Academic Press [A subsidiary of Harcourt Brace Jovanovich, Publishers], New York-London, 1973, pp. xiii+441 (cit. on p. 91).

[SU09] Plamen Stefanov and Gunther Uhlmann. “Thermoacoustic tomography with variable sound speed”. In: *Inverse Problems* 25.7 (2009), pp. 075011, 16. DOI: 10.1088/0266-5611/25/7/075011 (cit. on p. 6).

[Tay+98] Amanda L Taylor, Brian A Kudlow, Kevin L Marrs, Dieter C Gruenert, William B Guggino, and Erik M Schwiebert. “Bioluminescence detection of ATP release mechanisms in epithelia”. In: *American Journal of Physiology-Cell Physiology* 275.5 (1998), pp. C1391–C1406 (cit. on p. 8).

[Wan+06a] Ge Wang, Wenxiang Cong, Kumar Durairaj, Xin Qian, Haiou Shen, Patrick Sinn, Eric Hoffman, Geoffrey McLennan, and Michael Henry. “In vivo mouse studies with bioluminescence tomography”. In: *Opt. Express* 14.17 (2006), pp. 7801–7809 (cit. on p. 10).

[Wan+06b] Ge Wang, Haiou Shen, Kumar Durairaj, Xin Qian, and Wenxiang Cong. “The first bioluminescence tomography system for simultaneous acquisition of multiview and multispectral data”. In: *International journal of biomedical imaging* 2006 (2006) (cit. on pp. 9, 11, 72).

[WLJ04] Ge Wang, Yi Li, and Ming Jiang. “Uniqueness theorems in bioluminescence tomography”. In: *Medical physics* 31 (2004), p. 2289 (cit. on pp. 6, 7, 19, 22).

[Wu+03] Joseph C Wu, Ian Y Chen, Gobalakrishnan Sundaresan, Jung-Joon Min, Abhijit De, Jian-Hua Qiao, Michael C Fishbein, and Sanjiv S Gambhir. “Molecular imaging of cardiac cell transplantation in living animals using optical bioluminescence and positron emission tomography”. In: *Circulation* 108.11 (2003), pp. 1302–1305 (cit. on p. 8).

[Yam93] M Yamamoto. “Conditional stability in determination of force terms of heat equations in a rectangle”. In: *Mathematical and computer modelling* 18.1 (1993), pp. 79–88 (cit. on p. 118).

[Yam94] Masahiro Yamamoto. "Conditional stability in determination of densities of heat sources in a bounded domain". In: *Control and estimation of distributed parameter systems: nonlinear phenomena*. 1994, pp. 359–370 (cit. on p. 118).

[YFY08] Liang Yan, Chu-Li Fu, and Feng-Lian Yang. "The method of fundamental solutions for the inverse heat source problem". In: *Engineering Analysis with Boundary Elements* 32.3 (2008), pp. 216–222 (cit. on p. 118).